LIB. G.K.V.

R
06.063
22 P.
V. LV

PROC. OF THE
INDIAN ACADEMY OF SC.

VOL. 62

112120

गुरुकुल कांगड़ी विश्वविद्यालय, हरिद्वार
पुस्तकालय

विषय संख्या R 506·063
पुस्तक संख्या B22P V·LV
आगत पंजिका संख्या

पुस्तक पर किसी प्रकार का निशान लगाना वर्जित है। कृपया १५ दिन से अधिक समय तक पुस्तक अपने पास न रखें। 8079

यह पुस्तक वितरित न की जाय
NOT TO BE ISSUED

सन्दर्भ ग्रन्थ
REFERENCE BOOK

स्टाक प्रमाणीकरण १९८४-१९८५

REGISTERED No. BG. 315

PROCEEDINGS
OF THE
INDIAN ACADEMY
OF SCIENCES

VOL. LV] *SECTION A* [No. 5

8079

MAY 1962

CHECKED 1973
Initial

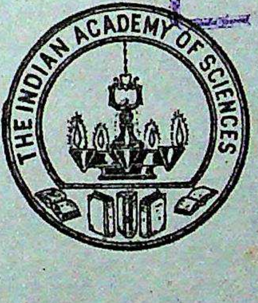

Price Rs. 4 or 6 Sh. *Annual Subscription Rs. 36*

IMPORTANT

Notice to the Subscribers of the "Proceedings of the Indian Academy of Sciences"

As from 1st January 1962, the following subscription prices for the *Proceedings of the Indian Academy of Sciences* will come into effect:—

Annual Subscription Rates

	Sections A & B	Section A	Section B
Inland ..	Rs. 72 00 nP.	Rs. 36 00 nP.	Rs. 36 00 nP.
Foreign ..	$ 18 00 cts. or £ 6-0-0	$ 9 00 cts. or £ 3-0-0	$ 9 00 cts. or £ 3-0-0

The *Proceedings of the Indian Academy of Sciences*, a monthly, which commenced its publication in July 1934 in two Sections, A and B, comprising of papers in physical and biological sciences respectively, has since then maintained an unbroken record of punctual issue on the last date of every month. Two volumes in each Section are issued every year and the 55th volume is now running. Each volume contains between pages 350 to 400 of text, 15 to 20 full-page plates and a large number of figures in the text. The *Proceedings* embody the results of the scientific research of the highest quality carried out in India.

The subscription price, which was originally fixed in July 1934, has remained unaltered all these years. The printing costs have progressively increased and are at present nearly three times the original ones. It has therefore become inevitable that the subscription rates are enhanced to enable the *Proceedings* to continue to offer to our subscribers the same volume of material and the same quality of paper, printing and illustrations as at present.

PRINTED AT THE BANGALORE PRESS, BANGALORE CITY, BY T. K. BALAKRISHNAN,
SUPERINTENDENT, AND PUBLISHED BY THE INDIAN ACADEMY OF
SCIENCES, BANGALORE

112120

112120

THE MANY ELECTRON WAVE EQUATION IN THE SCHRÖDINGER-PAULI FORM

By K. S. Viswanathan, F.A.Sc.
(*National Aeronautical Laboratory, Bangalore-1*)

Received January 20, 1962

I. Introduction

A generalisation of the Dirac equation for systems containing many electrons will find its applications in several branches of physics and will be of use especially in calculating the relativistic effects in many electron systems as well as in understanding precisely chemical binding and spins in complex molecular systems. It was shown in an earlier paper[1] that by considering a four vector whose components denote respectively the three components of the total momentum and the total energy of a dynamical system, one can obtain a generalisation of the Dirac equation. For a single electron moving in a field, the magnitude of the momentum four vector is equal to *imc*, *m* being the rest mass of the particle, and the magnitude can also be expressed as $\sum_{\mu=1}^{4} \gamma_\mu [P_\mu + (e/c) A_\mu]$ where the γ's are four-dimensional matrices satisfying the relations $\gamma_\mu\gamma_\nu + \gamma_\nu\gamma_\mu = 2\delta\mu\nu$. Equating these two expressions and making them operate on the state vector $|\Psi\rangle$, one obtains an alternative elegant method of deriving the Dirac equation. It therefore appears obvious that a natural generalisation of the Dirac equation should proceed from a consideration of the magnitude of the *total momentum* four vector whose components (three momenta and the energy of the system) represent quantities of utmost physical significance. Such an equation involves no approximation, and it was further shown that a representation of the generalised Dirac equation in the product space of the electrons leads to equation (1) of the present paper which is a generalisation of the Breit equation for systems containing two electrons.

Equation (1) is correct to terms of the order (v^2/c^2), and includes the retardation effects arising from the fact that the velocity of propagation of interactions is finite in relativity theory and is equal to the velocity of light. The matrices α are of order 4^N, and the wave function Ψ has also got 4^N components. Of these, only 2^N components have large values, the rest being small. For two electron systems, Breit[2,3] has earlier obtained an equation satisfied by the four large components, which involves the Pauli matrices only. It is the object of the present paper to generalise Breit's reduced equation for many electron systems, and to derive an equation in the 2^N large components of the wave equation by eliminating all the remaining small components from equation (1).

II. THE WAVE EQUATION

It has been shown in a previous paper that the many electron wave equation can be written as

$$\left\{\left(\mathrm{P}_0 + \frac{e}{c}\mathrm{A}_0\right) + \sum_{i=1}^{N}\sum_{k=1}^{3} \alpha_k{}^i \mathrm{P}_k{}^i + mc\left(\sum_{i=1}^{N}\beta^i\right)\right.$$
$$\left. + \frac{e^2}{2c}\left[\sum_{\substack{ij\\ i<j}} \frac{\alpha^i\cdot\alpha^j}{r_{ij}} + \sum_{\substack{ij\\ i<j}} \frac{(\alpha^i\cdot r_{ij})\,(\alpha^j\cdot r_{ij})}{r^3{}_{ij}}\right]\right\}\Psi = 0 \qquad (1)$$

where

$$\mathrm{P}_0 = \frac{i\hbar}{c}\frac{\partial}{\partial t};$$

$$\mathrm{P}_k{}^i = -\,i\hbar\frac{\partial}{\partial x_k{}^i}; \qquad (2)$$

$$\alpha_k{}^i = \mathrm{I}_4 \times \mathrm{I}_4 \times \cdots \times \alpha_k \times \mathrm{I}_4 \cdots \times \mathrm{I}_4;$$
$$\beta^i = \mathrm{I}_4 \times \mathrm{I}_4 \times \cdots \times \beta \times \mathrm{I}_4 \cdots \times \mathrm{I}_4. \qquad (3)$$

In the above, the upper suffix i corresponds to the i-th electron, and $(x_1{}^i,\ x_2{}^i,\ x_3{}^i)$ denote the co-ordinates of the i-th electron. I_4 denotes the unit matrix of order four, and α_1, α_2, α_3 and β have the representations (1) of Appendix I. Further in (3), α_k and β occur in the i-th place and the × denotes direct product multiplication. Since the direct product of two square matrices of orders m and n is of order mn, $\alpha_k{}^i$ and β^i are of order 4^N. The wave function Ψ has consequently 4^N components, and we denote a general component by $\psi_{i_1 i_2 \ldots i_N}$ where i_1, i_2, $\cdots$ i_N are integers which assume one of the values 1, 2, 3 or 4. These suffixes signify the four different spin states of the electrons 1, 2, $\cdots$ N respectively.

If the electrons are moving in an external electric field U then A_0 is given by

$$\mathrm{A}_0 = \sum_{i=1}^{N}\mathrm{U}(r_i) - \sum_{i<j}\frac{e}{r_{ij}}. \qquad (4)$$

Equation (1) was derived on the assumption that the electrons are moving in an electric field only; when a magnetic field is present, we have for P_k^i the following expression.

$$P_k^i = -i\hbar \frac{\partial}{\partial x_k^i} + \frac{e}{c} A_k^i \tag{2 a}$$

where A_k^i ($k = 1, 2, 3$) are the components of the vector potential for the i-th electron.

Now

$$\dot{x}_k^i = [x_k^i, H] \tag{5}$$

where

$$H = -c \left\{ \frac{e}{c} A_0 + \sum_{i=1}^{3} \sum_{k=1}^{3} \alpha_k^i P_k^i + mc \sum_{i=1}^{N} \beta^i \right.$$

$$\left. + \frac{e^2}{2c} \sum_{i<j} \left[\frac{\alpha^i \cdot \alpha^j}{r_{ij}} + \frac{(\alpha^i \cdot r_{ij})(\alpha^j \cdot r_{ij})}{r_{ij}^3} \right] \right\}. \tag{6}$$

Further A_0, A_1, A_2, A_3 are functions of the positions of the particles or the interelectronic distances and do not involve the momenta. Hence x_k^i commutes with them. Again

$$[x_k^i, P_s^m] = \delta_{im}\delta_{ks} \tag{7}$$

so that

$$\left[x_k^i, \sum_i \sum_k \alpha_k^i P_k^i \right] = \alpha_k^i. \tag{8}$$

Hence

$$\dot{x}_k^i = -c\alpha_k^i \tag{9}$$

or

$$v^i = -c\alpha^i.$$

Thus the matrices α^i represent the velocities of the particles as in the one electron theory.

III. FIRST APPROXIMATION

Let us consider the t-th component of the wave equation where

$$t = \sum_{r=1}^{N} (i_r - 1)\, 4^{N-r}. \tag{10}$$

The t-th component of

$$\left(P_0 + \frac{e}{c} A_0\right) \Psi \text{ is obviously}$$

$$\left(P_0 + \frac{e}{c} A_0\right) \psi_{i_1 i_2 \ldots i_N}.$$

Now β is a diagonal matrix with $+1$ along the first two diagonal elements and -1 along the last two diagonal elements. Thus

$$\begin{aligned}(\beta^r \Psi)_{i_1 i_2 \ldots i_N} &= \sum_{i_1' \ldots i_N'} (I_4)_{i_1 i_1'} (I_4)_{i_2 i_2'} \cdots (\beta)_{i_r i_r'} \cdots (I_4)_{i_N i_N'} \psi_{i_1' \ldots i_N'} \\ &= \sum_{i_1' \ldots i_N'} \delta_{i_1 i_1'} \delta_{i_2 i_2'} \cdots (\beta)_{i_r i_r'} \cdots \delta_{i_N i_N'} \psi_{i_1' \ldots i_N'} \\ &= \sum_{i_r'} (\beta)_{i_r i_r'} \psi_{i_1 \ldots i_r' \ldots i_N} = \epsilon_r \psi_{i_1 \ldots i_N}\end{aligned} \tag{11}$$

where $\epsilon_r = +1$ if $i_r = 1$ or 2, and is equal to -1 if $i_r = 3$ or 4. Thus

$$(mc \Sigma \beta^r \Psi)_{i_1 \ldots i_N} = mc \left(\sum_{r=1}^{N} \epsilon_r \right) \psi_{i_1 \ldots i_N}. \tag{12}$$

The maximum value of $\Sigma \epsilon_r$ is equal to N and this happens when all the i_r's have the values 1 or 2. Similarly when $i_1, i_2, \cdots i_N$ all assume one of the values 3 or 4, we reach the other extreme value of $\sum_{r=1}^{N} \epsilon_r$ which is equal to $-$N. The sum $\Sigma \epsilon_r$ takes the $(N+1)$ values N, $(N-2), \cdots -N$ depending on the values of the indices $i_1, i_2, \cdots i_N$.

In the sequel, we shall use the indices $s_1, s_2, \cdots s_N$ to denote the numbers 1 or 2 and the indices $l_1, l_2, \cdots l_N$ to denote the numbers 3 or 4. A general component of the wave function has the form $\psi_{s_1 s_2 \ldots l_r \ldots l_N}$. There are 2^N components (the large components) of the type $\psi_{l_1 l_2 \ldots l_N}$ with all the indices having the value 3 or 4; $\binom{N}{1} 2^N$ components of the form $\psi_{l_1 l_2 \ldots s_r \ldots l_N}$

in which on index (s_r) is *small* and the rest are all large; and finally $\binom{N}{N}2^N$ components of the form $\psi_{s_1\ldots s_N}$ with all indices small.

Now in the first approximation,

$$\left(P_0 + \frac{e}{c}A_0\right) \sim Nmc.$$

We have seen that the minimum value of $mc\,\Sigma\,\epsilon_r$ occurs when all the i_r's take the values 3 or 4, and this is equal to $-$ N*mc*. Thus

$$\left[\left(P_0 + \frac{e}{c}A_0 + mc\sum_{r=1}^{N}\beta^r\right)\Psi\right]_{l_1\ldots l_N} = 0$$

in the first approximation. The components $\psi_{l_1\ldots l_N}$ in which all the indices have the value 3 or 4 are therefore large. Consider now the component ($l_1, l_2, \cdots s_r, \cdots l_N$) of the wave equation, in which one index corresponding to the r-th electron is small and the rest are all large. In this case $mc\sum_{r=1}^{N}\epsilon_r$ is equal to $-(N-2)\,mc$. The last term in the square bracket in (1) is of one order higher than the rest and we shall neglect it for the time being. We have seen in the appendix that the effect of α^r on a component ($i_1, i_2, \cdots s_r, \cdots i_N$) is to transform it into the component ($i_1, i_2, \cdots l_r, \cdots i_N$) whose r-th index is a large one and conversely. α^r thus changes l_r into s_r, and s_r into l_r. Thus $(\alpha_k{}^r\Psi)_{l_1l_2\ldots s_r l\ldots l_N}$ is a large component. It can be seen from equation (21) that all the $\binom{N}{1}2^N$ components of the type $\psi_{l_1l_2\ldots s_r\ldots l_N}$ with only one small index are of the order (v/c). In general, a component with m small indices is of order $(v/c)^m$.

Now $(\alpha_k{}^i\Psi)_{l_1\ldots s_r\ldots l_N}$ ($i \neq r$) is a component which has two indices (the i-th and the r-th ones), small and hence is of the order $(v/c)^2$. On the contrary $(\alpha_k{}^r\Psi)_{l_1\ldots s_r\ldots l_N}$ is a large component. Thus from (14) of appendix, we see that correct to terms of the order (v/c),

$$\left\{P_0 + \frac{e}{c}A_0 - (N-2)\,mc\right)\psi_{l_1l_2\ldots s_r\ldots l_N} + (P^r\sigma^r\Psi)_{l_1\ldots(s_r+2)\ldots l_N} = 0 \tag{13}$$

where

$$\sigma^r = I_2 \times I_2 \times \cdots \times \sigma \times \cdots I_2. \tag{14}$$

In the above matrix product, we follow the convention that the elements of I_2 as well as σ are numbered as 3 and 4 instead of as 1 and 2 as is usually done. If we set

$$\left(P_0 + \frac{e}{c} A_0\right) = Nmc$$

in equation (13) we get to a first approximation that*

$$\psi_{l_1 l_2 \ldots s_r \ldots l_N} = - \frac{1}{2mc} (P^r \sigma^r \Psi)_{l_1 l_2 \ldots (s_r+2) \ldots l_N} \tag{15}$$

IV. SECOND APPROXIMATION

Consider now the $(l_1, l_2, \cdots s_a, \cdots s_b, \cdots l_N)$-th component of the wave equation (1). In this, two suffixes s_a and s_b are small and the rest are all large. Hence $mc \Sigma \epsilon_r = -(N-4) mc$ and thus

$$\left(P_0 + \frac{e}{c} A_0\right) + mc \sum \epsilon_r \sim 4mc.$$

Now $(\alpha_k{}^i \Psi)_{l_1 \ldots s_a \ldots s_b \ldots l_N}$ is equal to a component which involves three small indices, namely i, a and b and is therefore of the order $(v/c)^3$. We are here striving for an approximation of the order $(v/c)^2$ only and hence $(4mc)^{-1} (\alpha_k{}^i \Psi)_{l_1 \ldots s_a \ldots s_b \ldots l_N}$ which is of the order $(v/c)^4$ can be neglected. Similarly

$$(4mc)^{-1} \frac{e^2}{cr} (\alpha^i \cdot \alpha^j \Psi)_{l_1 \ldots s_a \ldots s_b \ldots l_N} \quad (i,\ j \neq a,\ b)$$

involves four small indices and hence is of the order $(v/c)^6$. Again

$$\frac{1}{4mc} \frac{e^2}{cr} (\alpha^a \cdot \alpha^j \Psi)_{l_1 \ldots s_a \ldots s_b \ldots l_N} \quad (j \neq b)$$

is of the order $(v/c)^4$ and hence can be neglected. Hence the only term in the second summation which is of the order $(v/c)^2$ corresponds to the case for which $i, j = a, b$. Thus correct to terms of the order $(v/c)^2$, we have

$$\left[\left\{P_0 + \frac{e}{c} A_0 - (N-4) mc + \sum_{k=1}^{3} (\alpha_k{}^a P_k{}^a + \alpha_k{}^b P_k{}^b) + \frac{e^2}{2c}\left(\frac{\alpha^a . \alpha^b}{r_{ab}} + \frac{(\alpha^a . r_{ab})\ (\alpha^b . r_{ab})}{r^3{}_{ab}}\right)\right\} \Psi \right]_{l_1 l_2 \ldots s_a \ldots s_b \ldots l_N} = 0. \tag{16}$$

---

* The representations for σ_i used by Breit are the negative of the Pauli matrices and there will be thus a difference in sign in all terms that depend linearly on σ between the results of Breit's paper and the present one, when the latter are reduced to two electron systems.

Now

$$\begin{aligned}(\alpha_k{}^a\Psi)_{l_1 l_2 \ldots s_a \ldots s_b \ldots l_N} &= \sum_{l_a=3}^{4} (\sigma_k)_{s_a+2,\, l_a}\, \psi_{l_1 l_2 \ldots l_a \ldots s_b \ldots l_N} \\ &= -\frac{1}{2mc} \sum_{l_a=3}^{4} (\sigma_k)_{s_a+2,\, l_a} (\mathbf{P}^b \boldsymbol{\sigma}^b \Psi)_{l_1 l_2 \ldots (s_b+2) \ldots l_N} \text{ from (15).}\end{aligned}$$

Thus

$$\sum_{k=1}^{3} (\alpha_k{}^a \mathrm{P}_k{}^a \Psi)_{l_1 l_2 \ldots s_a \ldots s_b \ldots l_N} = -\frac{1}{2mc} (\mathbf{P}^a \boldsymbol{\sigma}^a)(\mathbf{P}^b \boldsymbol{\sigma}^b \Psi)_{l_1 l_2 \ldots (s_a+2) \ldots (s_b+2) \ldots l_N}. \tag{17 a}$$

Similarly

$$\sum_{k} (\alpha_k{}^b \mathrm{P}_k{}^b \Psi)_{l_1 l_2 \ldots s_a \ldots s_b \ldots l_N} = -\frac{1}{2mc} (\mathbf{P}^b \boldsymbol{\sigma}^b)(\mathbf{P}^a \boldsymbol{\sigma}^a \Psi)_{l_1 l_2 \ldots (s_a+2) \ldots (s_b+2) \ldots l_N}. \tag{17 b}$$

From equation (13) (Appendix) it follows that

$$\begin{aligned}(\alpha_k{}^a \alpha_l{}^b \Psi)_{l_1 l_2 \ldots s_a \ldots s_b \ldots l_N} &= \sum_{i_a} \sum_{i_b} (\alpha_k)_{s_a i_a} (\alpha_l)_{s_b i_b}\, \psi_{l_1 l_2 \ldots i_a \ldots i_b \ldots l_N} \\ &= \sum_{l_a} \sum_{l_b} (\sigma_k)_{s_a+2,\, l_a} (\sigma_l)_{s_b+2,\, l_b}\, \psi_{l_1 \ldots l_a \ldots l_b \ldots l_N} \\ &= (\sigma_k{}^a \sigma_l{}^b \Psi)_{l_1 l_2 \ldots (s_a+2) \ldots (s_b+2) \ldots l_N}. \end{aligned} \tag{18}$$

Thus

$$\left[\left(\frac{\boldsymbol{\alpha}^a . \boldsymbol{\alpha}^b}{r_{ab}} + \frac{(\boldsymbol{\alpha}^a \cdot \boldsymbol{r}_{ab})(\boldsymbol{\alpha}^b . \boldsymbol{r}_{ab})}{r_{ab}{}^3}\right)\Psi\right]_{l_1 l_2 \ldots s_a \ldots s_b \ldots l_N} = \left[\left(\frac{\boldsymbol{\sigma}^a \cdot \boldsymbol{\sigma}^b}{r_{ab}} + \frac{(\boldsymbol{\sigma}^a . \boldsymbol{r}_{ab})(\boldsymbol{\sigma}^b . \boldsymbol{r}_{ab})}{r_{ab}{}^3}\right)\Psi\right]_{l_1 \ldots s_a+2 \ldots s_b+2 \ldots l_N}. \tag{19}$$

Hence setting

$$\mathrm{P}_0 + \frac{e}{c}\,\mathrm{A}_0 = \mathrm{N}mc$$

in (16), we get by virtue of (17) and (19) that

$$\begin{aligned}\psi_{l_1\ldots s_a\ldots s_b\ldots l_N} &= \frac{1}{4m^2c^2}\,(\mathbf{P}^a\boldsymbol{\sigma}^a)\,(\mathbf{P}^b\boldsymbol{\sigma}^b\Psi)_{l_1\ldots s_a+2\ldots s_b+2\ldots l_N}\\ &\quad - \frac{e^2}{8mc^2}\left[\frac{\boldsymbol{\sigma}^a.\boldsymbol{\sigma}^b}{r_{ab}}\,\Psi + \frac{(\boldsymbol{\sigma}^a\cdot\boldsymbol{r}_{ab})\,(\boldsymbol{\sigma}^b\cdot\boldsymbol{r}_{ab})}{r_{ab}{}^3}\,\Psi\right]_{l_1\ldots s_a+2\ldots s_b+2\ldots l_N}. \qquad (20)\end{aligned}$$

Next the $(l_1 l_2 \cdots s_a \cdots l_N)$-th component of the wave equation correct to terms of the order v^2/c^2 is given by

$$\begin{aligned}&\left\{\mathrm{P}_0 + \frac{e}{c}\,\mathrm{A}_0 - (\mathrm{N}-2)\,mc\right\}\psi_{l_1\ldots s_a\ldots l_N}\\ &+ \sum_i{}' \sum_k (\alpha_k{}^i\mathrm{P}_k{}^i\Psi)_{l_1\ldots s_a\ldots l_N} + \left[\sum_{k=1} \alpha_k{}^a\mathrm{P}_k{}^a\Psi\right.\\ &\left. + \frac{e^2}{2c}\sum_{\substack{j\\ j\neq a}}{}' \left\{\frac{\boldsymbol{\alpha}^a.\boldsymbol{\alpha}^j}{r_{aj}} + \frac{(\boldsymbol{\alpha}^a.\boldsymbol{r}_{aj})\,(\boldsymbol{\alpha}^j.\boldsymbol{r}_{aj})}{r_{aj}{}^3}\right\}\Psi\right]_{l_1\ldots s_a\ldots l_N} = 0. \qquad (21)\end{aligned}$$

Now by the application of equation (20) and of (8), (Appendix), it can be seen that

$$\begin{aligned}&\left(\sum_k \alpha_k{}^i\mathrm{P}_k{}^i\Psi\right)_{l_1\ldots s_a\ldots l_N}\\ &= (\boldsymbol{\sigma}^i\mathbf{P}^i)\left[\frac{1}{4m^2c^2}\,(\mathbf{P}^a\boldsymbol{\sigma}^a)\,(\mathbf{P}^i\boldsymbol{\sigma}^i)\,\Psi\right.\\ &\qquad\left. - \frac{e^2}{8mc^2}\left\{\frac{\boldsymbol{\sigma}^a.\boldsymbol{\sigma}^i}{r_{ia}} + \frac{(\boldsymbol{\sigma}^a.\boldsymbol{r}_{ia})\,(\boldsymbol{\sigma}^i.\boldsymbol{r}_{ia})}{r_{ia}{}^3}\right\}\Psi\right]_{l_1\ldots s_a+2\ldots l_N}. \qquad (22)\end{aligned}$$

Again

$$\left[\frac{\alpha^{a}\cdot\alpha^{j}}{r_{aj}}+\frac{(\alpha^{a}\cdot r_{aj})(\alpha^{j}\cdot r_{aj})}{r_{aj}^{3}}\right]_{l_1\ldots s_a\ldots l_N}$$

$$=-\frac{1}{2mc}\left\{\frac{\sigma^{a}\cdot\sigma^{j}}{r_{aj}}+\frac{(\sigma^{a}\cdot r_{aj})(\sigma^{j}\cdot r_{aj})}{r_{aj}^{3}}\right\}(\sigma^{j}\mathbf{P}^{j}\Psi)_{l_1\ldots(s_a+2)\ldots l_N}. \tag{23}$$

Thus substituting (22) and (23) in (21) we get

$$(2mc+f)\,\psi_{l_1\ldots s_a\ldots l_N}+(\mathbf{P}^{a}\sigma^{a}\Psi)_{l_1\ldots(s_a+2)\ldots l_N}+\sum_{i\neq a}{}'(\sigma^{i}\mathbf{P}^{i})$$

$$\times\left[\frac{1}{4m^{2}c^{2}}(\mathbf{P}^{a}\sigma^{a})(\mathbf{P}^{i}\sigma^{i})\Psi-\frac{e^{2}}{8mc^{2}}\left\{\frac{\sigma^{a}\cdot\sigma^{i}}{r_{ia}}\right.\right.$$

$$\left.\left.+\frac{(\sigma^{a}\cdot r_{ia})(\sigma^{i}\cdot r_{ia})}{r_{ia}^{3}}\right\}\Psi\right]_{l_1\ldots s_a+2\ldots l_N}-\frac{e^{2}}{4mc^{2}}\sum_{j}{}'\left\{\frac{\sigma^{a}\cdot\sigma^{j}}{r_{aj}}\right.$$

$$\left.+\frac{(\sigma^{a}\cdot r_{aj})(\sigma^{j}\cdot r_{aj})}{r_{aj}^{3}}\right\}(\sigma^{j}\mathbf{P}^{j}\Psi)_{l_1\ldots s_a+2\ldots l_N}=0 \tag{24}$$

where we have written

$$\mathrm{P}_0+\frac{e}{c}\mathrm{A}_0=\mathrm{N}mc+f. \tag{25}$$

Hence we have

$$\psi_{l_1 l_2\ldots s_a\ldots l_N}=-(2mc+f)^{-1}(\mathrm{F}_a\Psi)_{l_1\ldots(s_a+2)\ldots l_N} \tag{26}$$

where

$$\mathrm{F}_a=\left[(\mathbf{P}^{a}\sigma^{a})+\sum_{i}{}'(\mathrm{P}^{i}\sigma^{i})\left\{\frac{1}{4m^{2}c^{2}}(\mathbf{P}^{i}\sigma^{i})(\mathrm{P}^{a}\sigma^{a})\right.\right.$$

$$\left.-\frac{e^{2}}{8mc^{2}}\left(\frac{\sigma^{a}\cdot\sigma^{i}}{r_{ia}}+\frac{(\sigma^{a}\cdot r_{ia})(\sigma^{i}\cdot r_{ia})}{r^{3}_{ia}}\right)\right\}$$

$$\left.-\frac{e^{2}}{4mc^{2}}\sum_{j}{}'\left\{\frac{\sigma^{a}\cdot\sigma^{j}}{r_{ia}}+\frac{(\sigma^{a}\cdot r_{aj})(\sigma^{j}\cdot r_{aj})}{r_{aj}^{3}}\right\}(\sigma^{j}\mathbf{P}^{j})\right]. \tag{27}$$

Finally on making use of (18) and (23), we find that the $(l_1, l_2 \cdots l_N)$-th component of the wave equation is given by

$$\Bigg[\left(\mathrm{P}_0 + \frac{e}{c}\mathrm{A}_0 - \mathrm{N}mc\right)\Psi - \sum_{a=1}^{\mathrm{N}} (\sigma^a \mathrm{P}^a)\,(2mc + f)^{-1}\,\mathrm{F}_a \Psi$$

$$+ \frac{e^2}{2c} \sum_{\substack{ij \\ i<j}} \left(\frac{\sigma^i . \sigma^j}{r_{ij}} + \frac{(\sigma^i . r_{ij})\,(\sigma^j . r_{ij})}{{r_{ij}}^3}\right) \Big\{ \frac{1}{4m^2c^2} (\sigma^i \mathbf{P}^i)\;(\sigma^j \mathbf{P}^j)$$

$$- \frac{e^2}{8mc^2}\left(\frac{\sigma^i . \sigma^j}{r_{ij}} + \frac{(\sigma^i . r_{ij})(\sigma^j . r_{ij})}{{r_{ij}}^3}\right)\Big\}\,\Psi\,\Bigg]_{l_1 \ldots l_N} = 0. \tag{28}$$

Equation (28) does not involve any small components and is thus the reduced equation in the large components that we are seeking. It is, however, not in its simplest form since it involves products of the spin matrices. Though the spin matrices have representations of order 2^N, it is easy to see that the components of the spin of any electron satisfy the same commutation rules as those associated with the Pauli matrices; the spin matrices corresponding to the different particles of course commute with each other. Again in simplifying equation (28), the following results, which represent a small change in indices of the equations (46), (47) of Breit's paper, can be made use of:

If

$$\mathrm{X}_{ij} = \frac{\sigma^i . \sigma^j}{r_{ij}} + \frac{(\sigma^i . r_{ij})\,(\sigma^j . r_{ij})}{{r_{ij}}^3},$$

then

$${\mathrm{X}_{ij}}^2 = \frac{(6 - 4\sigma^i . \sigma^j)}{{r_{ij}}^2} + 2\,\frac{(\sigma^i . r_{ij})(\sigma^j . r_{ij})}{{r_{ij}}^4} \tag{29 a}$$

$$\frac{e^2}{8m^2c^3}\,[(\mathbf{P}^i\sigma^i)\,(\mathbf{P}^j\sigma^j)\,\mathrm{X}_{ij} + (\mathbf{P}^i\sigma^i)\,\mathrm{X}_{ij}\,(\mathbf{P}^j\sigma^j) + (\mathbf{P}^j\sigma^j)\,\mathrm{X}_{ij}\,(\mathbf{P}^i\sigma^i)$$

$$+ \mathrm{X}_{ij}\,(\mathbf{P}^i\sigma^i)\,(\mathbf{P}^j\sigma^j)]$$

$$= \frac{e^2}{2m^2c^3}\left[{r_{ij}}^{-1}\,(\mathbf{P}^i\mathbf{P}^j) + \sum_k \sum_l ({x_k}^i - {x_k}^j)\,({x_l}^i - {x_l}^j)\,\mathbf{P}_k{}^i\mathbf{P}_l{}^j\right]$$

$$+ \frac{e^2}{8m^2c^3} \langle (\mathbf{P}^i\sigma^i)\, (\mathbf{P}^j\sigma^j)\, \mathrm{X}_{ij} \rangle$$

$$+ \left(\frac{e^2{}_i}{2m^2c^3}\right) \{\langle \mathbf{P}^i r_{ij}^{-1} \rangle \times \mathbf{P}^j . \sigma^i + \langle \mathbf{P}^j r_{ij}^{-1} \rangle \times \mathbf{P}^i . \sigma^j\}. \quad (29\,b)$$

Again

$$\frac{1}{4m^2c^2} (\mathbf{P}^a\sigma^a)\, (2mc + f)^{-1}\, (\mathbf{P}^i\sigma^i)^2\, (\mathbf{P}^a\sigma^a)$$

$$= \frac{1}{8m^3c^3} (\mathbf{P}^a)^2\, (\mathbf{P}^i)^2. \quad (29\,c)$$

The second term in the right-hand side of the (29 *b*) contains singularities at $r_{ij} = 0$, and its behaviour at this point needs to be investigated carefully. For example making use of the relation

$$(a\sigma)\, (b\sigma) = (ab) + i\, (a \times b)\, .\, \sigma,$$

we have

$$\left(\frac{e^2}{8m^2c^3}\right) (\mathbf{P}^i\sigma^i)\, (\mathbf{P}^j\sigma^j)\, (\sigma^i\sigma^j)\, r_{ij}^{-1}$$

$$= \frac{e^2}{8m^2c^3} \{(\mathbf{P}^i\mathbf{P}^j)\, (1 - \sigma^i . \sigma^j) - i\, (\mathbf{P}^i \times \mathbf{P}^j)\, .\, (\sigma^i - \sigma^j)$$

$$+ (\mathbf{P}^i\sigma^j)\, (\mathbf{P}^j\sigma^i)\}\, r_{ij}^{-1}.$$

In view of the presence of the factor $(e^2/8m^2c^3)$, we can neglect $(e/c)\, \mathrm{A}_i$ in $\mathbf{P}^i$ in the above term and write $\mathbf{P}_i = -i\hbar \nabla_i$. Further, $\nabla_j = -\nabla_i$, as far as the effect of these operators on r_{ij}^{-1} is concerned, and thus $(\mathbf{P}^i\mathbf{P}^j)\, r_{ij}^{-1} = -4\pi\hbar^2 \delta\, (r_{ij})$. The behaviour of the term $\langle (\mathrm{P}^i\sigma^i)\, (\mathrm{P}^j\sigma^j)\, \mathrm{X}_{ij} \rangle$ at the singular point has been investigated by Sucher and Foley, and by making use of their result, we can write

$$\langle (\mathbf{P}^i\sigma^i)\, (\mathbf{P}^j\sigma^j)\, \mathrm{X}_{ij} \rangle = \mathrm{H}_{sp.}{}^{ij}$$

$$= -2\hbar^2 \left\{ \frac{1}{r_{ij}{}^3} \left[(\sigma^i . \sigma^j) - 3\, \frac{(\sigma^i r_{ij})\, (\sigma^j r_{ij})}{r_{ij}{}^2} \right]' - \frac{8\pi}{3} (\sigma^i\sigma^j)\, \delta\, (r_{ij}) \right\} \quad (29\,d)$$

112120

where the dash indicates that in evaluating the first term one should exclude a small sphere surrounding the vector r_i. If E represents the energy of the system, and $V = A_0$, then

$$P_0 + \frac{e}{c} A_0 = \frac{E + eV}{c}$$

and hence

$$f = P_0 + \frac{e}{c} A_0 - Nmc = \frac{(E + eV - Nmc^2)}{c}. \tag{25 a}$$

We have finally

$$\sum_{a=1}^{N} (\sigma^a \mathbf{P}^a)(2mc + f)^{-1}(\sigma^a \mathbf{P}^a)$$

$$= \frac{1}{2mc}\left[\sum_{i=1}^{N} (\mathbf{P}^i)^2 + \frac{e\hbar}{c}\sum_{i=1}^{N} (\mathbf{H}^i \sigma^i)\right]$$

$$- \frac{1}{4m^2c^2}\sum_{i=1}^{N}\left\{\frac{(E + eV - Nmc^2)}{c}(\mathbf{P}^i)^2 - \frac{ie\hbar}{c}\mathbf{P}^i . \mathcal{E}^i\right.$$

$$\left. - \frac{e\hbar}{c}\mathcal{E}^i . \mathbf{P}^i . \sigma^i\right\} \tag{30}$$

where

$$\mathbf{H}^i = \text{curl } A^i \quad \text{and} \quad \mathcal{E}^i = - \text{grad}^i V.$$

Substituting the equations (29) to (30) in (28) and solving for $(E + eV - Nmc^2)$, we get after some simplification that

$$\left[\frac{(E + eV - Nmc^2)}{c} - \left(\frac{1}{2mc}\right)\sum_{i=1}^{N} (\mathbf{P}^i)^2 + \left(\frac{1}{8m^3c^3}\right)(\mathbf{P}^i)^4\right.$$

$$- \left(\frac{eh}{4\pi mc^2}\right)\sum_{i=1}^{N} (\sigma^i \mathbf{H}^i) - \left(\frac{eh}{8\pi m^2c^3}\right)\sum_{i} (i\mathbf{P}^i . \mathcal{E}^i + \mathcal{E}^i \times \mathbf{P}^i . \sigma^i)$$

$$+ \sum_{i<s} \Big\{ \Big(\frac{e^2}{2m^2c^3}\Big) \Big[r_{is}^{-1} (\mathbf{P}^i\mathbf{P}^s) + \sum_{jk} (x_j{}^i - x_j{}^s)(x_k{}^i - x_k{}^s)$$

$$\times \mathrm{P}_j{}^i \mathrm{P}_k{}^s \Big] - \Big(\frac{e^2\hbar^2}{4m^2c^3}\Big) \Big[\Big(\frac{\sigma^i . \sigma^s}{r_{is}{}^3} - 3 \frac{(\sigma^i r_{is})(\sigma^s r_{is})}{r_{is}{}^5} \Big)'$$

$$- \frac{8\pi}{3} (\sigma^i \sigma^j)\, \delta(r_{is}) \Big] + \Big(\frac{ie^2}{2m^2c^3}\Big) [\langle \mathbf{P}^i r_{is}{}^{-1} \rangle \times \mathbf{P}^s . \sigma^i$$

$$+ \langle \mathbf{P}^s r_{is}{}^{-1} \rangle \times \mathbf{P}^i . \sigma^s] - \Big(\frac{e^4}{16mc^3}\Big) \mathrm{X}^2{}_{is} \Big\} \Big] \Psi = 0. \tag{31}$$

In this equation the bracket ⟨ ⟩ indicates that the operators operate only within the ⟨ ⟩.

V. THE REDUCED EQUATION IN THE LARGE COMPONENTS

Equation (31) is what one obtains on reducing the wave equation (1) to its large components. In his investigations on the relativistic wave equation for two electron systems, Breit (1932) has discussed in detail the validity of the term $(e^4/16mc^3)\,\mathrm{X}^2{}_{12}$ (the last term in 31) which involves neither the momentum operator nor the Planck's constant. He came to the conclusion that the Breit equation yields results consistent with field theory for energy calculations provided the last term in it is taken into account to the first order by perturbation theory working with sixteen components. Such a calculation will lead to all the terms in (31) excepting the last sum involving the terms $(e^4/16mc^3)\ \mathrm{X}_{ij})^2$. Since the arguments of Breit on the validity of this sum are quite general and are not restricted to two-electron systems only, we shall not repeat them here and shall content ourselves with stating that the correct wave equation is the one obtained by leaving out the sum $(e^4/16mc^3) \sum_{ij} \mathrm{X}_{ij}{}^2$ in equation (31). If we set $\epsilon = \mathrm{E} - \mathrm{N}mc^2$, then ϵ denotes the observable energy of the system, as its rest energy is equal to $\mathrm{N}mc^2$. Thus the wave equation for many electron systems is given by

$$\Big\{ \epsilon - \sum_{i=1}^{\mathrm{N}} \frac{(\mathbf{P}^i)^2}{(2m)} + e\mathrm{V} + \Big(\frac{1}{8m^3c^2}\Big) \sum_{i=1}^{\mathrm{N}} (\mathbf{P}^i)^4$$

$$- \Big(\frac{e\hbar}{2mc}\Big) \sum_i (\sigma^i \mathbf{H}^i) - \Big[\Big(\frac{eh}{8\pi m^2c^2}\Big) \sum_i \mathcal{E}^i \times \mathbf{P}^i . \sigma^i$$

$$- \left(\frac{e^2h}{4\pi m^2c^2}\right) \sum_{i,s}{}' (\nabla^i r_{is}{}^{-1}) \times \mathbf{P}^s . \sigma^i \Bigg] - \left(\frac{ieh}{8\pi m^2c^2}\right) \sum_i \mathbf{P}^i . \mathcal{E}^i$$

$$+ \left(\frac{e^2}{2m^2c^2}\right) \sum_{i<s} \left[\frac{\mathbf{P}^i . \mathbf{P}^s}{r_{is}} + \sum_{jk} (x_j{}^i - x_j{}^s)(x_k{}^i - x_k{}^s) \mathrm{P}_j{}^i \mathrm{P}_k{}^s \right]$$

$$- \left(\frac{e^2\hbar^2}{4m^2c^2}\right) \sum_{i<s} \Bigg[\frac{1}{r_{is}{}^3} \left(\sigma^i . \sigma^s - 3\, \frac{(\sigma^i r_{is})(\sigma^s r_{is})}{r_{is}{}^2} \right)'$$

$$- \frac{8\pi}{3} (\sigma^i \sigma^s)\, \delta\,(r_{is}) \Bigg] \Bigg\} \Psi = 0. \qquad (32)$$

The first three terms in the above equation constitute the Schrödinger equation for many electron systems. The fourth and fifth terms give respectively the relativistic variation of mass with velocity and the interaction energy between the spins and the magnetic field acting on them. The sixth term in the square bracket gives the well-known spin-orbit coupling energy. The term

$$\frac{e^2h}{4\pi m^2c^2} (\nabla_i r_{is}{}^{-1}) \times \mathbf{P}^s . \sigma^i$$

can be interpreted as the energy of interaction of the spin of the i-th electron with the angular momentum of the s-th electron about the line joining these two particles. The seventh term is imaginary and does not lend itself easily to physical interpretation. It is characteristic of Dirac theory, and can also be written as

$$\sum + \frac{ieh}{8\pi m^2c^2} \mathcal{E}^i . \mathbf{P}^i,$$

and the expectation values of both the expressions will be equal as pointed out by Bethe and Salpeter. This term also involves singularities of the type $\delta\,(r_i)$ and $\delta\,(r_{ij})$. The last two terms give respectively the orbit-orbit and the spin-spin interactions.

We can replace $\mathbf{P}_i$ by its $- i\hbar \nabla_i$ in all terms of the equation (32) excepting the term $- \Sigma\,(\mathrm{P}_i{}^2/2m)$ and this term has the value

$$\sum \left\{ \frac{\hbar^2}{2m} \nabla_i{}^2 - \frac{e}{cm} \mathbf{A}^i . \mathbf{P}^i - \frac{e^2}{2mc^2} (\mathbf{A}^i)^2 \right\} .$$

One may notice that when there is no external magnetic field, the symmetry of the equation (31) is the same as that of the potential field V, and the wave function Ψ also will thus exhibit this symmetry.

VI. THE SPIN STATES

If the wave function Ψ is normalised so that $\int \Psi^* \Psi d\tau = 1$ where $d\tau = dx_1 \cdots dx_N$ denotes an element of volume in the configuration space and Ψ^* is the transpose of Ψ, then $\Psi^* \Psi d\tau$ can be interpreted as the probability of finding the electrons 1, 2 $\cdots$ N in the volume elements dx_1, dx_2, dx_N respectively. In particular, $\Psi^2{}_{33\cdots3}$ denotes the probability of finding all the electrons with parallel spins and of finding the electrons 1, 2 $\cdots$ N respectively in the volume elements $dx_1, \cdots dx_N$. Similarly $(\Sigma \psi^2{}_{l_1 l_2 \ldots l_N})$ where the summation covers all the components for which m out of the N numbers l_i have the value 3 and the rest the value 4, denotes the probability of finding m electrons with spins quantised along the positive direction of the z-axis and the remaining $(N - m)$ electrons with spins quantised in the opposite direction. The number of terms in the above summation is obviously

$$\binom{N}{m} = \frac{N!}{(N-m)!\,m!}.$$

Thus the number of terms contained in the probability distributions of finding N, (N $-$ 1) $\cdots$ 0 electrons having the positive spin are given by the different terms of the binomial expansion $(1+1)^N$. If N is even, obviously the term having the greatest value corresponds to the case for which $m = (N/2)$ or to the case wherein each electron finds its spin compensated by another electron of the opposite spin. It must however be borne in mind that in an approximation that ignores terms of the order (v^2/c^2), the wave function is an eigenfunction of S^2 and S_z, and thus the components which correspond to the solution of the Schrödinger equation will have the largest values; the other components can be expected to have the order of magnitude of the relativistic corrections.

Now to satisfy the Pauli Exclusion Principle, the wave function should be anti-symmetric with respect to an interchange of any two electrons. From (32) we see that the Hamiltonian remains invariant under any permutation of the space co-ordinates as well as the spin co-ordinates. Thus Pauli's Exclusion Principle will be satisfied if the components of Ψ satisfy the following relations :

$$\begin{aligned} &\psi_{l_1 \ldots l_i \ldots l \ldots l_N}(x_1 \cdots x_i \cdots x_j \cdots x_N) \\ &\quad = -\,\psi_{l_1 \ldots l_j \ldots l_i \ldots l_N}(x_1 \cdots x_j \cdots x_i \cdots x_N) \\ &\qquad\qquad (i, j = 1,\ 2, \cdots N). \end{aligned} \tag{33}$$

If $l_i = l_j$ or in other words if the spins of the i-th and the j-th electrons are the same, the function $\psi_{l_1 \ldots l_i \ldots l_j \ldots l_N}$ is anti-symmetric in the co-ordinates of these two electrons. Thus the Exclusion Principle demands that the components should be anti-symmetric with respect to the co-ordinates of all electrons that have the same spin, while they can behave as a mixture of symmetric and anti-symmetric functions as far as interchange of electrons with opposite spins are concerned. In both cases equations (33) give the conditions which Pauli's Exclusion Principle demands on the components of the wave function. As an example, the Heitler-London theory for the hydrogen molecule corresponds to the case for which the two anti-symmetric components ψ_{33} and ψ_{44} are identically equal to zero while ψ_{34} and ψ_{43} are taken as symmetric functions satisfying the relation $\psi_{34}(1, 2) = -\psi_{43}(2, 1)$.

The author's grateful thanks are due to Dr. P. Nilkantan, Director, National Aeronautical Laboratory, for his keen interest in this work and encouragement.

SUMMARY

The paper deals with the reduction of the generalised Dirac equation for a system containing N electrons to its 2^N large components. The wave equation for many electron systems has been derived in its Schrödinger-Pauli form, and this includes higher order relativistic effects such as the mass change of the particles with their velocities, the spin-orbit, the orbit-orbit and the spin-spin interactions. A few remarks are made on the physical interpretation of the components of the wave function and the relations which they should obey in order to satisfy the Pauli Exclusion Principle.

REFERENCES

1. Viswanathan, K. S. .. *Proc. Ind. Acad. Sci.*, 1960, **42**, 35.
2. Breit, G. .. *Phys. Rev.*, 1929, **34**, 553.
3. ———— .. *Ibid.*, 1932, **39**, 616.
4. Sucher, J. and Foley, H. .. *Ibid.*, 1954, **95**, 966.
5. Bethe, H. A. and Salpeter, E. E. *Handbuch der physik*, Springer—Verlag, Berlin, 1957, **35**.
6. Weyl, H. .. *The Theory of Groups and Quantum Mechanics*, Methuen & Company, Limited, 1931, pp. 90–91.

APPENDIX

If $(x_1, x_2, \cdots x_m)$ are components of a vector r in a vector space R of dimension m, and similarly if $(y_1, y_2, \cdots y_n)$ denote the components of a vector η in a vector space G of dimension n, then the direct product of $R \times G$ is of dimensions mn and is associated with the transformation properties of the vector $z = r \times \eta$ whose components are given by $z_l = z_{ik} = x_i y_k$ $(l = 1, 2, \cdots mn)$. With the linear correspondences A in R and B in G: $x'_{i'} = \sum_i a_{i'i} x_i$; $y'_{k'} = \sum_k b_{k'k} y_k$

is associated the linear correspondence $C = A \times B$ in the product space:

$$x'_{i'} y'_{k'} = \sum_{i,k} a_{i'i}\, b_{k'k} x_i\, y_k$$

or

$$z'_{l'} = \sum_l c_{l'l}\, z_l; \quad c_{l'l} = a_{i'i} b_{k'k} \tag{A}$$

if we associate the numbers l and l' with the pairs (ik) and $(i'k')$. For the sake of definiteness, we arrange the components $x_i y_k$ in such a way that a component $x_i y_k$ precedes another component $x_{i'} y_{k'}$ if $i < i'$, and when $i = i'$ if $k < k'$. The same convention will be adopted to evaluate the direct product of N matrices also. Thus a component $\psi_{i_1 i_2 \dots i_N}$ of the wave function will precede another component $\psi_{j_1 j_2 \dots j_N}$ if $i_1 < j_1$, and when $i_1 = j_1$; $i_2 = j_2$; $\cdots i_l = j_l$ then $\psi_{i_1 i_2 \dots i_N}$ precedes $\psi_{j_1 j_2 \dots j_N}$ if $i_{l+1} < j_{l+1}$. The matrices α_k and β are given by

$$\alpha_k = \begin{pmatrix} 0 & \sigma_k \\ \sigma_k & 0 \end{pmatrix}; \quad \beta = \begin{pmatrix} I_2 & 0 \\ 0 & -I_2 \end{pmatrix} \tag{1}$$

where σ_1, σ_2, σ_4 are the Pauli matrices and I_2 is the unit matrix of order 2. Further for the Pauli matrices, we choose the usual representations

$$\sigma_1 = \begin{pmatrix} 0 & 1 \\ 1 & 0 \end{pmatrix}; \quad \sigma_2 = \begin{pmatrix} 0 & -i \\ i & 0 \end{pmatrix}; \quad \sigma_3 = \begin{pmatrix} 1 & 0 \\ 0 & -1 \end{pmatrix} \tag{2}$$

Now if $A = (a_{ij})$ and $B = (b_{kl})$ are two square matrices of order m and n respectively, then the direct product can be represented as the partitioned matrix

$$A \times B = \begin{pmatrix} a_{11}B & a_{12}B & \cdots & a_{1m}B \\ a_{21}B & a_{22}B & \cdots & a_{2m}B \\ \cdots & \cdots & \cdots & \cdots \\ \cdots & \cdots & \cdots & \cdots \\ a_{m1}B & a_{m2}B & \cdots & a_{mm}B \end{pmatrix} \tag{3}$$

Further the direct product of i unit matrices of order four is a unit matrix of order 4^i. Hence from (3, section II) and (3), we see that $\alpha_k{}^i$ is given by a partitioned matrix of order 4^{i-1}; we have

$$\alpha_k{}^i = \begin{pmatrix} a_k{}^i & 0 & \cdots & 0 \\ 0 & a_k{}^i & \cdots & 0 \\ \cdots & \cdots & \cdots & \cdots \\ \cdots & \cdots & \cdots & \cdots \\ 0 & 0 & \cdots & a_k{}^i \end{pmatrix} \tag{4}$$

In the above, each element is a matrix of order 4^{N-i+1} and $a_k{}^i$ is given by the matrix

$$a_k{}^i = \begin{pmatrix} 0 & \sigma_k \times I_{N_i} \\ \sigma_k \times I_{N_i} & 0 \end{pmatrix} \tag{5}$$

where $N_i = 4^{N-i}$ and I_{N_i} is a unit matrix of order 4^{N-i}. Similarly β^i is given by the following partitioned diagonal matrix of order 4^{i-1}

$$\beta^i = \begin{pmatrix} b^i & 0 & \cdots & 0 \\ 0 & b^i & \cdots & 0 \\ \cdots & \cdots & \cdots & \cdots \\ \cdots & \cdots & \cdots & \cdots \\ 0 & 0 & \cdots & b^i \end{pmatrix} \tag{6}$$

where

$$b^i = \beta \times I_{N_i} = \begin{pmatrix} I_{N_i} & 0 & 0 & 0 \\ 0 & I_{N_i} & 0 & 0 \\ 0 & 0 & -I_{N_i} & 0 \\ 0 & 0 & 0 & -I_{N_i} \end{pmatrix}. \tag{7}$$

Now

$$\alpha_k{}^r = I_4 \times I_4 \times \cdots \times \alpha_k \times \cdots I_4.$$

From a generalisation of the equations (A) to N vectors, we see that

$$\begin{aligned} (\alpha_k{}^r \Psi)_{i_1 i_2 \ldots i_N} &= \sum_{i_1' \ldots i_N'} (I_4)_{i_1 i_1'} \cdots (\alpha_k)_{i_r i_r'} \cdots (I_4)_{i_N i_N'} \psi_{i_1' \ldots i_N'} \\ &= \sum_{i_1' \ldots i_N'} \delta_{i_1 i_1'} \cdots (\alpha_k)_{i_r i_r'} \cdots \delta_{i_N i_N'} \psi_{i_1' \ldots i_N'} \\ &= \sum_{i_r'} (\alpha_k)_{i_r i_r'} \psi_{i_1 i_2 \ldots i_r' \ldots i_N}. \end{aligned} \tag{8}$$

The same result could be proved with the aid of the matrix for α_k^r given by (4) but this is more tedious.

If $A_1, A_2, \cdots A_N$ and $B_1, B_2, \cdots B_N$ are matrices of the same order, then $(A\times A_1 \ \ (B\times B_1) = AB\times A_1B_1$. (9)

Hence applying the above result to one more matrix, we get

$$(A\times A_1\times A_2)\ (B\times B_1\times B_2) = [(A\times A_1)\ (B\times B_1)]\ \times A_2B_2$$
$$= \ AB\times A_1B_1\times A_2B_2$$

Thus $(A\times A_1 \cdots \times A_N)\ (B\times B_1\times \cdots B_N) = AB\times A_1B_1\times \cdots \times A_NB_N.$ (10)

Thus we find that

$$\alpha_k{}^r\alpha_l{}^s = I_4 \times I_4 \times \cdots \times \alpha_k \times \cdots \times \alpha_l \times \cdots I_4 \tag{11}$$

Again we find that the matrices $\alpha_k{}^r$ satisfy the commutation rules

$$\alpha_k{}^r\alpha_l{}^r + \alpha_l{}^r\alpha_k{}^r = 2\delta_{kl}. \tag{12}$$

From (11) we find that

$$\begin{aligned}(\alpha_k{}^r\alpha_l{}^s\Psi)_{i_1i_2\ldots i_N} &= \sum_{i'_1\ldots i_N'} (I_4)_{i_1i_1'}\cdots(\alpha_k)_{i_ri_r'}\cdots(\alpha_l)_{i_si_s'}\cdots(I_4)_{i_Ni_N'}\psi_{i_1'\ldots i_N'}\\ &= \sum_{i_1'\ldots i_N'} \delta_{i_1i_1'}\cdots(\alpha_k)_{i_ri_r'}\cdots(\alpha_l)_{i_si_s'}\cdots\delta_{i_Ni_N'}\psi_{i_1'\ldots i_N'}\\ &= \sum_{i_r'}\sum_{i_s'}(\alpha_k)_{i_ri_r'}(\alpha_l)_{i_si_s'}\psi_{i_1i_2\ldots i_r'\ldots i_s'\ldots i_N}.\end{aligned} \tag{13}$$

Now α_k is of the form $\begin{pmatrix}0 & \sigma_k\\ \sigma_k & 0\end{pmatrix}$ and thus if $i_r=1$ or 2, we have $(\alpha_k)_{i_ri_r'}=0$ for $i_r'=1$ or 2 and it is equal to $(\sigma_k)_{i_r(i_r-2)}$ for $i_r'=3$ or 4. Similarly when $i_r=3$ or 4, we have $(\alpha_k)_{i_ri_r'}=(\sigma_k)_{(i_r-2)i_r'}$ if $i_r'=1$ or 2, and is equal to zero if $i_r'=3$ or 4. Thus from (8) we see that the effect of $\alpha_k{}^r$ on Ψ is to transform a component $(i_1, i_2, \cdots i_r \cdots i_N)$ into another component $(i_1, i_2, \cdots i_r' \cdots i_N)$ whose r-th index is large if i_r is small and *vice versa*. In other words, if i_r is large (having the value 3 or 4) then α^r transforms it into a small one and conversely α^r transforms a component whose r-th index is small into a component whose r-th index is large.

If now we follow the convention that the row and column indices of the two-dimensional Pauli matrices be denoted by the numbers 3 and 4 instead of by 1 and 2, then it follows from (8) that

$$\begin{aligned}(\alpha_k{}^r\Psi)_{l_1l_2\ldots s_r\ldots l_N} &= \Sigma\,(\alpha_k)_{s_ri_r}\,\psi_{l_1l_2\ldots i_r\ldots l_N}\\ &= \sum_{l_r=3}^{4}(\sigma_k)_{(s_r+2)l_r}\,\psi_{l_1l_2\ldots l_r\ldots l_N}\\ &= (\sigma_k{}^r\Psi)_{l_1l_2\ldots(s_r+2)\ldots l_N}.\end{aligned} \tag{14}$$

DIAMAGNETIC BEHAVIOUR OF BINARY LIQUID MIXTURES

By R. Gopalakrishna

(*Department of Physics, Sri Venkateswara University, Tirupati*)

Received April 12, 1962

(Communicated by Dr. S. Ramachandra Rao, F.A.SC.)

INTRODUCTION

DIAMAGNETIC susceptibilities of a large number of liquid mixtures have been measured by different workers (Selwood, 1956) and attempts are made to fit them to Wiedemann's law. It has also been pointed out by some workers (Angus and Tilston, 1940 and 1947) that deviations from this ideal behaviour are traceable to probable sources of error in measurements. In the physics laboratories of Sri Venkateswara University, we are engaged in a detailed study of the thermodynamic behaviour of liquid mixtures. A part of these studies, the ultrasonic behaviour of liquid mixtures of triethylamine with a number of liquids, have been reported in a recent note (Reddy and Subrahmanyam, 1962). The present communication deals with the diamagnetic behaviour of 10 liquid mixtures with triethylamine as a common component. It has been possible to establish a considerable amount of similarity in the ultrasonic and magnetic behaviours of these mixtures.

EXPERIMENTAL

Mixtures were prepared by mixing weighed amounts of extra pure liquids. Densities of the mixtures were determined by the hydrostatic method. Magnetic susceptibilities were measured by the Gouy method. Effect of magnetic impurities were eliminated by standard methods from measurements made at different field strengths in the range 4,000 to 10,000 Gauss. As a result of care taken in maintaining the fields steady, it was possible to realise an accuracy better than 1 per cent. in the value of susceptibilities.

RESULTS AND DISCUSSION

In this series of measurements it was noticed that the measured value of the susceptibility of the mixture deviated considerably from the value expected on the basis of the linear law. In order to bring out the nature of these differences with greater clarity, the excess susceptibility, χ^E defined as the difference between the experimental value and the linear law value, is represented in Fig. 1 as a function of molar concentration n_2 of the second component, the molar concentration of the common component being n_1. It is seen from these curves that aniline and *o*-Nitrotoluene mixtures conform to the linear law. In all other cases the deviation can be expressed by an empirical formula

$$\chi^{E} / n_1 n_2 = A + B(n_1 - n_2) + C(n_1 - n_2)^2.$$

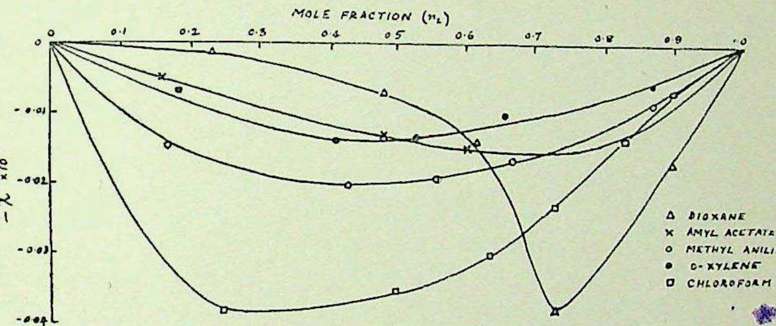

FIG. 1

The values of these constants are given in Table I.

TABLE I

Values of constants

System		A×10⁸	B×10⁸	C×10⁸
Triethylamine-pyridine	..	−10·00	14·20	−14·90
" -chloroform	..	−14·00	6·70	− 5·60
" -dioxane ..	..	− 3·20	17·10	21·40
" -diphenyl ether	..	−12·00	6·80	− 2·20
" -methylaniline	..	− 7·20	− 2·60	− 3·44
" -*o*-xylene	..	− 4·80	0	− 0·31
" -*m*-xylene	..	− 4·80	1·56	2·05
" -amyl acetate	..	− 6·40	0·17	6·90

We find that a correspondence in behaviour can be established by considering excess compressibility β^{E} and excess susceptibility χ^{E}. Table II brings out the essential features of this correspondence.

TABLE II

Component 2	Nature of β^E	Nature of χ^E	Concentration at which χ^E is maximum	Concentration at which χ^E is maximum
Dioxane ..	Linear	Concave	..	0·75
Diphenyl ether ..	Concave	Concave	0·48	0·32
Amyl acetate ..	Concave	Concave	0·51	0·68
Aniline ..	Concave	Linear	0·30	..
Pyridine ..	Concave	Concave	0·42	0·33
o-Xylene ..	Concave	Concave	0·45	0·50
m-Xylene ..	Concave	Concave	0·50	0·52
Chloroform ..	Concave	Concave	..	0·33
Methylaniline ..	Concave	Concave	0·40	0·44
o-Nitrotoleune ..	Linear	Linear	..	..

It is seen that the behaviours of χ^E and β^E are similar in all cases except the mixtures of dioxane and aniline. On the basis of this comparison Triethylamine-*o*-Nitrotoluene mixtures are to be regarded as ideal.

Departures from this ideal behaviour are often attributed to the formation of complexes. The concentration at which a maximum in β^E or χ^E occurs is to be taken as a measure of the molecular complex; thus $n_2 = 0 \cdot 50$ means 1 : 1 complex, $n_2 = 0 \cdot 33$ would mean a 2 : 1 complex, and $n_2 = 0 \cdot 66$ indicates a 1 : 2 complex. From this point of view, it is seen that the same complex appears to control the magnetic and ultrasonic behaviour of *o*-Xylene, *m*-Xylene and methylaniline mixtures.

In other cases different complexes appear to control the magnetic and the ultrasonic behaviours of the mixtures; for example, in amyl acetate the ultrasonic behaviour indicates a 1 : 1 complex whereas the magnetic data indicate a 1 : 2 complex. These differences are engaging our further attention.

SUMMARY

Diamagnetic susceptibilities of 10 mixtures with triethylamine as the common component have been determined. Deviations from linearity

have been observed in all cases except in aniline and *o*-Nitrotoluene. The magnetic behaviour has been compared with the ultrasonic behaviour of these mixtures.

ACKNOWLEDGEMENT

The author takes this opportunity to offer his grateful thanks to Prof. S. Ramachandra Rao and Dr. J. Bhimasenachar for their valuable suggestions and constant encouragement.

I thank the authorities of Sri Venkateswara University for giving me the necessary facilities.

REFERENCES

Angus *et al.*	.. *Trans. Faraday Soc.*, 1940, **36**, 923.
——— and Tilston	.. *Ibid.*, 1947, **43**, 235.
Reddy and Subrahmanyam	.. *Curr. Sci.* (under publication).
Selwood, P. W.	.. *Magnetochemistry*, Interscience Publishers, Inc., New York, 1956, p. 107.

STUDIES IN THE FORMATION OF HETEROCYCLIC RINGS CONTAINING NITROGEN

Part IX. Condensation of Thiourea with Aromatic Aldehydes and Ammonium Acetate

BY KHALIL AHMED AND N. V. SUBBA RAO, F.A.SC.

(Department of Chemistry, Osmania University)

Received September 29, 1961

THE reaction between thiourea and aliphatic aldehyde-ammonias or the aldehyde and ammonia has been studied by a number of workers[1-4] who reported the formation of *s*-triazine derivatives (I). Paquin[5] used primary amines in place of ammonia and obtained alkyl derivatives. Formaldehyde did not yield the normal product when ammonia was used but behaved normally with primary amines.[6]

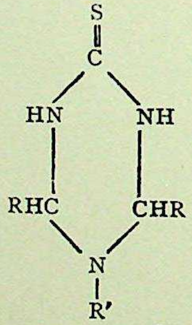

I

According to Paquin[5] the reaction between thiourea, aliphatic aldehydes and ammonia or aldehyde-ammonias followed a step-wise course through an intermediate sym-di-(aminoalkyl) thiourea.

In the preceding paper,[7] the condensation between urea (one mole), aromatic aldehydes (two moles) and ammonium acetate (one mole) was described by us and the optimum conditions have been reported for the synthesis of 2-keto-4, 6-diaryl hexahydro-*s*-triazines. In the present work the reaction has been extended to thiourea leading to the synthesis of 2-thioketo-4, 6-diaryl hexahydro-*s*-triazines and to a comparative study of the reaction with urea and thiourea. As in the case of urea, the reaction may be represented by a similar step-wise mechanism to explain the formation of 2-thio-keto-4, 6-diaryl hexahydro-*s*-triazine (II) and 1, 3-bis-(arylidene) thioureas (III). Compounds of the type (IV) may be considered to be more stable than the corresponding urea compounds on the basis of the observation by Pollak,[8] that thiourea under weakly acidic conditions condensed with formaldehyde producing dimethylol thiourea, whereas urea was reported to produce methylene type of compounds under similar conditions. Hence under weakly acidic conditions employed in the present work, the chances should be better for the intermediate (IV) to react with ammonia resulting in better yields of the thioketo-*s*-triazines.

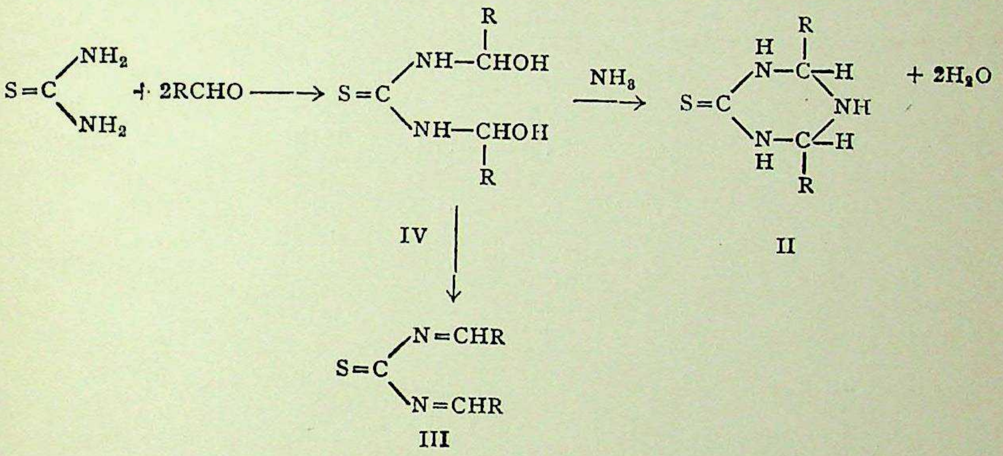

Two moles of eight aromatic aldehydes have been condensed with thiourea (one mole) and ammonium acetate (one mole) under the conditions worked out for the urea condensation. The nature and the relative yields of the products are presented in Table I.

In almost all the cases, the thioketo triazines have been obtained in better yields compared to those of the corresponding keto triazines with the exception of *o*-chlorobenzaldehyde condensation. The benzylidene thioureas have been obtained in the case of *o*-nitro, *o*-chloro and 2, 4-dichlorobenzaldehydes. The latter did not exhibit any tendency for polymerisation as in the case of some arylidene ureas. These results support the assumption that 1, 3-bis-(α-hydroxybenzyl) thioureas are more stable compared to 1, 3-bis-(α-hydroxybenzyl) ureas providing greater chance for the reaction with ammonia to take place resulting in better yields of thioketo triazines. 2-Thioketo-4, 6-diphenylhexahydro-*s*-triazine has been found to exhibit a high intensity band at 249 $m\mu$ ($\log. \epsilon_{max.} = 4.29$) in 95% ethanol and 2-thioketo-4, 6-di-(*p*-methoxyphenyl) hexahydro-*s*-triazine between 274–285 $m\mu$ ($\log. \epsilon_{max.} = 4 \cdot 41$) in the ultraviolet region. In the infra-red region, 2-thio-keto-4, 6-diphenyl hexahydro-*s*-triazine gave three bands at 1180 cm.$^{-1}$ ($8 \cdot 46\ \mu$), 1170 cm.$^{-1}$ ($8 \cdot 55\ \mu$) and 1149 cm.$^{-1}$ ($8 \cdot 7\ \mu$) which may be assigned to $> C = S$ stretching frequency.

TABLE I

Products of condensation of thiourea with aromatic aldehydes and ammonium acetate: Time of reaction: six hours

No.	Name of aldehyde	Percentage yield of 2-thioketo-4, 6-diaryl hexahydro-*s*-triazine	Percentage yield of 1, 3-bis-arylidene thiourea
1	Benzaldehyde	82·2	..
2	Salicylaldehyde	38·0	..
3	Anisaldehyde	10·7	..
4	*o*-Nitrobenzaldehyde	50·0	7·3
5	*m*-Nitrobenzaldehyde	66·6	..
6	*p*-Nitrobenzaldehyde	47·5	..
7	*o*-Chlorobenzaldehyde	56·8	18·7
8	2, 4-Dichlorobenzaldehyde	29·4	11·1

EXPERIMENTAL

All m.p.'s are uncorrected.

General procedure for the Condensation of Thiourea with Aromatic Aldehydes and Ammonium Acetate

Thiourea (one mole), aromatic aldehydes (two moles) and ammonium acetate (one mole) were heated with excess of ethyl alcohol (95%), first to dissolve the solids and then under reflux conditions in general, for a period of six hours. The reaction mixture was worked out, either by cooling it to room temperature and leaving overnight or by removing the solvent under reduced pressure if the solids did not separate on standing overnight. The crude product was fractionated by using suitable solvents. The substances isolated in this manner were purified and characterised.

2-*Thioketo*-4, 6-*diphenyl hexahydro-s-triazine*.—Thiourea, benzaldehyde, ammonium acetate and 95% ethanol were refluxed on a steam-bath. The orange yellow solution was left overnight, resulting in an yellow granular solid which was filtered, washed with hot water and dried. Two recrystallisations from ethanol yielded pale yellow needles, *m.p.* 175° (Found: C, 67·1; H, 5·9; N, 15·9; $C_{15}H_{15}N_3S$ requires C, 66·9; H, 5·5; N, 15·6%).

2-*Thioketo*-4,6-*di*-(*o-hydroxyphenyl*) *hexahydro-s-triazine*. — Thiourea, salicylaldehyde and ammonium acetate were condensed in ethanol and the reaction mixture was subjected to steam distillation to remove the unreacted salicylaldehyde. The orange yellow residue left in the flask could be purified by dissolving in ethyl alcohol and precipitation with water. Further purification from ethyl acetate gave yellow plates which did not melt sharply but decomposed at 250° (Found: C, 60·1; H, 4·9; N, 13·8; $C_{15}H_{15}N_3O_2S$ requires C, 59·8; H, 4·9; N, 13·9%).

2-*Thioketo*-4, 6-*di*-(*p-methoxyphenyl*) *hexahydro-s-triazine*.—Thiourea, anisaldehyde and ammonium acetate were condensed in ethanol and the solvent was removed under reduced pressure. The pale brown solid left in the flask was washed with hot water and a little ether resulting in a colourless solid. Four recrystallisations from ethanol gave colourless plates, m.p. 148–49° (Found: C, 62·0; H, 5·8; N, 12·4; $C_{17}H_{19}N_3O_2S$ requires C, 62·0; H, 5·7; N, 12·4%).

2-*Thioketo*-4, 6-*di*-(*o-nitrophenyl*) *hexahydro-s-triazine*.—Thiourea, *o*-nitrobenzaldehyde and ammonium acetate were condensed in ethanol. The reaction mixture was cooled and the solid that separated was filtered and washed with hot water. The solid was extracted with excess of cold acetone. The acetone insoluble part was repeatedly recrystallised from ethyl acetate, giving yellow needles, m.p. 195° (Found: C, 50·5; H, 3·3; N, 19·4; $C_{15}H_{13}N_5O_4S$ requires C, 50·1; H, 3·6; N, 19·5%).

1, 3-*Bis*-(*o-nitrobenzylidene*) *thiourea*.—The acetone-soluble portion from the above experiment was recrystallised twice from dilute acetone giving light brown rods, m.p. 175° (Found: C, 53·0; H, 3·0; N, 16·6; $C_{15}H_{10}N_4O_4S$ requires C, 52·6; H, 2·9; N, 16·3%).

2-*Thioketo*-4,6-*di*-(*m-nitrophenyl*) *hexahydro-s-triazine*.—Thiourea, *m*-nitrobenzaldehyde and ammonium acetate were condensed in ethanol. The solid that separated was dissolved in pyridine, cooled and kept overnight. Pale yellow square plates, m.p. 208–9°, were deposited. (Found: C, 50·6; H, 3·9; N, 19·4; $C_{15}H_{13}N_5O_4S$ requires C, 50·1; H, 3·6; N, 19·5%).

2-*Thioketo*-4, 6-*di*-(*p-nitrophenyl*) *hexahydro-s-triazine*.—Thiourea, *p*-nitrobenzaldehyde and ammonium acetate were condensed in ethanol. The dark brown solid that separated was filtered, washed with hot water and then with ether. Two recrystallisations from acetone and finally once from ethyl acetate gave the pure thioketo-triazine, reddish-brown plates, m.p. 240° (Found: C, 50·0; H, 3·4; N, 19·4; $C_{15}H_{13}N_5O_4S$ requires C, 50·1; H, 3·6; N, 19·5%).

2-*Thioketo*-4,6-*di*-(*o-chlorophenyl*) *hexahydro-s-triazine.*—Thiourea, *o*-chlorobenzaldehyde and ammonium acetate were condensed in ethanol. The pale yellow solid that separated on cooling was fractionated into (i) alcohol-soluble and (ii) alcohol-insoluble fractions. The alcohol-soluble fraction was purified by recrystallisation from ethyl acetate, colourless needles, m.p. 176° (Found: C, 53·1; H, 3·9; N, 12·3; $C_{15}H_{13}Cl_2N_3S$ requires C, 53·2; H, 3·8; N, 12·4%).

1, 3-*Bis*-(*o-chlorobenzylidene*) *thiourea.*—The alcohol-insoluble fraction could be purified from benzene. The compound on two recrystallisations from the solvent yielded colourless plates, m.p. 171°. (Found: C, 55·6; H, 3·6; N, 8·5; $C_{15}H_{12}Cl_2N_2S$ requires C, 56·0; H, 3·1; N, 8·7%.)

2-*Thioketo*-4, 6-*di*-(2′, 4-′*dichlorophenyl*) *hexahydro-s-triazine.*—Thiourea, 2, 4-dichlorobenzaldehyde and ammonium acetate were condensed in ethanol. To the reaction mixture excess of distilled water was added with slow agitation, when a white granular solid separated. The colourless solid was taken up in boiling ethanol and the solution cooled in ice, depositing a little unreacted thiourea. The solution was filtered, concentrated and left for eighteen hours at the room temperature. Pale yellow crystalline solid separated, which on further recrystallisation from ethyl acetate gave white rectangular plates, m.p. 190° (Found: C, 44·3; H, 2·9; N, 10·4; $C_{15}H_{11}Cl_4N_3S$ requires C, 44·2; H, 2·7; N, 10·3%).

1, 3-*Bis*-(2′, 4′-*dichlorobenzylidene*) *thiourea.*—The mother liquor from the above experiment was treated with excess of water resulting in the precipitation of pale yellow needles. It was dissolved in benzene and kept for three days, when pale yellow fine needles, m.p. 65°, were obtained. (Found: C, 46·1; H, 2·2; N, 7·1; $C_{15}H_8Cl_4N_2S$ requires C, 46·1; H, 2·1; N, 7·1%.)

SPECTROPHOTOMETRIC DETERMINATIONS

(*a*) *Ultraviolet absorption spectra.*—The compounds were thoroughly purified before taking the spectra. Ethanol (95%) was used as solvent. The readings were recorded on Unicam Spectrophotometer Model S.P. 500, in the ultraviolet region. Quartz cells of one cm. thickness and narrow slit-width (0·12 mm.) were used.

(i) 2-thioketo-4, 6-diphenyl hexahydro-*s*-triazine.—

λ_m 249 mμ (log. $\epsilon_{\text{max.}} = 4{\cdot}29$)

(ii) 2-Thioketo-4, 6-di-(*p*-methoxyphenyl) hexahydro-*s*-triazine.—

$\lambda_{max.}$ 274—285 mμ (log. $\epsilon_{max.} = 4 \cdot 41$).

(*b*) *Infra-red absorption spectrum*.—The absorption was recorded on a Perkin-Elmer Model 21, double beam infrared spectrophotometer using rock-salt prism. The characteristic absorptions in the wave numbers are given below with the intensity of the bands in brackets:

2-*Thioketo*-4, 6-*diphenyl hexahydro-s-triazine*.—2891 (*m*), 1515 (*m*), 1504 (*m*), 1414 (*m*), 1401 (*m*), 1377 (*m*), 1277 (*m*), 1180 (*m*), 1170 (*m*), 1149 (*w*), 1075 (*w*), 1027 (*w*), 984 (*w*), 957 (*w*), 917 (*w*), 907 (*w*), 856 (*w*), 850 (*w*), 827 (*m*), 818 (*m*), 808 (*m*), 756 (*m*), 723 (*m*), 701 (*w*), 693 (*w*), 668 (*w*).

SUMMARY

Under the optimum conditions worked out for the condensation of urea, aromatic aldehydes and ammonium acetate, the reaction has been extended to thiourea. 2-Thioketo-4, 6-diaryl hexahydro-*s*-triazines have been obtained in all the cases in better yields; 1, 3-bis-arylidene thioureas could be isolated only in a few cases. The ultraviolet and infrared absorption data for some of the thioketo-hexahydro-*s*-triazines are recorded and the $>C = S$ stretching frequency in these compounds has been assigned.

We thank Dr. K. Babu Rao for the microanalysis.

REFERENCES

1. Nencki .. *Ber.*, 1874, 7, 158.
2. Dixon .. *J. Chem. Soc.*, 1888, **53**, 411.
3. ———— .. *Ibid.*, 1892, 509.
4. Steindorff and Paquin .. Ger. Patent, 5,282,203; *C.A.*, 1933, **27**, 5160; U.S. Patent, 2,304,624; *C.A.*, 1943, **37**, 2852.
5. Paquin .. *Angew. Chem.*, 1948, **60 A**, 267.
6. Burke .. *J. Am. Chem. Soc.*, 1947, **69**, 2136.
7. Ahmed and Rao .. *Proc. Ind. Acad. Sci.*, 1962, **55**, 185.
8. Pollak .. *Modern Plastic*, 1939, **16** (10, 45, 74, 76); *C.A.*, 1939, **33**, 6249.

THE RAMAN SPECTRUM OF RUTILE

BY D. KRISHNAMURTI, F.A.SC.

(*Memoir No.* 132 *from the Raman Research Institute, Bangalore*-6*)

Received April 16, 1962

1. INTRODUCTION

TITANIUM dioxide occurs in three different crystalline modifications, *viz.*, rutile, brookite and anatase. Rutile is uniaxial and exhibits a remarkably high refraction and birefringence. The study of its Raman spectrum is of much interest especially in view of the relative simplicity of its crystal structure. The Raman effect in rutile was first reported by Narayanan (1950). Dayal (1950) and Matossi (1951) have discussed the theoretical aspects of the subject in the light of the experimental facts. The polarisation characters of the Raman lines and their identification had been dealt with by Narayanan in another paper (1953).

The theoretical and experimental investigations cited above have not resulted in an unambiguous identification of all the fundamental Raman frequencies of the crystal. The conclusions of the different authors are also in conflict with each other and hence a re-examination of the subject appeared to be called for. The Raman spectrum of rutile observed at room temperature exhibits several broad and diffuse bands, the number of which much exceeds that theoretically expected. It therefore appeared to be desirable to study the Raman effect in rutile at room temperature as well as at the temperature of liquid air. The sharpening of the Raman frequencies to be expected at the low temperature is actually observed and this circumstance is of assistance in the interpretation of the results.

2. THE CRYSTAL STRUCTURE OF RUTILE

Rutile belongs to the space-group D_{4h}^{14} of the tetragonal system and contains two TiO_2 groups per unit cell. The titanium atoms are situated at the corners and body-centres of the tetragonal lattice, the two non-equivalent titaniums being those at the corner and the body-centre. The oxygen atoms are so arranged that it is possible to identify a linear symmetrical TiO_2

---

* Present address: Department of Physics (Post-graduate Studies and Research), University of Mysore, "Manasa Gangotri", Mysore.

group at each corner and body-centre of the lattice; the two non-equivalent TiO_2 groups lie on the two diagonals perpendicular to each other and passing respectively through the corner and the body-centre. In effect, each titanium atom has as first neighbours six oxygen atoms which are approximately octahedrally co-ordinated around it. Particular mention may be made here of the fact that the two Ti–O distances of each of the linear TiO_2 groups lying perpendicular to the fourfold axis are actually slightly greater than the four other Ti–O distances which are inclined to the fourfold axis. The following are the parameters of the structure of rutile.

$a = 4 \cdot 594$; $c = 2 \cdot 959$ A.U. The titaniums are at $(0, 0, 0)$ and $(\frac{1}{2}, \frac{1}{2}, \frac{1}{2})$, their site symmetry being D_{2h}. The oxygens are at $\pm (x, x, 0)$ and $\pm (\frac{1}{2} + x, \frac{1}{2} - x, \frac{1}{2})$ with $x = 0 \cdot 306$, the site symmetry of the oxygens being C_{2v}. The axes of reference here are of course the three orthogonal crystal axes.

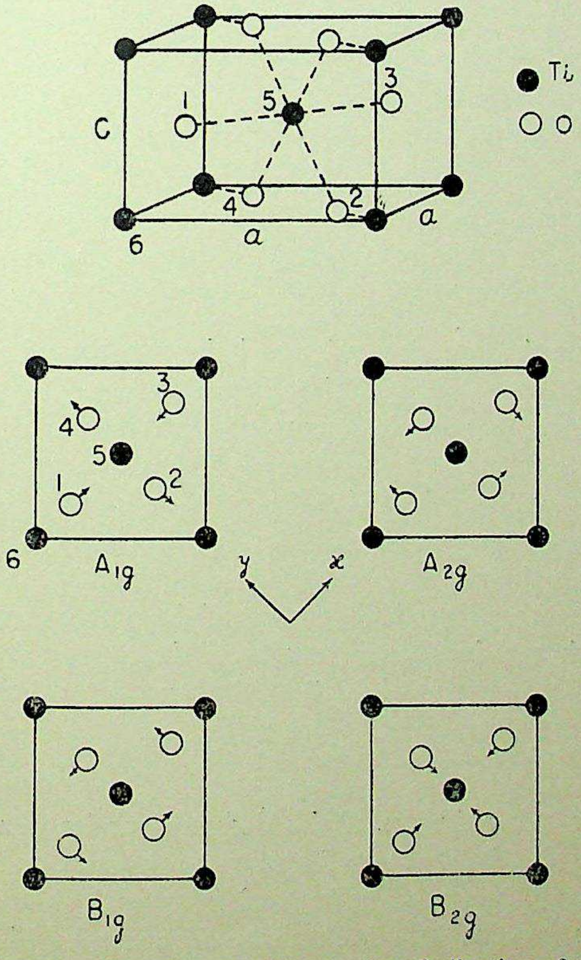

TEXT-FIG. 1. The structure and some of the modes of vibration of rutile symmetric with respect to the centre of inversion.

3. THE DYNAMICS OF THE RUTILE LATTICE

TABLE I

D^{14}_{4h}	n_i	T	n_i'	Activity	
				R.E.	I.R.
A_{1g}	1	0	1	p	f
A_{2g}	1	0	1	f	f
B_{1g}	1	0	1	p	f
B_{2g}	1	0	1	p	f
E_g	1	0	1	p	f
A_{1u}	0	0	0	f	f
A_{2u}	2	1	1	f	p (M_z)
B_{1u}	2	0	2	f	f
B_{2u}	0	0	0	f	f
E_u	4	1	3	f	p (M_x, M_y)

n_i: total number of vibrations including pure translations.

T: pure translations.

n'_i: total number of vibrations excluding pure translations.

R.E.: Raman effect. I.R.: Infra-red. p: permitted; f: forbidden; M_x, M_y, M_z represent the directions of the oscillatory dipole moments.

Table I shows the selection rules and the number of vibrations under each one of the different species. The different normal modes of vibration can be grouped into two sets, *viz.*, symmetric and antisymmetric with respect to the centre of symmetry. Amongst the former there are four species A_{1g}, B_{1g}, B_{2g} and E_g; under each of these there is only one vibration and these four are the theoretically permitted Raman-active fundamentals. In the antisymmetric class there is one normal mode under the species A_{2u} which should be active in the infra-red absorption of the extraordinary ray; besides this there occur three other normal modes of the doubly degenerate species E_u which should be active in the infra-red absorption of the ordinary ray. The vibrations appearing under A_{2g} and B_{1u} are inactive both in Raman effect and infra-red absorption.

The symmetry co-ordinates of the different modes can be derived by standard procedure. The species referred to by Matossi as B_{2u} in his paper is denoted here by B_{1u} so as to be in conformity with the notation adopted by Wilson in his treatise on 'Molecular Vibrations'. The following are the symmetry co-ordinates for the vibrations of the different species.

$$\begin{array}{lll}
\omega_1: & A_{1g}: & x_1 = -y_2 = -x_3 = y_4 \\
\omega_2: & A_{2g}: & y_1 = x_2 = -y_3 = -x_4 \\
\omega_3: & B_{1g}: & -y_1 = x_2 = y_3 = -x_4 \\
\omega_4: & B_{2g}: & x_1 = y_2 = -x_3 = -y_4 \\
\omega_5: & E_g: & z_1 = z_2 = -z_3 = -z_4 \\
\quad\text{or} & & z_1 = -z_2 = -z_3 = z_4 \\
\omega_6: & A_{2u}: & z_1 = z_2 = z_3 = z_4;\ z_5 = z_6 \\
 & & \text{with the condition } Mz_5 + 2mz_1 = 0 \\
\omega_8\ \&\ \omega_9: & B_{1u}: & z_1 = -z_2 = z_3 = -z_4;\ z_5 = -z_6 \\
\omega_{10}, \omega_{11}\ \&\ \omega_{12}: & E_u & x_1 = y_2 = x_3 = y_4; \\
 & & y_1 = x_2 = y_3 = x_4; \\
 & & x_5 = y_6;\quad y_5 = x_6 \\
\quad\text{or} & & x_1 = -y_2 = x_3 = -y_4; \\
 & & y_1 = -x_2 = y_3 = -x_4; \\
 & & x_5 = -y_6;\quad y_5 = -x_6 \\
 & & \text{with the condition} \\
 & & 2m(x_1 + x_2) + M(x_5 + x_6) = 0.
\end{array}$$

4. EXPERIMENTAL RESULTS AND DISCUSSION

The Raman spectra were recorded with the aid of two instruments, one a large aperture ($f/4\cdot5$) two-prism Huet glass spectrograph and the other a Hilger medium glass spectrograph of slightly higher dispersion. A synthetic specimen of rutile in the form of a boule of length 3 cm. and diameter 2 cm. was used to obtain the spectra; only the λ 4358 radiation of the mercury arc could be used to excite the Raman effect as the crystal was pale yellow in colour and was strongly absorbing even in the near ultra-violet region of the spectrum. With slit widths of about 0·075 mm. exposures of the order of 50 hours were given to obtain intense records of the spectrum.

For recording the spectrum at the liquid air temperature a demountable Dewar flask was constructed. The flask consisted of two parts, one an inner vessel of brass to hold the liquid air and the other an outer jacket of glass which was silvered inside; the two vessels were provided with flanges at their upper ends and to get a good vacuum-tight joint between them at the low temperature, silicone DC4 grease proved to be quite useful. A copper block was attached to the lower end of the inner vessel and the crystal was

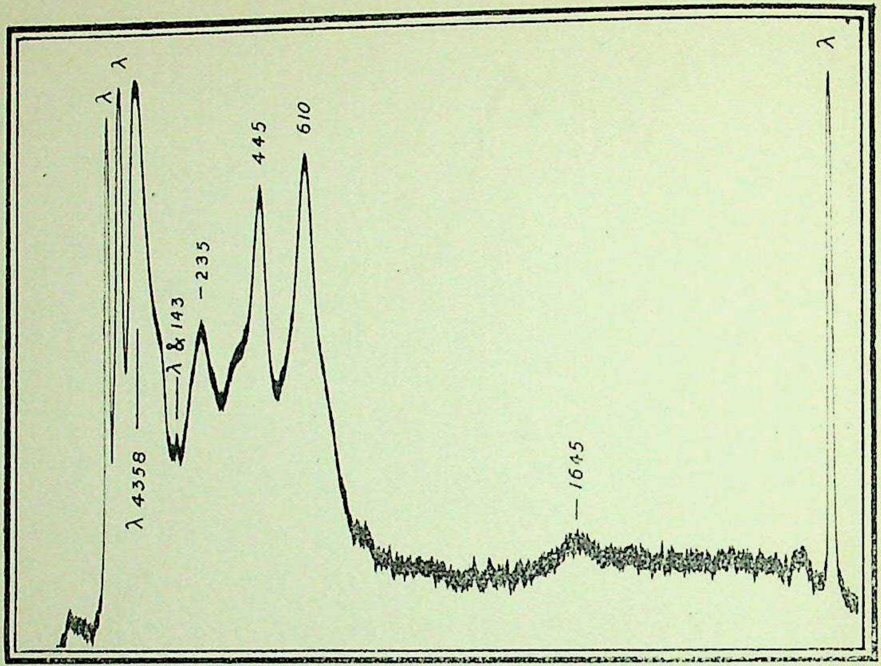

TEXT-FIG. 2. Microphotometer record of the Raman spectrum of rutile recorded at room temperature.

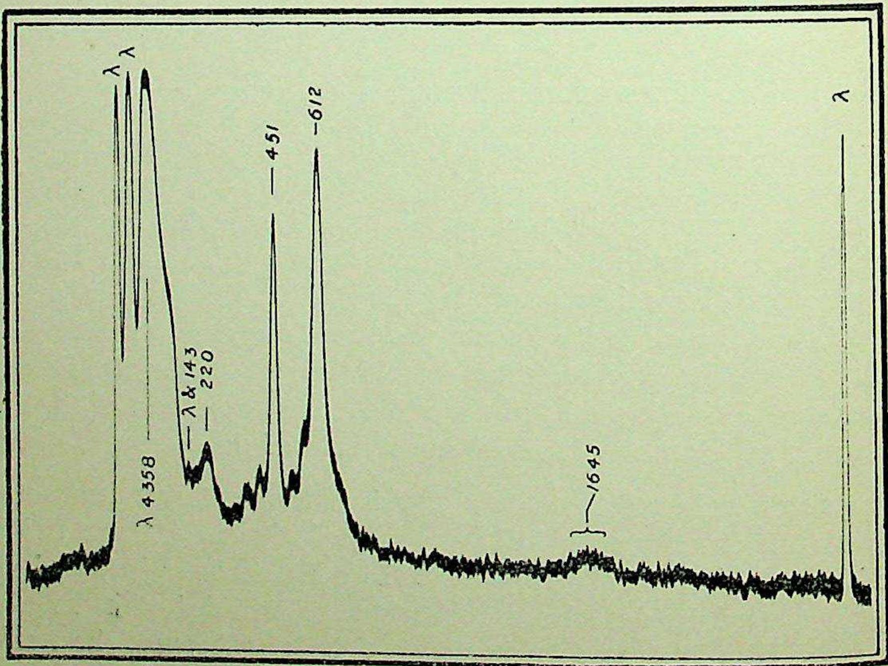

TEXT-FIG. 3. Microphotometer record of the Raman spectrum of rutile recorded at liquid air temperature.

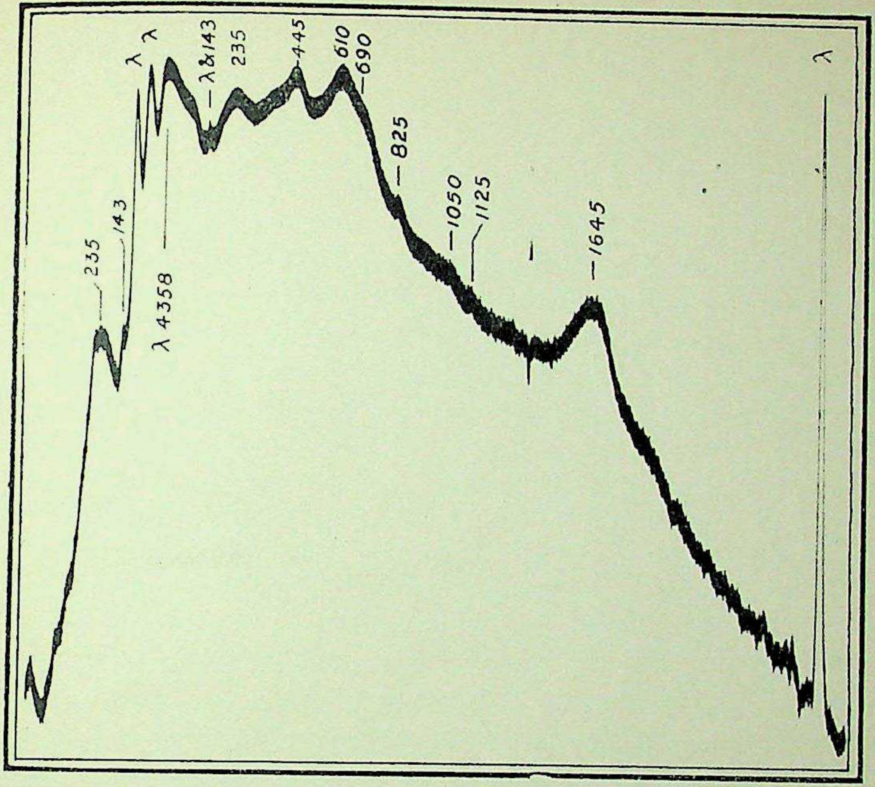

TEXT-FIG. 4. Microphotometer record of a heavily exposed spectrogram exhibiting the weaker Raman lines of rutile at room temperature.

embedded in the copper block with Wood's alloy to secure good thermal contact. The space between the inner vessel and the outer glass jacket was kept continuously evacuated. The outer glass vessel was provided at its lower end with two windows respectively for the entry of the exciting radiations and for the exit of the transversely scattered light.

Plate XXII accompanying the text and the microphotometer records produced in the Text-Figs. 2, 3 and 4 illustrate the different features of the Raman spectrum of rutile. The two very intense Raman lines of shifts 445 and 610 cm.$^{-1}$ constitute the prominent features manifested by even moderately exposed spectrograms. Under prolonged exposures, there appear several other Raman lines of shifts respectively 143 (m), 235 (st), 690 (w), 825 (w), 1050 (w), 1125 (w) and 1645 (w) cm.$^{-1}$ Of these the frequency shifts at 143 and 825 cm.$^{-1}$ are comparatively sharp and the shifts at 235 and 1645 cm.$^{-1}$ are quite broad and diffuse. The spectrum recorded at liquid air temperature exhibits a pronounced sharpening of the lines as may be clearly noticed in the case of the two prominent lines whose shifts at the low temperature are respectively 451 and 612 cm.$^{-1}$ The broad line at 235 cm.$^{-1}$ appears to be diminished in its intensity relatively to the other Raman shifts, and in addition, surprisingly enough, the value of this frequency shift at the low temperature is definitely lower than the room temperature value by about fifteen wave numbers.

The two frequency shifts of 445 cm.$^{-1}$ and 610 cm.$^{-1}$ which are very intense and which appear quite sharp and strong at low temperature obviously represent two of the four theoretically permitted Raman-active fundamentals. In fact, the polarisation studies undertaken by Narayanan definitely show that the frequency shift 610 cm.$^{-1}$ belongs to the totally symmetric species A_{1g} and the other one of shift 445 cm.$^{-1}$ belongs to the doubly degenerate species E_g.

We now proceed to identify the other two Raman-active fundamentals belonging to the species B_{1g} and B_{2g} and also furnish an explanation for the other observed features. From an inspection of the diagrams representing the Raman-active modes A_{1g}, B_{1g} and B_{2g} shown in Fig. 1 in the text it may be noticed that the vibrational frequency of the mode B_{1g} should be extremely low in view of the fact that the movements of *all* the oxygens surrounding any titanium are all strictly perpendicular to the bonds and involve no changes in the Ti-O bond-lengths. (The changes in the O–O distances are also quite small.) On the other hand, in the case of the mode B_{2g} all the oxygens move *simultaneously* towards or away from the central titanium. These movements involve changes in the Ti-O bond-lengths and hence it is obvious that the frequency of this mode should be quite high. The only Raman lines observed in the very low frequency region are the two shifts 235 cm.$^{-1}$ and 143 cm.$^{-1}$ Of these the frequency shift at 143 cm.$^{-1}$ is sharp even at room temperature as can be clearly seen from its appearance on the anti-Stokes side of the record in Text-Fig. 4. On the Stokes side this Raman line is masked by a weak mercury line in this region. The sharpness with which this Raman frequency appears in the spectrum precludes any other explanation for its origin except that of identifying it with the mode B_{1g}.

Matossi has derived detailed expressions for the different normal modes of vibration in rutile in terms of a set of bond-stretching and bond-bending force constants. Without making any approximations whatever regarding the magnitudes of the forces, it may be seen from his paper that there exist the following relationships between the frequencies of the different normal modes:

$$\omega_4^2 - \omega_2^2 = \omega_1^2 - \omega_3^2 \tag{1}$$

where ω_1, ω_2, ω_3 and ω_4 represent the circular frequencies of the modes A_{1g}, A_{2g}, B_{1g} and B_{2g} respectively.

$$\frac{\omega_2{}^2}{\omega_3{}^2} = \left(\frac{\cos\psi + \sin\psi}{\cos\psi - \sin\psi}\right)^2 = 16\cdot 544 \qquad (2)$$

where ψ is a constant connected with the parameters of the structure. With the aid of the above two equations it may readily be seen that the values of the frequencies of the modes A_{2g} and B_{2g} can be calculated assuming the values of the frequencies for the modes A_{1g} and B_{1g}. The calculated values for A_{2g} (inactive in both Raman effect and infra-red) and B_{2g} (Raman-active) are respectively 582 and 831 cm.$^{-1}$ The Raman spectrum indeed exhibits a sharp and well-defined frequency shift of 825 cm.$^{-1}$ which obviously arises from the normal mode B_{2g}.

From the above calculations it also emerges that the bond-stretching force constant k'' between the two oxygen atoms 4 and 1 has a value $4\cdot 226 \times 10^4$ dynes/cm. In addition to the relations which we have cited above there exists one another from which it is possible to calculate the frequency of the absorption maximum to be observed in the extraordinary ray, *i.e.*, mode A_{2u}. This relation is obtained by neglecting to a first approximation the bond angle bending force constant d_1 corresponding to the atoms 1, 5 and 3 which are in a line and are comparatively farther apart from each other. This relation is given by

$$m\omega_5{}^2 - 8k'' \cos^2\chi = \omega_6{}^2 \left(\frac{mM}{2m + M}\right)$$

where k'' is the constant mentioned above, m and M are respectively the masses of the oxygen and titanium atoms; ω_5 and ω_6 are the circular frequencies corresponding to the modes E_g and A_{2u}; $\cos\chi$ has a value $= 0\cdot 53$. If we assume the observed value of the frequency shift corresponding to the mode E_g (ω_5), *i.e.*, 445 cm.$^{-1}$ the calculated value for A_{2u} emerges as 344 cm.$^{-1}$ in fair agreement with the observed value of 333 cm.$^{-1}$ reported in the literature. This agreement again confirms our identification of the frequency shift 143 cm.$^{-1}$ as arising due to the mode B_{1g}. The other Raman shifts observed are explicable as overtones and combinations of the Raman-active and infra-red-active frequencies as shown in Table II.

It may be mentioned here that the two broad bands observed (in the spectra recorded at room temperature) on the short-wavelength side of the shifts 445 cm.$^{-1}$ and 610 cm.$^{-1}$ have till now hampered the proper identification of the four fundamental Raman frequencies. However, in the present investigation the spectra recorded at the low temperature clearly show them to be the Raman shifts 445 and 610 cm.$^{-1}$ excited by the two satellites of λ 4358 and hence these are eliminated from consideration. Obviously at the room temperature, these shifts, because of their considerable width, merge together to give the observed bands.

TABLE II

Vibrational frequencies of rutile

Observed value in cm.$^{-1}$	Observed in	Identification	Calculated value in cm.$^{-1}$
143	R.E.	B_{1g}	..
235	R.E.	?	..
256	I.R.	E_u	..
333	I.R.	A_{2u}	344
445	R.E.	E_g	..
610	R.E.	A_{1g}	..
690	R.E.	$A_{2u} \times A_{2u}$	688
825	R.E.	B_{2g}	831
1050	R.E.	$A_{1g} \times E_g$	1055
1125	R.E.	$A_{2g} \times A_{2g}$?	1164
1645	R.E.	$B_{2g} \times B_{2g}$	1650
..	Inactive in both I.R. and R.E.	A_{2g}	582

Besides the frequencies listed in Table II, studies on the infra-red reflection spectrum of rutile by early investigators (*vide Landolt Bornstein Tables*, 1955, Vol. I, Part IV) have revealed the following maxima, *viz.*, 256, 385, 540, 625 and 690 cm.$^{-1}$ in the ordinary ray and 333 (shown in Table II), 451, 518 and 625 cm.$^{-1}$ in the extraordinary ray. Calculation of frequencies of the infra-red-active species E_u (ordinary ray) and those of the inactive species B_{1u} involves the values of a number of force constants, not all of which could be estimated with the available data. Some of the above maxima, however, may arise by violation of selection rules due to causes to be considered presently.

It is highly probable that the Raman shift of 235 cm.$^{-1}$ arises due to an infra-red-active (but theoretically Raman inactive) doubly degenerate mode of species E_u present in this region—*i.e.*, corresponding to the maximum at 256 cm.$^{-1}$ given above. The origin of the Raman activity of this species in violation of the selection rules can be traced to the fact that there are five

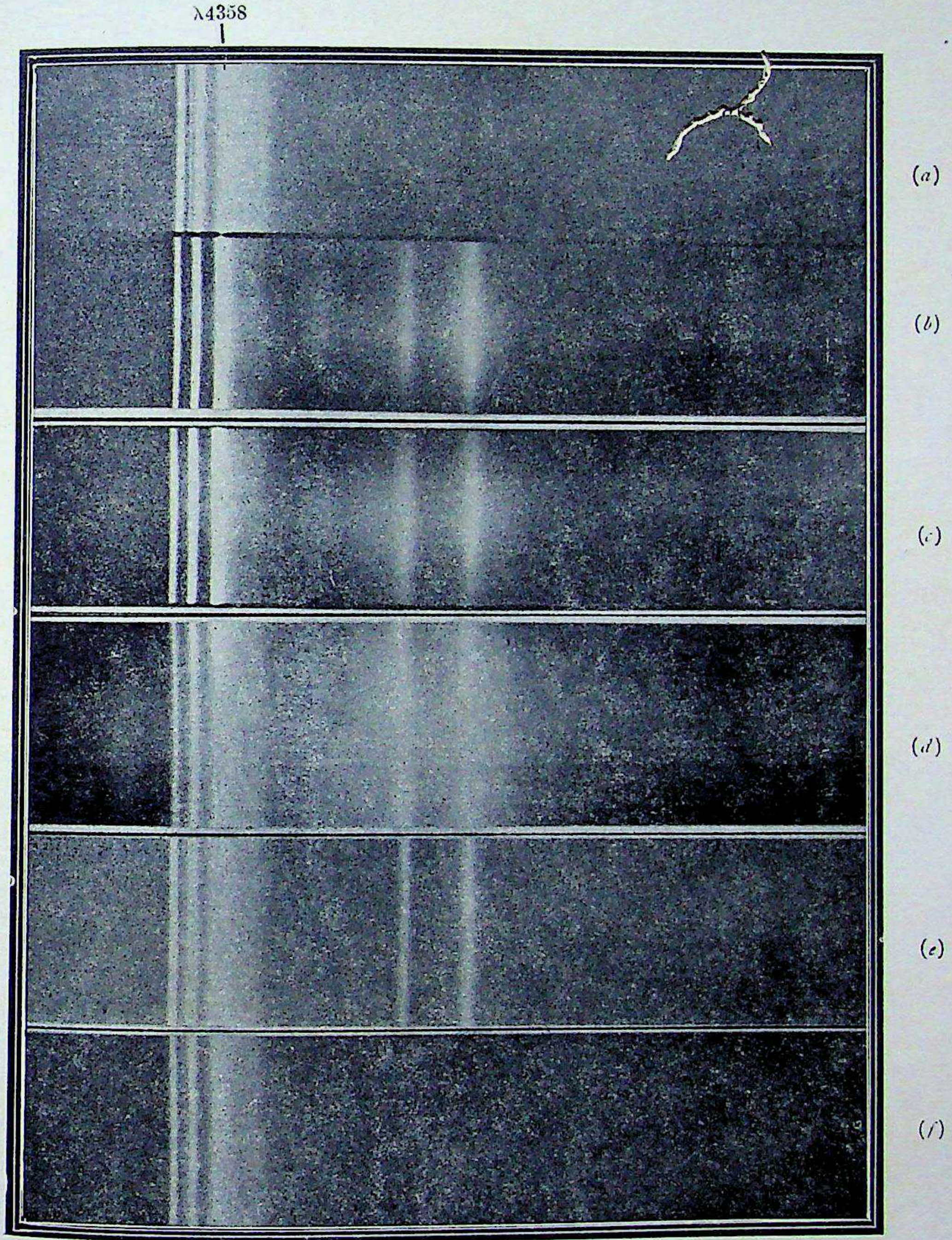

(*a*) Spectrum of the mercury arc; (*b*) and (*c*) Raman spectrum of rutile at room temperature for two different orientations of the crystal; (*d*) Heavily exposed Raman spectrum of rutile at room temperature; (*e*) The spectrum of the rutile at liquid air temperature; (*f*) Spectrum of the mercury arc.

naturally occurring isotopes of titanium of atomic weights 46, 47, 48, 49 and 50 and with relative abundances of 7·95%, 7·75%, 73·45%, 5·51%, 5·34% respectively. Whereas, the selection rules and symmetry modes are derived on the basis that all titaniums are of equal mass, the actual situation is that approximately only three quarters of the total number of titanium atoms are of identical mass, the others varying from 48, the maximum variation being two units either way. It could therefore be expected that the infra-red-active species E_u (which involves also the movements of the titaniums) would become Raman-active, and the low value of the frequency (235 cm.$^{-1}$) is suggestive of this view. In the case of α-quartz, modes of the species B have been observed to be weakly Raman-active in violation of the selection rules and an analogous explanation had been offered by the author (1958). It is also not possible to identify the frequency 235 cm.$^{-1}$ with the mode B_{1g} (instead of 143 cm.$^{-1}$ as has been done), since it leads to a theoretical value of 973 cm.$^{-1}$ for the Raman-active mode B_{2g} and no Raman frequency shift of that value in rutile has been observed.

Finally, it may be pointed out that in the case of mode A_{2g} (Text-Fig. 1) here occur comparatively greater changes in the O–O distances than in the case of the mode B_{1g}, thereby leading to a theoretically calculated value of 582 cm.$^{-1}$ which is greater than that of B_{1g} (143 cm.$^{-1}$), even though both modes are such that no changes in the Ti-O bond-lengths are involved.

In conclusion, the author wishes to express his sincere thanks to Prof. Sir C. V. Raman, F.R.S., N.L., for his kind interest in this investigation.

5. SUMMARY

The Raman spectrum of rutile has been investigated both at room temperature and at the temperature of liquid air. The Raman lines which, at room temperature are quite wide, are observed to sharpen greatly at the low temperature. The different Raman-active fundamentals are identified and the paper also elucidates the several subsidiary features which are observed in spectrograms recorded with prolonged exposures.

6. REFERENCES

1. Dayal, B. .. *Proc. Ind. Acad. Sci.*, 1950, **32 A**, 304.
2. Krishnamurti, D. .. *Ibid.*, **1958**, **47 A**, 276.
3. Matossi, F. .. *Jour. Chem. Phys.*, 1951, **19**, 1543.
4. Narayanan, P. S. .. *Proc. Ind. Acad. Sci.*, 1950, **32 A**, 279.
5. ——— .. *Ibid.*, 1953, **37 A**, 411.

SPECTROSCOPIC STUDIES OF THE CRESOLS

III. Emission and Absorption Spectra of meta-Cresol in the Near Ultra-violet Region*

By P. Ramakoteswara Rao**

(*Department of Spectroscopy, Banaras Hindu University*)

Received January 15, 1962

(Communicated by Dr. R. K. Asundi, F.A.SC.)

PART A. THE EMISSION SPECTRUM

Experimental Procedure

The meta-cresol used in the investigations was the laboratory reagent variety of the B.D.H. Company. It was purified by distillation before use. The emission spectrum of meta-cresol was excited by means of an uncondensed transformer discharge through the flowing vapour of the substance. The discharge tube employed and the electrical arrangement used for exciting the spectrum are similar to those described elsewhere (Ramakoteswara Rao, 1962, Part I). Even by running the discharge under the controlled conditions described in the paper on ortho-cresol (Ramakoteswara Rao, 1962, Part II), it was not possible to get the 'pure' emission spectrum of meta-cresol, *i.e.*, without the simultaneous appearance of the CO third positive bands. This meant that even under the mild conditions of excitation employed, some meta-cresol molecules dissociated with the consequent formation and excitation of the CO molecules. Therefore, still milder conditions of excitation were tried. Under these conditions, the discharge was not continuous. The total time for which the discharge took place varied between fifty and seventy-five per cent. of the actual time of exposure. Secondly, a mercury diffusion pump was included in the evacuating arrangement so that the rate of flow of the vapour and the rate of clearance from the discharge tube of the dissociation products were more rapid. Still, the CO bands persistently appeared on the spectrograms. Since only one CO band, the one at 2833·1 Å, appeared in the region of the meta-cresol emission bands, no further attempts were made to get the emission spectrum of meta-cresol free from all traces of CO bands. The voltage applied between the electrodes of the discharge tube varied between 1800 and 2050 volts. When the discharge was taking place, a feeble white glow could be seen in the discharge tube if there was complete darkness around it.

---

* This paper is based on a part of the author's thesis accepted for the Ph.D. degree (1958) of the Banaras Hindu University, Banaras, India.

** Present address: Analytical Division, Atomic Energy Establishment, Trombay, Bombay, India.

The emission spectrum of meta-cresol was recorded on the Hilger medium quartz (E_2) spectrograph. Kodak III–0 plates were used to photograph the spectrum and exposure times varied from eight to about thirty hours.

RESULTS

The emission spectrum of meta-cresol consists of fifteen bands in the region 2750–2920 Å, superposed over a continuum beginning at about 2770 Å and extending to beyond 3100 Å. The continuum has its intensity maximum at about 2960 Å and fades away towards both ends, the fading towards the long wavelength side being more gradual. The bands are, in general, diffuse. A typical emission spectrum of meta-cresol is shown in Fig. 1.

The spectrograms are measured on a Hilger comparator having a least count of 0·001 mm. The wavelength data presented in Table I are the averages of nine measurements on three spectrograms. The intensity of many of the bands does not differ much from that of the continuum over which they are superposed. The stronger bands are correct to within 8 cm.^{-1} and the rest to about 15 cm.^{-1}

ANALYSIS AND DISCUSSION

A comparison of the emission spectrum with the near ultra-violet absorption spectrum of meta-cresol vapour, photographed on the same plate, has shown that the two are parts of the same band system. It is, therefore, clear that the carrier of the emission spectrum is the meta-cresol molecule.

It is assumed, as was done for the other two cresols, that the CH_3 and OH groups of meta-cresol 'behave' as single particles and that this near ultra-violet band system corresponds to the 2600 Å, $^1B_{2u}-{}^1A_{1g}$, system of benzene. It then follows that meta-cresol molecule has C_s symmetry and that the band system under discussion involves the transition $^1A'-{}^1A'$.

From a study of the absorption spectrum of meta-cresol vapour the zero-zero band was fixed at 35985 cm.^{-1} (*see* Part B). Hence the band occurring in the emission spectrum of meta-cresol at 35983 cm.^{-1} with medium strong intensity is taken as the zero-zero band.

A noteworthy feature in the emission spectrum of meta-cresol is the occurrence of two intense bands (more intense than the zero-zero band) on the short wavelength side of the zero-zero band. These two bands, which also occur with high intensity in the absorption spectrum of meta-cresol, are interpreted as due to transitions respectively from the 116 cm.$^{-1}$ and 188 cm.$^{-1}$ vibrational levels of the excited state of meta-cresol to the zero-vibrational level of its electronic ground state. The high intensity of these bands is to be understood in terms of the Franck-Condon principle and the change in equilibrium distances on electronic excitation, between atoms predominantly involved in the 116 cm.$^{-1}$ and 188 cm.$^{-1}$ excited state vibrations. The only other band to the short wavelength side of the zero-zero band is 251 cm.$^{-1}$ away from it. This frequency difference is also suggested as an excited state vibrational frequency.

The medium intensity bands at 35248 cm.$^{-1}$ and 34980 cm.$^{-1}$ are separated from the zero-zero band by 735 and 1003 cm.$^{-1}$ respectively. These frequency differences are taken as frequencies of fundamental vibrations in the ground state of the molecule. The Raman spectrum of meta-cresol (Herz, 1943) shows two strongly polarized lines of outstanding intensity at 734 cm.$^{-1}$ and 1000 cm.$^{-1}$ It is obvious that the suggested ground state frequencies correspond to those involved in the above two Raman lines. Higher quanta of these frequencies are not observed in the emission spectrum.

The 1003 cm.$^{-1}$ vibration of meta-cresol is interpreted as the carbon ring 'breathing vibration' corresponding to the 992 cm.$^{-1}$ vibration of benzene. The 998 cm.$^{-1}$ vibration of meta-xylene, which obviously involves the same vibrational mode as the 1003 cm.$^{-1}$ vibration of meta-cresol, has been similarly interpreted by Pitzer and Scott (1943) and Singh (1956).

The 724 cm.$^{-1}$ vibration of meta-xylene (Pitzer and Scott, 1943 and Singh, 1956), the 745 cm.$^{-1}$ vibration of meta-dihydroxybenzene (Beck, 1950) and the 735 cm.$^{-1}$ vibration of meta-cresol seem very likely to involve similar modes of vibration. Pitzer and Scott (1943) assign the 724 cm.$^{-1}$ frequency of meta-xylene to the C–C–C parallel bending vibration corresponding to the b_{1u} 1011 cm.$^{-1}$ vibration of benzene. Singh (1956), however, assigns it to the C–CH_3 valence vibration. Beck (1950) ascribes the 745 cm.$^{-1}$ vibration of meta-dihydroxybenzene to the C–OH valence vibration. From the fact that these vibrations appear but with slightly different values in three different substituted benzene molecules, it appears that they are more likely to be associated with the carbon-ring vibrations rather than the carbon-substituent vibrations.

The 204 cm.$^{-1}$ frequency involved in the weak band at 35779 cm.$^{-1}$ is also suggested as a ground state vibrational frequency. This has also been observed in the absorption spectrum. This frequency is correlated with the depolarized Raman line at 215 cm.$^{-1}$ The weak band at 35579 cm.$^{-1}$ separated from the zero-zero band by 404 cm.$^{-1}$ may also involve a ground state vibration. In the absorption spectrum of meta-cresol a weak band occurs at 398 cm.$^{-1}$ on the red side of the zero-zero band. The mean of these two values, namely, 401 cm.$^{-1}$ is suggested as a possible ground state frequency. This frequency does not have support from the Raman spectrum.

The − 85 cm.$^{-1}$ and 54 cm.$^{-1}$ frequencies appearing in the weak bands at 35898 and 36037 cm.$^{-1}$ are difference frequencies involving $v - v$ and $v - v'$ transitions. These will be referred to in Part B.

The vibrational analysis of the emission spectrum of meta-cresol is presented in Table I.

TABLE I

Emission spectrum of meta-cresol

Wave-length Å	Wave-number cm.$^{-1}$	Intensity	Separation from 0–0 band	Assignment
2758·5	36241	2 *d*	258	0+251
63·5	175	8 *d*	192	0+188
69·2	101	9	118	0+116
74·1	037	2 *d*	54	0+54
78·3	35983	6	0	0−0
84·9	898	2	− 85	0−82
94·1	779	3	− 204	0−204
2809·8	579	3	− 404	0−401
15·7	505	2	− 478	0−401−82
36·2	248	5	− 735	0−735
42·8	166	4 *d*	− 817	0−735−82
48·9	091	4 *d*	− 892	0−735−2×82
57·9	34980	4 *d*	−1003	0−1003
98·3	493	5	−1490	
2919·5	242	3 *d*	−1741	0−735−1003

d, diffuse.

The origin of the continuous emission spectrum occurring in the region of the discrete bands and beyond has not been investigated.

PART B. ABSORPTION SPECTRUM

The absorption spectrum of meta-cresol vapour was investigated in the temperature range 0°–32° C. using absorption cells of lengths 100, 150, 200 and 250 cm. The experimental details are similar to those given elsewhere (Ramakoteswara Rao, 1962, Part I). The absorption spectrum was photographed on the Hilger large quartz (E_1) spectrograph (dispersion 3·5 Å/mm. at 2700 Å) Kodak B-4 and B-20 plates were employed to photograph the spectrum and exposure times ranged between half an hour and forty-five hours.

RESULTS

The absorption spectrum of meta-cresol, recorded under the above-mentioned experimental conditions consists of about fifty-five bands in the region 2580–2810 Å. On spectrograms corresponding to smaller cell lengths and lower temperatures, two band groups, headed on their short wavelength sides by the bands at 36173 cm.$^{-1}$ and 37139 cm.$^{-1}$, can be recognized. The longer wavelength band group, namely, the one headed by the band at 36173 cm.$^{-1}$ is the more prominent one. On spectrograms corresponding to longer absorption paths, both the band groups expand on either side resulting in a number of discrete absorption bands. In the spectrogram corresponding to 250 cm. absorption path and 30° C. temperature, there is total absorption in the region 2580–2810 Å and beyond.

The absorption bands of meta-cresol can be classified regarding their appearance, into four broad categories. There are bands which are diffuse and exhibit on closer examination a degradation towards the long wavelength side. Over fifty per cent. of the total bands come under this category. There are eight to ten bands which are diffuse and very broad, the width of an individual band being 15 cm.$^{-1}$ or more. Then there are bands which are narrow and line-like and those which show a sharp degradation towards the long wavelength side. About half a dozen bands come under each of these two categories. A typical absorption spectrum of meta-cresol vapour is reproduced in Fig. 2.

The wavelengths of the absorption bands are given in Table II. They are the average results of eight measurements made on four spectrograms. The stronger and sharper bands are correct to 5 cm.$^{-1}$ and the rest to 12 cm.$^{-1}$

TABLE II

Absorption spectrum of meta-cresol

Wave-length Å	Wave-number cm.$^{-1}$	Intensity	Separation from 0–0 band	Assignment
2809·2	35587	2	− 398	0−401
03·6	658	2 *d*	− 327	0−4×82
2799·4	711	3 *d*	− 274	0−200−82
97·4	737	4	− 248	0−248; 0−3×82
93·6	785	5	− 200	0−200
90·8	821	4	− 164	0−2×82
87·9	859	5	− 126	0−126
84·4	903	6	− 82	0−82
81·8	938	6	− 47	0−47
78·1	985	9	0	0−0
74·7	36029	9	44	0+44
73·6*	043	9 *b*	58	0+58
69·2	101	10	116	0+116
67·1	128	6	143	0+188−47
63·7	173	10 *b*	188	0+188
58·9	236	6	251	0+251
54·5	294	5	309	0+188+116; 0+469−2×82
52·0	326	2	341	0+469−126
49·9	354	2	369	0+696−4×82
47·9	381	2	396	0+469−82
45·5	412	4	427	
42·4	454	5	469	0+469
40·1	484	2	499	0+696−200
2737·4	36520	4	535	0+696−2×82
34·5	559	2	574	0+469+116; 0+696−126
31·3	602	4	617	0+696−82
28·1	645	4 *b*	660	0+469+188
25·4	681	9	696	0+696
17·1	793	6	808	0+696+116; 0+964−2×82
14·7	826	4	841	0+964−126
11·8	865	6 *d*	880	0+696+188; 0+964−82
05·6	949	8 *b*	964	0+964
00·7	37016	8 *b*	1031	0+1031
2697·4	062	8 *d*	1077	0+964+116; 0+964+188 −82

TABLE II—(*Contd.*)

Wave-length Å	Wave-number cm.$^{-1}$	Intensity	Separation from 0–0 band	Assignment
96·2	079	6	1094	0+1031+58
91·8	139	8 *d*	1154	0+964+188; 0+1031+116; 0+696+469
87·0	205	5 *b*	1220	0+964+251; 0+1031+188; 0+2×696−2×82
82·2	272	4	1287	0+1031+251; 0+696+469 +116
81·0	289	5	1304	0+2×696−82
74·7	376	5	1391	0+2×696
71·4	422	4 *d*	1437	0+964+469
67·1	483	6	1498	0+1031+469
59·5	590	5 *d*	1605	
55·4	648	6	1663	0+964+696
51·2	708	5 *d*	1723	0+1031+696
47·5	760	5 *d*	1775	0+964+696+116
2643·0	37825	5 *d*	1840	0+964+696+188; 0+1031 +696+116; 0+2×964 −82
37·1	909	4	1924	0+2×964; 0+1031+696 +188
32·0	983	3 *d*	1998	0+1031+964; 0+3×696 −82
28·9	38027	3 *d*	2042	0+2×964+116
25·3	080	3 *d*	2095	0+3×696
07·2	344	3 *d*	2359	0+2×696+964
2599·7	454	3 *d*	2469	0+1031+964+469
89·2	610	4	2625	0+2×964+696
85·1	672	1	2687	0+1031+964+696
82·8	706	1	2721	

b, broad. *d*, diffuse.

ANALYSIS AND DISCUSSION

The band at 35985 cm.$^{-1}$, one of the strongest bands in the absorption spectrum, is taken as the zero-zero band. The band is sharp and degraded towards the red.

The vibrational analysis presented in this section (*see* Table II) assumes seven excited state vibrational frequencies 116, 188, 251, 469, 696, 964 and 1031 cm.$^{-1}$, three ground state frequencies 200, 248 and 401 cm.$^{-1}$ and five difference frequencies 44, 58, − 47, − 82 and − 126 cm.$^{-1}$ One of the ground state frequencies proposed here, namely, the 248 cm.$^{-1}$ frequency, is not observed in the emission spectrum.

The bands involving the 116 cm.$^{-1}$ and 188 cm.$^{-1}$ excited state frequencies appear very prominently in both the absorption and the emission spectra of meta-cresol. In emission spectrum they are more intense than the zero-zero band. These frequencies appear in combination with all the other excited state frequencies. The 116 cm.$^{-1}$ and 188 cm.$^{-1}$ excited state frequencies are correlated with the 200 cm.$^{-1}$ (Raman effect 215 cm.$^{-1}$) and 248 cm.$^{-1}$ (Raman effect 243 cm.$^{-1}$) ground state frequencies respectively.

The 696 cm.$^{-1}$ and 964 cm.$^{-1}$ frequencies involve two very intense bands in the absorption spectrum of meta-cresol. They form progressions of three and two members respectively and occur in combination with all the other excited state frequencies and with many difference frequencies. Cave and Thompson (1950) and Sreeramamurty (1951) also reported these excited state frequencies from their analysis of the absorption spectrum of meta-cresol. The 696 cm.$^{-1}$ and 964 cm.$^{-1}$ excited state frequencies are correlated with the 735 cm.$^{-1}$ and 1003 cm.$^{-1}$ ground state frequencies observed in the emission spectrum.

Some correlations have been suggested between the remaining excited state frequencies and some ground state frequencies observed in the Raman spectrum (*see* Table III). Those ground state frequencies have not been observed in the emission spectrum.

The strong bands at 36029 cm.$^{-1}$ separated from the zero-zero band by 44 and 58 cm.$^{-1}$ respectively, are interpreted as involving $v - v'$ transitions.

The bands on the longer wavelength side of the zero-zero band and separated from it by − 47, − 82 and − 126 cm.$^{-1}$ can, as usual, be understood as resulting from 1–1 transitions, mostly involving non-totally symmetric vibrations. Of these, the − 82 cm.$^{-1}$ frequency is the most prominent. Four multiples of this difference frequency appear superposed on the zero-zero band and its second and third multiples appear in association with a number of excited state frequencies. The 116 cm.$^{-1}$ excited state-frequency has been correlated above with the 200 cm.$^{-1}$ ground state frequency. It appears very likely that the − 82 cm.$^{-1}$ difference frequency is due to 1–1 transition involving the 200 cm.$^{-1}$ ground state frequency. The occur-

TABLE III

Fundamental vibrational frequencies of meta-cresol molecule

Ground state frequencies in cm.$^{-1}$		Excited state frequencies in cm.$^{-1}$		
Raman effect (Herz, 1943)	Near u-v. emission spectrum. Present research	Near u-v. absorption spectrum		
		Present research	Sreeramamurty (1951)	Cave & Thompson (1950)
215	200*	116*		
243	248†	188*	183	
			199	
303		251*		
	401*			
				423
518 540		469		
734	735	696	696	693
			808	
			950	
1000	1003	964	962	963
1086		1031		
			1150	
				1199
			1219	

* These frequencies are observed both in the absorption and emission spectra.

† This frequency is observed only in the absorption spectrum.

rence of higher multiples of the − 82 cm.$^{-1}$ difference frequency can be understood in view of the low value of the ground state vibration with which it is associated.

The analysis of the absorption spectrum of meta-cresol is given in Table II. In cases where a band has more than one assignment, the various assignments have been arranged in the order of decreasing significance. It can be seen from Table II that, in the absorption spectrum of meta-cresol, a fairly large number of transitions of the type $0 + v_i + v_j + v_k$ occur. Table III gives most of the fundamental vibrational frequencies of the ground and excited states of meta-cresol suggested so far.

A word may be said in the end about the diffuseness characteristic of the meta-cresol bands. The diffuseness is a characteristic of the bands of only meta-cresol and not so much of ortho and para-cresol. A similar situation is met with in the near ultra-violet band systems of the isomeric xylenes. Cooper and Sponer (1952) traced the diffuseness of meta-xylene bands to the following possible causes:

(1) due to overlapping $v - v$ transitions;

(2) due to the overlapping of gross and fine structures of band; and

(3) due to internal rotation of the CH_3 group; the potential restricting such a rotation being only 500 cal./mole.

The first two in this list are of a general nature and apply not only to meta-xylene but also (may be to different extents) to other polyatomic molecules for example to ortho- and para-xylene and to other substituted benzene molecules. The third cause should effect the spectra of meta-xylene and para-xylene molecules to the same extent, since the potential hindering the rotation of the CH_3 group about the C–C bond in para-xylene is about the same as that in meta-xylene (Pitzer and Scott, 1943). Therefore it appears that there are other more important reasons responsible for the diffuseness of the bands in the spectra of meta-xylene and meta-cresol.

SUMMARY

Part A:—The emission spectrum of meta-cresol, obtained by means of a controlled transformer discharge through the flowing vapour, is recorded on the Hilger medium quartz (E_2) spectrograph. The emission spectrum consists of fifteen bands in the region 2750–2920 Å superposed over a continuum beginning at about 2770 Å and extending to beyond 3100 Å. The discrete emission spectrum is the counterpart of the near ultra-violet absorption spectrum of meta-cresol vapour (Part B). The electronic transition involved in the discrete band system is interpreted as $^1A' - {}^1A'$. A vibrational analysis of the band system is proposed in terms of the ground state vibrational frequencies 200, 401, 735 and 1003 cm.$^{-1}$ and the excited state frequencies 116, 188 and 251 cm.$^{-1}$

Part B:—The absorption spectrum of meta-cresol vapour, using absorption paths ranging from 100–250 cm. and temperatures from 0–30° C., is recorded on the Hilger large quartz (E_1) spectrograph. About fifty-five bands are obtained in the region 2580–2810 Å. A vibrational scheme for the band system is proposed in terms of the excited state vibrational frequencies 116, 188, 251, 469, 696, 964 and 1031 $cm.^{-1}$ and the ground state frequencies 200, 248 and 401 $cm.^{-1}$

ACKNOWLEDGEMENTS

The author is highly indebted to Professor R. K. Asundi for his interest in this work, to Dr. Nand Lal Singh for helpful guidance and encouragement and to Mr. T. V. Krishnan for his help in this paper. The author expresses his thanks to the Council of Scientific and Industrial Research for financial assistance during the period of this work.

REFERENCES

Beck, C. A. ..	*J. Chem. Phys.*, 1950, **18**, 1135.
Cave, W. T. and Thompson, H. W.	*Disc. Farad. Soc.*, 1950, **9**, 35.
Cooper, C. D. and Sponer, H. ..	*J. Chem. Phys.*, 1952, **20**, 1248.
Herz, E. ..	*Monatsch. Chem.*, 1943, **74**, 160.
Pitzer, K. S. and Scott, D. W. ..	*J. Am. Chem. Soc.*, 1943, **65**, 803.
Ramakoteswara Rao, P. ..	Communicated to *Proc. Ind. Acad. Sci.*, Part I.
——————— ..	*Ibid.*, Part II.
Singh, I. S. ..	Ph.D. Thesis, 1956, Benares Hindu University, Benares, India.
Sreeramamurty, K. ..	*Curr. Sci.*, 1951, **20**, 291.

EXPLANATION OF PLATES

PLATE XXIII

FIG. 1. Emission spectrum of meta-cresol photographed on Hilger medium quartz (E_2) spectrograph; exposure time 15 hours.

PLATE XXIV

FIG. 2. Absorption spectrum of meta-cresol obtained with 100 cm. absorption path at 30° C. Spectrogram taken on Hilger large quartz (E_1) spectrograph; exposure time 10 hours.

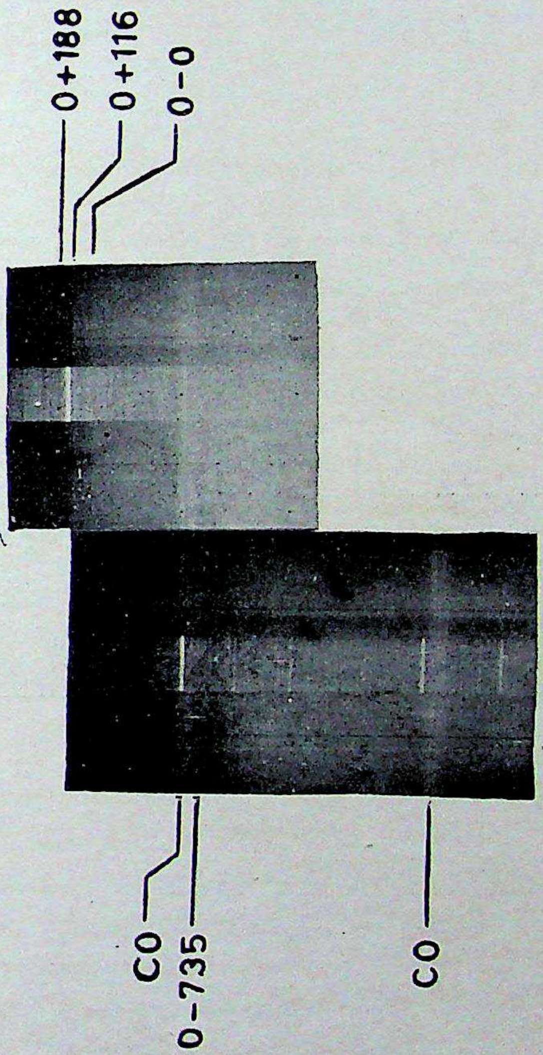
0+188
0+116
0-0
CO
0-735
CO

FIG. 1

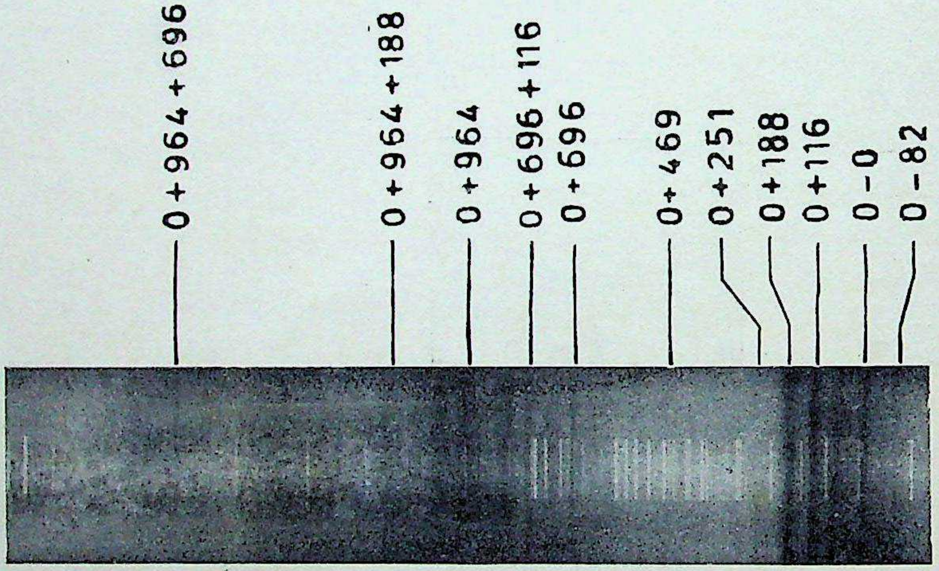
0+964+696
0+964+188
0+964
0+696+116
0+696
0+469
0+251
0+188
0+116
0-0
0-82

FIG. 2

THE ANISOTROPY OF ELASTIC WAVE PROPAGATION IN CRYSTALS

By R. VENKATARAMAN

(*National Aeronautical Laboratory, Palace Road, Bangalore-1*)

Received March 24, 1962

(Communicated by Dr. K. S. Viswanathan, F.A.SC.)

I. INTRODUCTION

IN an isotropic solid, there are three types of elastic wave-fronts moving in any direction, of which two are transverse and the third longitudinal. A crystal also admits three sets of wave-fronts in any direction inside it and the vibration directions of these wave-fronts are orthogonal to each other, but the vibration direction of each wave-front is generally obliquely inclined to its direction of propagation. With the exception of certain directions, which are determined by the symmetry of the lattice, elastic waves inside a crystal are not strictly longitudinal or transverse. It was shown in an earlier paper[1] that the maximum inclination of the vibration direction of a wave with its direction of propagation is of the order of ten to twelve degrees for Diamond, Magnesium oxide and Copper, which belong to the cubic class of symmetry. In the present paper these calculations have been extended to a few crystals belonging to other classes also. We may mention that this phenomenon of anisotropy in elastic wave propagation is strikingly manifested by the crystal Ammonium di-hydrogen phosphate which crystallizes in the tetragonal system, and for this substance the maximum inclination of the vibration direction with its direction of propagation exceeds slightly thirty-four degrees for the quasi-longitudinal branch.

Another problem of importance in elastic wave propagation concerns the form of the elastic wave-surface for solids. The wave-surface gives us an insight into the nature of the wave-fronts divulging from a point source inside a crystal, where a disturbance has been initially set up. It is generally defined as the envelope of all planes $(lx + my + nz - v) = 0$ where (l, m, n) denotes the direction of propagation of an elastic wave and v is the velocity in this direction. Since the velocity of a wave is a function of its direction, the wave surface for a crystal is not spherically symmetric. In view of the significant deviation which the vibration direction maintains with that of the direction of propagation for the crystal ADP, it was thought desirable to carry out calculations to determine the form of the wave-surface also for this crystal. These are reported in Section III and it is shown here that the direction of the ray which signifies the direction of transport of energy has a maximum inclination of twenty-eight degrees with its direction of propagation.

II. THE VIBRATION DIRECTIONS

If $\vec{A}$ $(= Ax, Ay, Az)$ represents the amplitude of a plane elastic wave propagating in the direction (l, m, n) of a crystal, then the components of the displacement Ax, Ay and Az as well as the velocities of propagation of the three types of elastic waves are given by

$$R\vec{A} = 0 \tag{1}$$

where

$$R = \begin{bmatrix} A - \rho v^2 & \alpha\beta & \gamma\alpha \\ \alpha\beta & \beta - \rho v^2 & \beta\gamma \\ \gamma\alpha & \beta\gamma & C - \rho v^2 \end{bmatrix} \tag{1.a}$$

and

$$\begin{aligned}
A &= C_{11}l^2 + C_{66}m^2 + C_{55}n^2 + 2C_{56}mn + 2C_{15}ln + 2C_{16}lm \\
B &= C_{66}l^2 + C_{22}m^2 + C_{44}n^2 + 2C_{24}mn + 2C_{46}ln + 2C_{26}lm \\
C &= C_{55}l^2 + C_{44}m^2 + C_{33}n^2 + 2C_{34}mn + 2C_{35}ln + 2C_{45}lm \\
\beta\gamma &= C_{56}l^2 + C_{24}m^2 + C_{34}n^2 + (C_{23} + C_{44})\,mn + (C_{36} + C_{45})\,ln \\
&\quad + (C_{25} + C_{46})\,lm \\
\gamma\alpha &= C_{15}l^2 + C_{46}m^2 + C_{35}n^2 + (C_{36} + C_{45})\,mn + (C_{13} + C_{55})\,ln \\
&\quad + (C_{14} + C_{56})\,lm \\
\alpha\beta &= C_{16}l^2 + C_{26}m^2 + C_{45}n^2 + (C_{25} + C_{46})\,mn + (C_{14} + C_{56})\,ln \\
&\quad + (C_{12} + C_{66})\,lm.
\end{aligned} \tag{1.b}$$

The direction of the vector $\vec{A}$ is different from the direction (l, m, n) and in the sequel we study the inclination of these for a few crystals belonging to different classes of symmetry.

(*i*) *Hexagonal system.*—For the hexagonal system there are only five independent constants, namely, C_{11}, C_{33}, C_{44}, C_{12} and C_{13} and there exists relations of the type $C_{11} = C_{22}$; $C_{44} = C_{55}$; $C_{13} = C_{23}$; and $C_{66} = (C_{11} - C_{12})/2$.

All other elastic constants vanish. Applying these conditions, equation (1) reduces to

$$\begin{bmatrix} C_{11}l^2 + C_{66}m^2 + C_{44}n^2 - \rho v^2 & lm\,(C_{12} + C_{66}) & ln\,(C_{13} + C_{55}) \\ lm\,(C_{12} + C_{66}) & C_{66}l^2 + C_{11}m^2 + C_{44}n^2 - \rho v^2 & mn\,(C_{23} + C_{44}) \\ ln\,(C_{13} + C_{55}) & mn\,(C_{23} + C_{44}) & C_{55}l^2 + C_{44}m^2 + C_{33}n^2 - \rho v^2 \end{bmatrix} \vec{A} = 0. \tag{2}$$

Considering the wave propagation along the xy plane, *i.e.*, $n = 0$, we find that the waves become strictly longitudinal or transverse. Thus wave propagation is completely isotropic over the whole of the xy plane. This is obviously because of the relation $C_{66} = (C_{11} - C_{12})/2$ which is similar to the relation $C_{44} = (C_{11} - C_{12})/2$ that exists for isotropic solids. We may mention that of all the crystal classes, an isotropy in wave propagation over a whole plane exists for the hexagonal system only.

Passing the yz plane, the set of equations derived from (2) split into

$$\left.\begin{aligned} &Ax\left(\frac{C_{11} - C_{12}}{2}m^2 + C_{44}n^2 - \rho v^2\right) = 0 \\ &Ay\,(C_{11}m^2 + C_{44}n^2 - \rho v^2) + Az\,(C_{13} + C_{44})\,mn = 0 \\ &Ay\,(C_{13} + C_{44})\,mn + A_z\,(C_{44}m^2 + C_{33}n^2 - \rho v^2) = 0 \end{aligned}\right\}. \tag{3}$$

The wave-front having the velocity

$$V = \left\{\frac{\left(\frac{C_{11} - C_{12}}{2}m^2 + C_{44}n^2\right)}{\rho}\right\}^{\frac{1}{2}}$$

is transverse.

The other two values of v, which we denote by v_+ and v_-, give respectively the velocities of the quasi-longitudinal and quasi-transverse modes of vibration.

The angles which the vibrations directions of these two wave-fronts make with that of the direction of propagation (0, m, n) are given by

$$\cos \phi_{\pm} = \frac{n}{D_{\pm}} [(C_{13} + C_{44})\, m^2 + (\rho v_{\pm}{}^2 - C_{11} m^2 - C_{44} n^2)] \qquad (4.a)$$

where

$$D_{\pm}{}^2 = (C_{13} + C_{44})^2\, m^2 n^2 + (\rho v_{\pm}{}^2 - C_{11} m^2 - C_{44} n^2)^2 \qquad (4.b)$$

The values of ϕ_- for the quasi-transverse mode as a function of θ, where θ is the angle between the wave-normal and y-axis, are plotted in Fig. 1 for the crystals Beryllium and β quartz. The graph of ϕ_+ for quasi-longitudinal mode *versus* θ is similar to the graph of ϕ_- *versus* θ since both the modes are mutually orthogonal. For Beryllium, the values of the elastic constants are based on the results of Gold,[2] *viz.*,

$$C_{11} = 30 \cdot 8 \times 10^{11};\quad C_{33} = 35 \cdot 7 \times 10^{11};\quad C_{44} = 11 \cdot 0 \times 10^{11};$$
$$C_{12} = -\,5 \cdot 8 \times 10^{11};\quad C_{13} = 8 \cdot 7 \times 10^{11} \text{ dynes/cm.}^2$$

For β quartz, the values are taken from those of Kammer, Pardue and Frissell,[3] *viz.*,

$$C_{11} = 11 \cdot 66 \times 10^{11};\quad C_{33} = 11 \cdot 04 \times 10^{11};\quad C_{44} = 3 \cdot 606 \times 10^{11};$$
$$C_{12} = 1 \cdot 67 \times 10^{11};\quad C_{13} = 3 \cdot 28 \times 10^{11} \text{ dynes/cm.}^2$$

The maximum deviation of the wave-fronts from either longitudinality or transversality is very small for the crystal Beryllium and is of the order of 4° only; for β quartz, it is of the order of 10°.

(*ii*) *Tetragonal system.*—For the tetragonal system, equation (1) reduces to

$$\begin{bmatrix} C_{11} l^2 + C_{66} m^2 + C_{44} n^2 - \rho v^2 & lm\,(C_{12} + C_{66}) & ln\,(C_{13} + C_{44}) \\ lm\,(C_{12} + C_{66}) & C_{66} l^2 + C_{11} m^2 + C_{44} n^2 - \rho v^2 & mn\,(C_{13} + C_{44}) \\ ln\,(C_{13} + C_{44}) & mn\,(C_{13} + C_{44}) & C_{44}\,(l^2 + m^2) + C_{33} n^2 - \rho v^2 \end{bmatrix} \vec{A} = 0. \qquad (5)$$

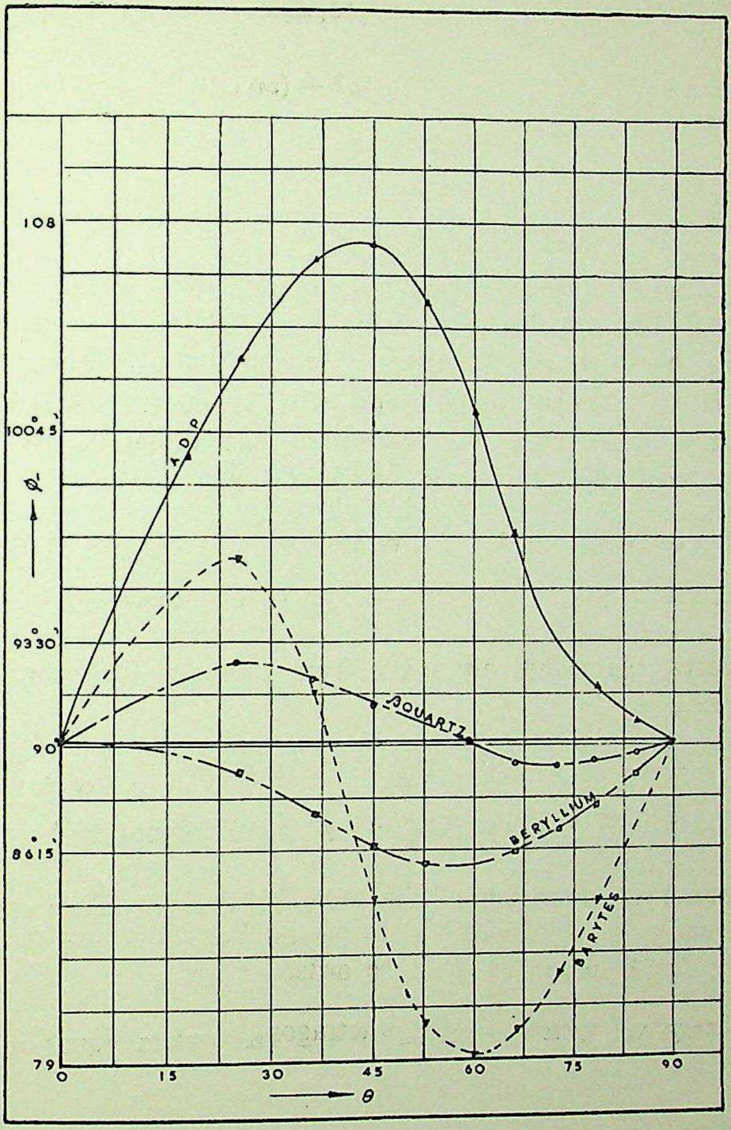

Fig. 1. Plot of ϕ_- as a function of θ in the case of ADP, Barytes, Beryllium and β quartz (ϕ_- is the angle between the vibration direction of the wavefront of quasi-transverse mode with that of the wave-normal and θ is the angle between the wave-normal and y-axis.

Considering the propagation along the xy plane we get the equations,

$$\left.\begin{aligned} &\mathrm{A}x\,(\mathrm{C}_{11}l^2 + \mathrm{C}_{66}m^2 - \rho v^2) + \mathrm{A}y\,(\mathrm{C}_{12} + \mathrm{C}_{66})\,lm = 0 \\ &\mathrm{A}x\,(\mathrm{C}_{12} + \mathrm{C}_{66})\,lm + \mathrm{A}y\,(\mathrm{C}_{66}l^2 + \mathrm{C}_{11}m^2 - \rho v^2) = 0 \\ &\mathrm{A}z\;\,(\mathrm{C}_{44} - \rho v^2) = 0 \end{aligned}\right\}. \qquad (6)$$

The wave-front having the velocity $(C_{44}/\rho)^{\frac{1}{2}}$ is transverse. The inclinations of the other two wave-fronts with that of the wave-normal $(l, m, 0)$ are given by,

$$\cos\phi_{\pm} = \frac{m}{D_{\pm}}\left[l^2(C_{12} + C_{66}) + (\rho v_{\pm}{}^2 - C_{11}l^2 - C_{66}m^2)\right] \tag{7.a}$$

where

$$D_{\pm}{}^2 = (C_{12} + C_{66})^2 l^2 m^2 + (\rho v_{\pm}{}^2 - C_{11}l^2 - C_{66}m^2)^2 \tag{7.b}$$

The deviations are calculated for the crystal Ammonium di-hydrogen phosphate. The values of $\phi_{\pm}$ as a function θ, where θ is the angle between the wave-normal and x-axis, are plotted in Figs. 2 and 3 respectively. The maximum values of ϕ_+ and ϕ_- are 35° and 125° and so the deviations exhibited by this crystal are strikingly large. The steep fall of the curve at $\theta = 45°$ is surprising, and to understand this phenomenon the value of $(d\phi/d\theta)$ at $\theta = 45°$ was evaluated.

In fact

$$\left(\frac{d\phi}{d\theta}\right)_{\theta=45°} = \frac{C_{11} - C_{66}}{C_{12} + C_{66}} - 1.$$

This has a value of the order of 57 for ADP and gives a slope angle for the curve 89° approximately. The large value of the slope angle for ADP is due to the fact that C_{12} is negative and C_{66} is small and thus the denominator $(C_{12} + C_{66})$ in the expression for $(d\phi/d\theta)$ becomes very small. The slope of the curve at $\theta = 45°$ is not so pronounced for other crystals.

Turning to the yz plane we find that

$$\cos\phi_{\pm} = \frac{n}{D_{\pm}}\left[(C_{13} + C_{44})^2 m^2 + (\rho v_{\pm}{}^2 - C_{11}m^2 - C_{44}n^2)\right] \tag{8.a}$$

where

$$D_{\pm}{}^2 = (C_{13} + C_{44})^2 m^2 n^2 + (\rho v_{\pm}{}^2 - C_{11}m^2 - C_{44}n^2)^2. \tag{8.b}$$

For this plane the maximum inclinations are found to be 17° and 117° for the quasi-longitudinal branch and quasi-transverse branch respectively. Again the deviations are substantial. For the elastic constants, the following values given by Mason and Matthias[4] were used:

$C_{11} = 6 \cdot 2 \times 10^{11}$; $C_{33} = 3 \times 10^{11}$; $C_{44} = 0 \cdot 91 \times 10^{11}$;
$C_{66} = 0 \cdot 61 \times 10^{11}$; $C_{12} = -0 \cdot 5 \times 10^{11}$; $C_{13} = 1 \cdot 4 \times 10^{11}$
dynes/cm.^{2}

(*iii*) *Orthorhombic system.*—Finally for the orthorhombic system, the equation (1) simplifies to

$$\begin{bmatrix} C_{11}l^2 + C_{66}m^2 & lm\,(C_{12} + C_{66}) & ln\,(C_{13} + C_{55}) \\ \quad + C_{55}n^2 - \rho v^2 & & \\ lm\,(C_{12} + C_{66}) & C_{66}l^2 + C_{22}m^2 & mn\,(C_{23} + C_{44}) \\ & \quad + C_{44}n^2 - \rho v^2 & \\ ln\,(C_{55} + C_{13}) & mn\,(C_{23} + C_{44}) & (C_{55}l^2 + C_{44}m^2 \\ & & \quad + C_{33}n^2 - \rho v^2) \end{bmatrix} \vec{A} = 0. \tag{9}$$

For the xy plane, equation (9) reduces to:

$$\left.\begin{aligned} &Ax\,(C_{11}l^2 + C_{66}m^2 - \rho v^2) + Ay\,(C_{12} + C_{66})\,lm = 0 \\ &Ax\,(C_{12} + C_{66})\,lm + Ay\,(C_{66}l^2 + C_{22}m^2 - \rho v^2) = 0 \\ &Az\,(C_{55}l^2 + C_{44}m^2 - \rho v^2) = 0 \end{aligned}\right\}. \tag{10}$$

The wave-front advancing with the velocity

$$\left\{\frac{(C_{55}l^2 + C_{44}m^2)}{\rho}\right\}^{\frac{1}{2}}$$

is transverse. The deviations of the other two wave-fronts from the wave normal are given by

$$\cos\phi_{\pm} = \frac{m}{D_{\pm}}\,[(C_{12} + C_{66})\,l^2 + (\rho v_{\pm}{}^2 - C_{11}l^2 - C_{66}m^2)] \tag{11.a}$$

where

$$D_{\pm}{}^2 = (C_{12} + C_{66})^2\,l^2m^2 + (\rho v_{\pm}{}^2 - C_{11}l^2 - C_{66}m^2)^2. \tag{11.b}$$

The calculations have been carried out for Barytes using the values of the elastic constants given by Seshagiri Rao.[5] These values are

$$C_{11} = 8\cdot62 \times 10^{11};\quad C_{22} = 9\cdot17 \times 10^{11};\quad C_{33} = 10\cdot84 \times 10^{11};$$
$$C_{44} = 1\cdot2 \times 10^{11};\quad C_{55} = 2\cdot87 \times 10^{11};\quad C_{66} = 2\cdot74 \times 10^{11};$$
$$C_{12} = 5\cdot23 \times 10^{11};\quad C_{13} = 3\cdot41 \times 10^{11};\quad C_{23} = 3\cdot56 \times 10^{11}$$

dynes/cm.^{2}

The values of ϕ_+ and ϕ_- are plotted against θ in Figs. 2 and 3 respectively. Their maximum values are found to be 4° 30′ and 93° while their mean values lie about 3° and 91° respectively. The calculations have been extended to the other two planes, *i.e.*, *yz* and *zx* for which the angular deviations are respectively given by the equations

$$\cos \phi_{\pm} = \frac{n}{D_{\pm}} [(C_{23} + C_{44})\, m^2 + (\rho v_{\pm}{}^2 - C_{22}m^2 - C_{44}n^2)] \quad (12.a)$$

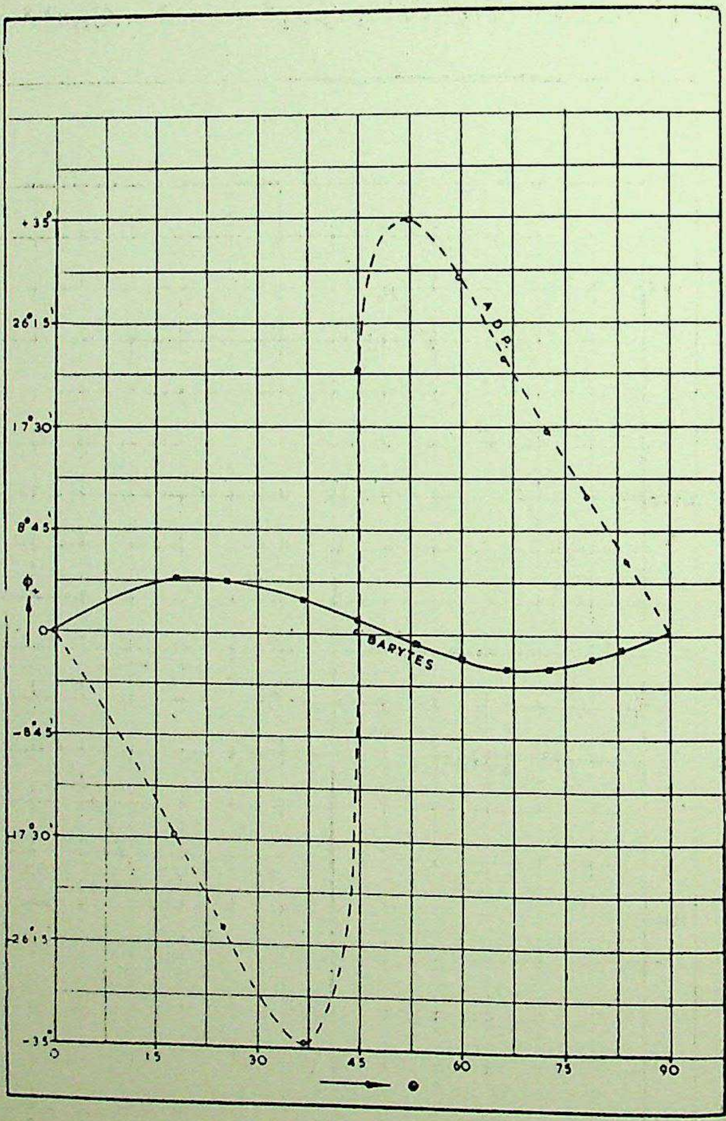

FIG. 2. Plot of ϕ_+ as a function of θ for ADP and Barytes ϕ_+ is the angle between the vibration direction of quasi-longitudinal mode and wave normal. θ is the angle between wave-normal and *x*-axis.

where

$$D_{\pm}{}^2 = (C_{23} + C_{44})^2\, m^2n^2 + (\rho v_{\pm}{}^2 - C_{22}m^2 - C_{44}n^2)^2 \quad (12.b)$$

and

$$\cos \phi_{\pm} = \frac{n}{D_{\pm}} \left[(C_{13} + C_{55})\, l^2 + (\rho v_{\pm}{}^2 - C_{11} l^2 - C_{55} n^2) \right] \qquad (13.a)$$

where

$$D_{\pm}{}^2 = (C_{13} + C_{55})^2\, l^2 n^2 + (\rho v_{\pm}{}^2 - C_{11} l^2 - C_{55} n^2)^2 \qquad (13.b)$$

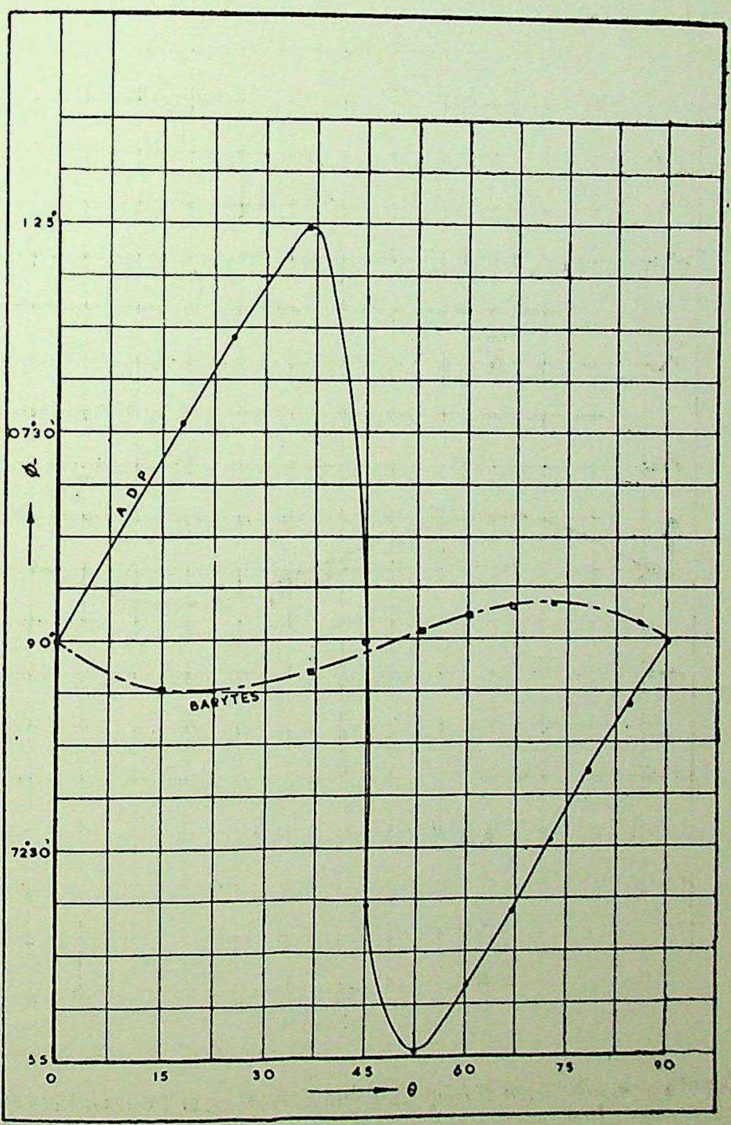

FIG. 3. Plot of ϕ_- as a function of θ for ADP and Barytes. ϕ_- is the angle between the vibration direction of quasi-transverse mode and wave-normal. θ is the angle between wave-normal and x-axis.

In the case of *yz* plane, the deviation is of the order of 10° and it is plotted in Fig. 1. For *zx* plane it is of the order of 6°.

III. WAVE-SURFACE

The wave-surface is the envelope of planes of the form

$$l\xi + m\eta + n\zeta - v = 0 \tag{14}$$

where (ξ, η, ζ) is a point on the wave-surface and v the phase velocity. Further l, m, n and v are subject to the conditions

$$l^2 + m^2 + n^2 = 1. \tag{15}$$

$$\frac{\alpha^2}{\rho v^2 - \mathrm{A} + \alpha^2} + \frac{\beta^2}{\rho v^2 - \mathrm{B} + \beta^2} + \frac{\gamma^2}{\rho v^2 - \mathrm{C} + \gamma^2} = 1. \tag{16}$$

Solving the equation (14) with the subsidiary conditions (15) and (16), we finally arrive at the following relations due to Musgrave[6]

$$\begin{aligned} v - \mathrm{A}' &= \frac{1}{2\rho v}\left[l\mathrm{L} + m\mathrm{M} + n\mathrm{N}\right] \\ \xi &= l\left[v - \frac{1}{2\rho v}(l\mathrm{L} + m\mathrm{M} + n\mathrm{N})\right] + \frac{\mathrm{L}}{2\rho v} \\ \eta &= m\left[v - \frac{1}{2\rho v}(l\mathrm{L} + m\mathrm{M} + n\mathrm{N})\right] + \frac{\mathrm{M}}{2\rho v} \\ \zeta &= n\left[v - \frac{1}{2\rho v}(l\mathrm{L} + m\mathrm{M} + n\mathrm{N})\right] + \frac{\mathrm{N}}{2\rho v} \end{aligned} \tag{17}$$

where A′ is an undetermined multiplier and L, M and N are given by

$$\begin{aligned} \mathrm{L} &= \left(\frac{p^2}{\alpha^2}\right)\mathrm{A}_l + \left(\frac{q^2}{\beta^2}\right)\mathrm{B}_l + \left(\frac{r^2}{\gamma^2}\right)\Gamma_l \\ \mathrm{A}_l &= \frac{\partial \alpha^2}{\partial l}(\rho v^2 - \mathrm{A}) + \alpha^2\frac{\partial \mathrm{A}}{\partial l} \\ \mathrm{B}_l &= \frac{\partial \beta^2}{\partial l}(\rho v^2 - \mathrm{B}) + \beta^2\frac{\partial \mathrm{B}}{\partial l} \\ \Gamma_l &= \frac{\partial \gamma^2}{\partial l}(\rho v^2 - c) + \gamma^2\frac{\partial c}{\partial l} \\ p : q : r &= \frac{\mathrm{A}x : \mathrm{A}y : \mathrm{A}z}{(\mathrm{A}x^2 + \mathrm{A}y^2 + \mathrm{A}z^2)^{\frac{1}{2}}}\,. \end{aligned} \tag{18}$$

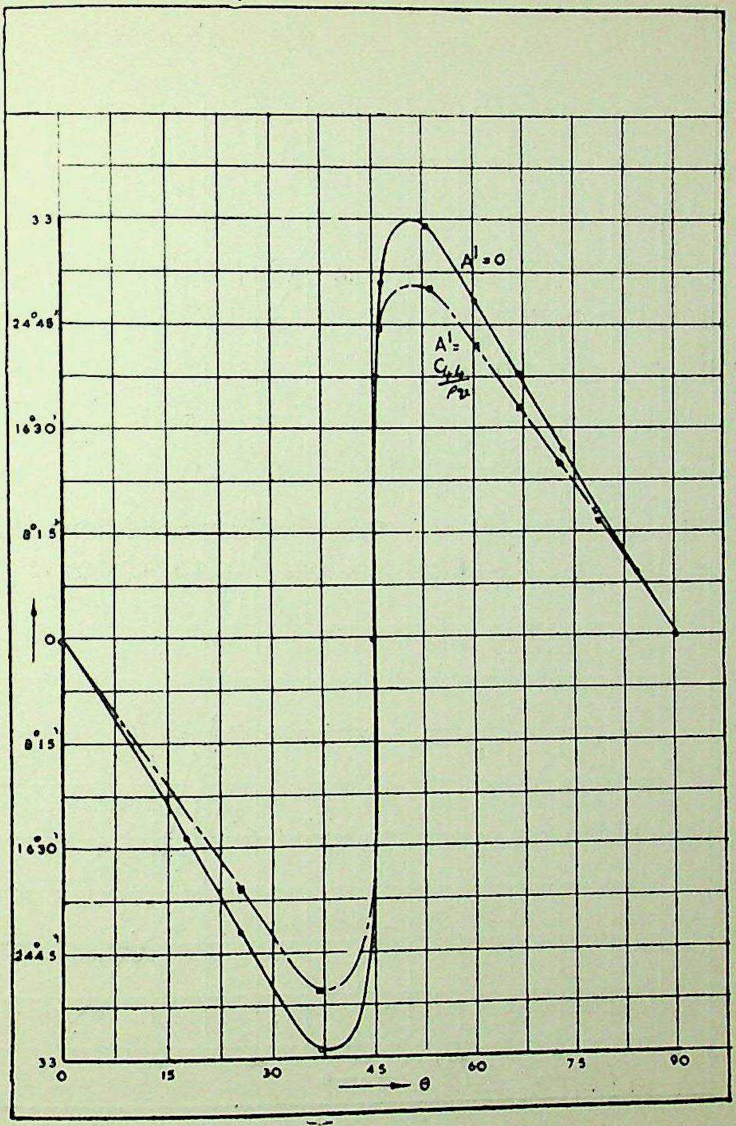

FIG. 4. Plot of ψ for xy plane as a function of θ for ADP for two values of A', A' = 0 and A' = $C_{44}/\rho v$. ψ is the angle between ray vector and wave-normal; θ is the angle between wave-normal and x-axis. A' is an arbitrary constant.

A, B, C, α, β and γ are given by the equation (1.*b*).

We have two similar equations for M and N.

The values of ξ, η, ζ are determined for the two cases, *viz.*, (*i*) $A' = 0$ and (*ii*) $A' = C_{44}/\rho v$.

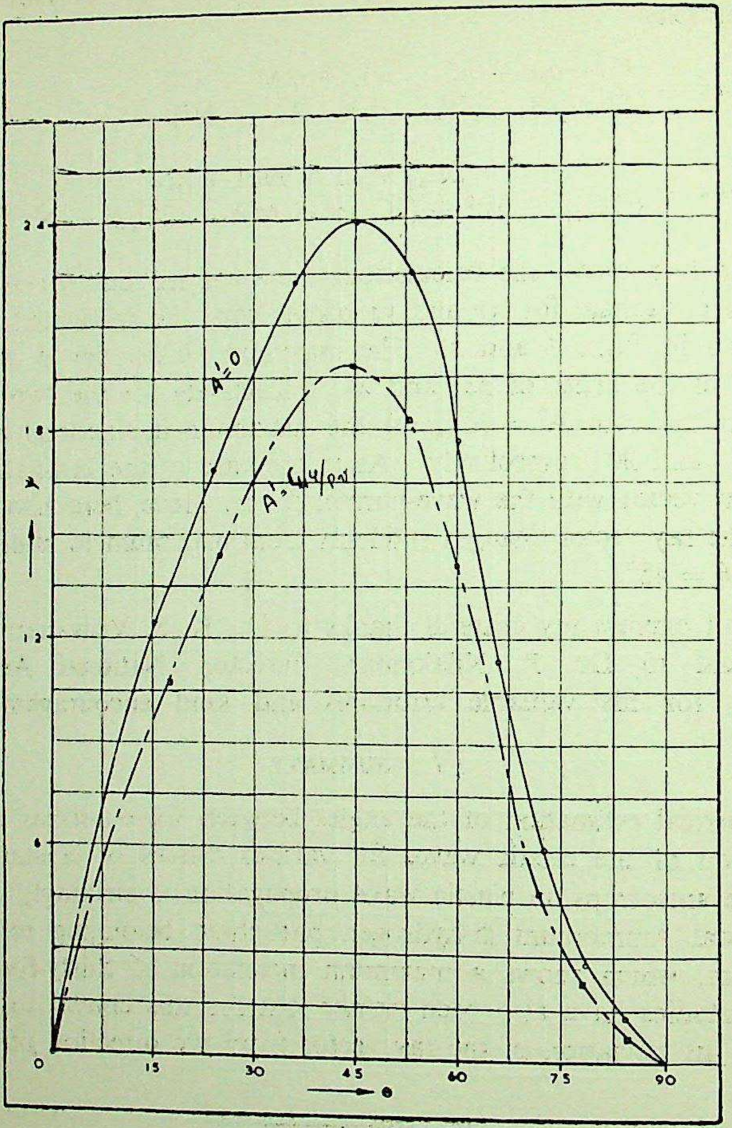

FIG. 5. Plot of ψ for yz plane as a function of θ for ADP and Barytes for two values of A', $A' = 0$ and $A' = (C_{44}/\rho v)$; ψ is the angle between the ray vector and wave-normal; θ is the angle between wave-normal and y-axis; A' is an arbitrary constant.

The co-ordinates ξ, η, ζ in these two cases are given by

$$(i)\ \xi = \frac{L}{2\rho v}\ ;\quad \eta = \frac{M}{2\rho v}\ ;\quad \zeta = \frac{N}{2\rho v} \tag{19}$$

$$(ii)\ \xi = \frac{2C_{44}l + L}{2\rho v}\ ;\quad \eta = \frac{2C_{44}m + M}{2\rho v}\ ;\quad \zeta = \frac{2C_{44}n + N}{2\rho v} \tag{20}$$

Further, the angles between the ray vector and wave-normal are given by the equations,

$$(i)\ \cos\psi = \frac{l\xi + m\eta + \eta\zeta}{(\xi^2 + \eta^2 + \zeta^2)^{\frac{1}{2}}} = \frac{l\mathrm{L} + m\mathrm{M} + n\mathrm{N}}{(\mathrm{L}^2 + \mathrm{M}^2 + \mathrm{N}^2)^{\frac{1}{2}}} \qquad (21)$$

$$(ii)\ \cos\psi = \frac{2\mathrm{C}_{44} + l\mathrm{L} + m\mathrm{M} + n\mathrm{N}}{\{(2\mathrm{C}_{44}l + \mathrm{L})^2 + (2\mathrm{C}_{44}m + \mathrm{M})^2 + (2\mathrm{C}_{44}n + \mathrm{N})^2)\}^{\frac{1}{2}}} \cdot \qquad (22)$$

For the two cases, the calculations were carried out for Ammonium di-hydrogen phosphate for xy and yz planes and the calculated values for ψ are shown in Figs. 4 and 5. The maximum values for ψ in the case $\mathrm{A}' = 0$ are of the order of 33° and 24° respectively for the two planes xy and yz. In the case $\mathrm{A}' = (\mathrm{C}_{44}/\rho v)$ the maximum inclinations are of the order of 28° and 20° respectively. As in the case of the inclination of the displacement vector with the wave-normal for xy plane, here also, the inclination of the ray vector changes suddenly from maximum to minimum near the point $\theta = 45°$.

Finally I express my grateful thanks to Dr. K. S. Viswanathan for his guidance and to Dr. P. Nilakantan, Director, National Aeronautical Laboratory, for his valuable criticisms and kind encouragement.

IV. SUMMARY

A numerical estimation of the angles between wave-normal and vibration direction of the elastic waves for various classes of crystal has been given. The anisotropy in elastic wave propagation is strikingly manifested by the crystal Ammonium di-hydrogen phosphate belonging to the tetragonal system, which shows a maximum inclination of thirty-four degrees. Numerical studies have also been carried out for this crystal to obtain an estimate of the deviation of the ray vector from the direction of the wave-normal.

V. REFERENCES

1. Viswanathan, K. S. and Venkataraman, R. *J. Sci. Ind. Res.*, 1961, **20 B**, 502–04.
2. Gold, L. .. *Phys. Rev.*, 1950, **77**, 390.
3. Kammer, E. W., Pardue, T. E. and Frissell, H. F. *J. Appl. Phys.*, 1948, **19**, 265.
4. Mason, W. P. and Matthias, B. T. *Phys. Rev.*, 1952, **88**, 477.
5. Seshagiri Rao, T. .. *Proc. Ind. Acad. Sci.*, 1951, **33**, 251.
6. Musgrave, M. J. P. .. *Proc. Roy. Soc.*, 1954, **226 A**, 339–55.

303-62. Printed at the Bangalore Press, Bangalore City, by T. K. Balakrishnan, Superintendent,
and Published by The Indian Academy of Sciences, Bangalore.

NOTICE TO AUTHORS

Scientific papers intended for publication in the *Proceedings of the Indian Academy of Sciences* can be accepted only when they are communicated by a Fellow of the Academy whose duty shall be to satisfy himself that such communications are fit to be read at the Meeting of the Academy and published in its *Proceedings*.

Papers should not ordinarily exceed fifty pages of foolscap. MSS. should be either typewritten or written in legible hand on one side of the paper. All papers should be carefully revised by the authors and should be absolutely in final form for printing. Position for text-figures should be indicated. Each paper shall conclude with a critical summary not exceeding 350 words.

Drawings, diagrams or other illustrations should be made on larger scale (preferably) twice the size than the ones in which they are intended to appear. They should be done in Indian ink on bristol board with lettering in pencil. Scale of magnification of camera lucida tracings should be indicated by the side of drawings. In certain special cases arrangements will also be made for monochrome lithographic and other colour plates. Reduction of illustrations desired should be indicated in pencil. Appropriate legends should accompany all drawings. Names of authors are to be marked in pencil on the left-hand corner of drawing sheets. Photomicrographs should be securely mounted with colourless paste.

All tables, quotations and footnotes which will be set hereafter (beginning from Vol. I, No. 2) in types smaller than the text, should be typewritten on separate sheets and placed with the text in proper sequence. Footnotes should be numbered in Arabic numerals.

References to literature in the text should be given, whenever possible, in chronological order, only the names of authors and years of publication, in brackets, being given. They should be cited in full after the summary, the authors' names following in alphabetical order. Thus,

Name or Names of author; Name of Journal (abbreviation) with a single underline; Year of publication; Number of Volume with a double underline, and lastly page. The following would be a useful illustration:—

Bergmann and Stather . . . . Z. Physiol. Chem., 1926, 152, 189.

Two copies of slip-proof and wherever possible, a page proof for final revision will be sent to authors. All corrections are best made on the slip-proof which should be transmitted to the Office of the Academy. All proof corrections involve heavy expenses which would be negligible if the papers are carefully revised by the authors before submission.

Fifty free reprints including plates and with cover will be supplied for each paper. Additional copies can be supplied at cost on previous intimation.

Blocks appearing in the *Proceedings* will be available for purchase by their respective authors. Orders for the same should be sent along with the corrected proofs and in any case not later than one month after the date of publication of the paper. The price charged would be 25% of the actual cost of the blocks *plus* freight and despatching charges. If the blocks are reproduced in other journals or publications, due acknowledgment should be made in them to the *Proceedings*.

The original drawings and plates of blocks appearing in the *Proceedings* will be returned to such of the authors as may require them provided the cost of despatching such originals is borne by them.

CONTENTS

PAGE

The Many Electron Wave Equation in the Schrödinger-Pauli Form . . . . K. S. Viswanathan 261

Diamagnetic Behaviour of Binary Liquid Mixtures . . . . R. Gopalakrishna 280

Studies in the Formation of Heterocyclic Rings Containing Nitrogen. Part IX. Condensation of Thiourea with Aromatic Aldehydes and Ammonium Acetate . . . . Khalil Ahmed and N. V. Subba Rao 284

The Raman Spectrum of Rutile . . . . D. Krishnamurti 290

Spectroscopic Studies of the Cresols. III. Emission and Absorption Spectra of Meta-Cresol in the Near Ultra-Violet Region . . . . P. Ramakoteswara Rao 300

The Anisotropy of Elastic Wave Propagation in Crystals . . . . By R. Venkataraman 311

8079

REGISTERED NO. BG. 315

PROCEEDINGS
OF THE
INDIAN ACADEMY
OF SCIENCES

VOL. LV] *SECTION A* [No. 6

JUNE 1962

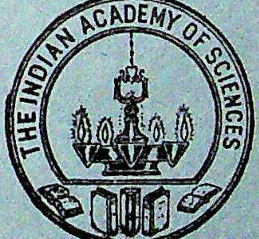

Price Rs. 4 or 6 Sh. *Annual Subscription Rs. 36*

IMPORTANT

Notice to the Subscribers of the "Proceedings of the Indian Academy of Sciences"

As from 1st January 1962, the following subscription prices for the *Proceedings of the Indian Academy of Sciences* will come into effect:—

Annual Subscription Rates

	Sections A & B	Section A	Section B
Inland ..	Rs. 72 00 nP.	Rs. 36 00 nP.	Rs. 36 00 nP.
Foreign ..	$ 18 00 cts.	$ 9 00 cts.	$ 9 00 cts.
	or	or	or
	£ 6-0-0	£ 3-0-0	£ 3-0-0

The *Proceedings of the Indian Academy of Sciences*, a monthly, which commenced its publication in July 1934 in two Sections, A and B, comprising of papers in physical and biological sciences respectively, has since then maintained an unbroken record of punctual issue on the last date of every month. Two volumes in each Section are issued every year and the 55th volume is now running. Each volume contains between pages 350 to 400 of text, 15 to 20 full-page plates and a large number of figures in the text. The *Proceedings* embody the results of the scientific research of the highest quality carried out in India.

The subscription price, which was originally fixed in July 1934, has remained unaltered all these years. The printing costs have progressively increased and are at present nearly three times the original ones. It has therefore become inevitable that the subscription rates are enhanced to enable the *Proceedings* to continue to offer to our subscribers the same volume of material and the same quality of paper, printing and illustrations as at present.

PRINTED AT THE BANGALORE PRESS, BANGALORE CITY, BY T. K. BALAKRISHNAN,
SUPERINTENDENT, AND PUBLISHED BY THE INDIAN ACADEMY OF
SCIENCES, BANGALORE

8079

ULTRA-VIOLET ABSORPTION SPECTRA AND HIGHER EXCITED STATES OF Nd^{3+} IN $LaCl_3$ AT 77° K.

BY R. M. AGRAWAL, R. K. ASUNDI, F.A.SC., R. C. NAIK, D. RAMAKRISHNAN AND SHOBHA SINGH

(Analytical Division, Atomic Energy Establishment, Trombay, Bombay, India)

Received February 26, 1962

INTRODUCTION

THE absorption spectrum of trivalent neodymium in crystals at low temperatures has been investigated by many workers in the past.[1-4] Recently a rather exhaustive work on the absorption and fluorescence spectra of Nd^{3+} in $LaCl_3$ was reported by Carlson and Dieke.[5] However, since the samples were mounted in glass tubes, their absorption data were limited to 30000 cm.$^{-1}$ only. In the present investigation we have extended the range and explored the region between 30000 and 40000 cm.$^{-1}$ by growing the experimental crystal in a vycor tube. Neodymium doped $LaCl_3$ single crystal has been selected for the reason that the lines obtained are sharp and the crystal has a higher symmetry (C_{3h}) for which the theory is rather well established.

EXPERIMENTAL DETAILS

Spectroscopically pure oxides of La and Nd supplied by Johnson and Matthey of England were used for the preparation of the chlorides. The single crystal was grown according to a modified Stockbarger method from the melt of anhydrous chlorides (5% Nd^{3+} in $LaCl_3$) contained in a sealed and tapering vycor tube filled with dry helium at a few centimetres pressure.[6] Absorption spectra at 77° K. have been photographed in the second order of the Jarrell Ash 3-metre Ebert grating spectrograph described earlier.[6] This gives a linear inverse dispersion of 2·5 A/mm. A high pressure 1,500 watt Xenon-arc lamp provided the necessary continuous spectrum. The intensity of the continuum begins to fall off in the ultraviolet but is sufficiently strong in the region explored. The light beam from this source is condensed by suitable quartz lenses and reflected along the axis of the spectrograph by a highly reflecting aluminised mirror obtained by depositing a fine film of aluminium on a glass plate by vacuum evaporation. Figure 1 shows the optical arrangement used. The tube containing the crystal was directly immersed in liquid nitrogen contained in a quartz dewar flask similar to one described earlier.[6] Observations were made with the crystal symmetry axis perpendicular to the light beam. Polarized spectra were obtained with a calcite rhomb kindly supplied by Professor P. K. Kichlu of Delhi University. Suitable filters were used to cut off the first-order spectrum. Kodak III–0 plates were used and the exposure times varied from 15–30 minutes at 3000 Å and 4–5 hours at 2500 Å. Different thicknesses of the crystal could be used and satisfactory results were obtained with thickness of 3–7 mm. Iron arc lines were recorded for standard lines.

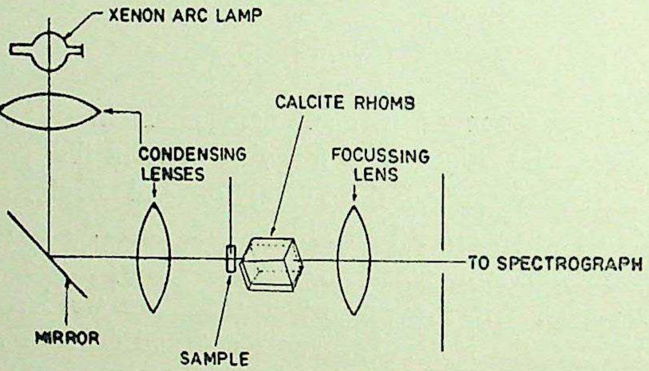

FIG. 1. Optical Arrangement for Absorption Studies

RESULTS AND DISCUSSION

Apart from the already known groups of absorption lines, five new groups of lines have been recorded in the present experiments in the region between 30000 and 40000 cm.$^{-1}$ Table I gives the wavelengths (in air) of absorption lines of these groups as obtained by measurements on several plates, together with the corresponding wave-numbers in vacuum, their observed polarisation and visually estimated intensities. The measurements are correct to ± ·02 A for the sharp lines, the accuracy being slightly lower for diffuse and/or broad lines. These lines are arranged in groups designated by letters N, O, P, Q and T, the groups R, S, A, B ···, etc., up to M being already reported by Carlson and Dieke.[5] Wybourne[7] has calculated the free ion energy values of the various states of Nd^{3+}. C. R. Sharma has also calculated* these values using Wong's method[8] of a Taylor series expansion of eigen-values. The correspondence between the calculated and observed positions of the levels is sufficiently close to allow the assignment of the newly observed groups as transitions from the ground state $^4I_{9/2}$ to the excited states $^2H_{9/2}$, $^2D_{3/2}$, ($^2H_{11/2}$ and $^2D_{5/2}$), $^2F_{5/2}$ and $^2F_{7/2}$ respectively.

---

* Private communication.

TABLE I

Absorption lines of Nd^{3+} at 77° K.

Group	State	Calculated free ion energy cm.$^{-1}$	λ in air Å	ν vac. cm.$^{-1}$	Visual intensity	Polarisation
N	$^2H_{9/2}$	32729	3069·49	32569·2	3	π
		(32495)	3068·02	32584·8	2	σ
			3067·30	32592·5	4*d*	π
			3058·80	32683·1	1*d*	π
			3056·00	32713·0	0	π
			3052·13	32754·5	7	σ
			3049·35	32784·3	10*b*	π
O	$^2D_{3/2}$	33771	3022·34	33077·3	4	π
		(33265)	3021·61	33085·3	4	σ
			3021·09	33091·0	1	σ
			3011·13	33200·5	7	σ
			3009·93	33213·7	10*b*	$\sigma\pi$
P	$^2H_{11/2}$	34119	2951·89	33866·7	2	$\sigma\pi$
	and	(33839)	2940·93	33992·9	1	π
	$^2D_{5/2}$	34970	2936·65	34042·5	8	$\sigma\pi$
		(34693)	2936·22	34047·4	4	σ
			2929·42	34126·5	8	$\sigma\pi$
			2920·25	34233·6	3	$\sigma\pi$
Q	$^2F_{5/2}$	39665	2624·38	38092·9	3	π
		(39405)	2623·87	38100·3	3	$\sigma\pi$
			2615·88	38216·7	5	σ or $\sigma\pi$
			2612·66	38263·7	3	$\pi\sigma$
T	$^2F_{7/2}$	41114	2536·66	39410·1	1	..
		(40812)	2533·05	39466·2	4	..
			2530·03	39513·4	1	..
			2529·02	39529·1	4	..
			2528·36	39539·4	2	..
			2522·20	39636·0	3	..
			2520·54	39662·1	1	..

Note.—Values in brackets in column 3 are calculated by C. R. Sharma by Wong's method.[8] Those not in brackets are from Wybourne.[7]

The relevant data are given in Table I. Group T is recorded with low intensity and it has not been possible to decide definitely about the polarisation of the lines of this group.

TABLE II

Selection rules for electric dipole transitions for an ion of configuration f^{2n+1} in a crystal field of C_{3h} symmetry

μ	$\pm 1/2$	$\pm 3/2$	$\pm 5/2$
$\pm 1/2$	..	σ	$\sigma\pi$
$\pm 3/2$	σ	π	σ
$\pm 5/2$	$\sigma\pi$	σ	..

As is seen from data in Table I, the groups appear more or less at expected positions, but it is not found possible to propose any analysis for all of them. It has been possible, however, to analyse group O completely, employing the selection rules for transitions treated as electric dipoles given in Table II, and assuming the μ-values and positions of the various stark levels of the ground state $^4I_{9/2}$ as given by Carlson and Dieke.[5] The excited state $^2D_{3/2}$ can have but two stark components with μ-values 1/2 and 3/2. From the lowest stark component of the ground state with $\mu = 5/2$, transitions to both these components are expected and observed. These lie at 33200·5 and 33213·7 cm.$^{-1}$ From the other stark components of the ground level at 115 cm.$^{-1}$ ($\mu = 1/2$) and 123 cm.$^{-1}$ ($\mu = 3/2$) which may be expected to be appreciably populated at 77° K., one and two lines respectively are expected to be observed in absorption to the levels in $^2D_{3/2}$. These are also observed. Other stark components of ground state lie too high (above 240 cm.$^{-1}$) and hence are not appreciably populated at 77° K. to give rise to any absorption lines. Thus five lines in all are expected to show up in absorption as a result of transitions from such of the stark components of the ground state as may be expected to be appreciably populated, to the stark components of $^2D_{3/2}$ and all these are observed in this group. The polarisation and intensity data support the proposed analysis. Plate XXV is a reproduction of the lines in the various groups and contains also the energy level diagram (analysis) of the transition $^2D_{3/2} \leftarrow {}^4I_{9/2}$, giving rise to the lines of the O group and their polarisation characteristics.

R. M. Agrawal and others *Proc. Ind. Acad. Sci., A, Vol. LV, Pl. XXV*

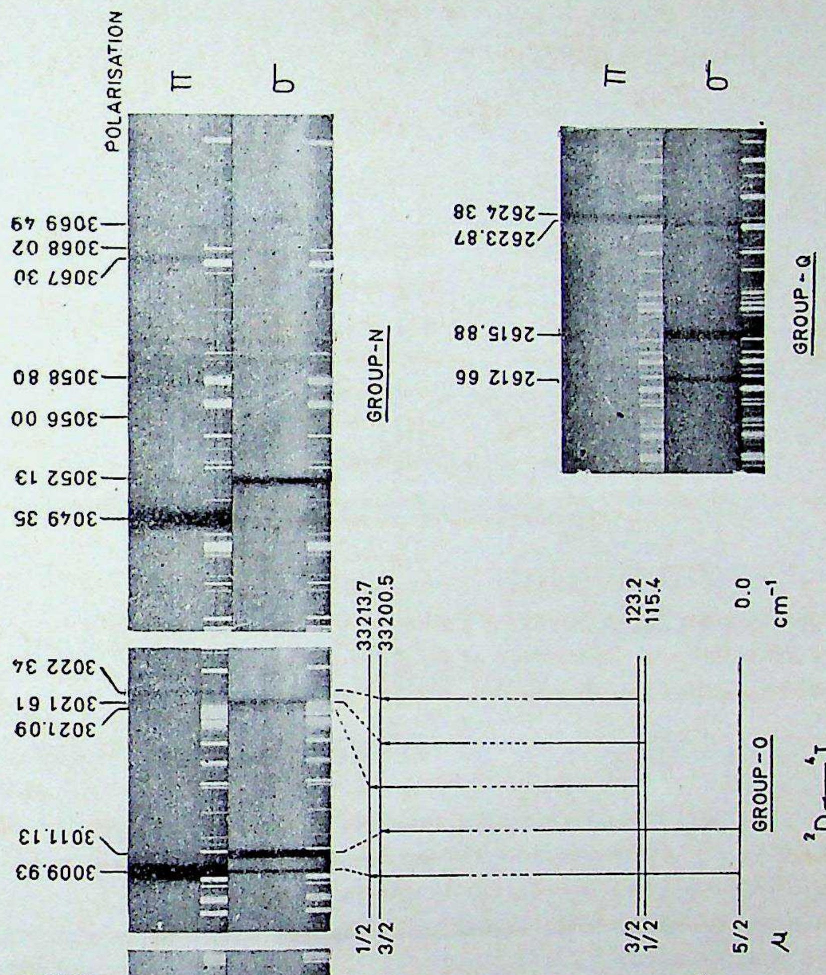

Ultra-violet Absorption Spectra of 5% Nd^{3+} in $LaCl_3$ at 77° K

More elaborate experiments at liquid helium temperature and Zeeman splitting data are necessary and may provide sufficient information to analyse the other groups recorded here.

SUMMARY

The paper deals with an extension towards shorter wavelengths of the absorption spectrum of Nd^{3+} employing a 5% Nd^{3+} doped LaCl$_3$ crystal. Five new groups of lines have been recorded and the analysis and interpretation of one of these groups, *viz.*, group O between 3010 and 3023 Å are given. The lines observed in this group are shown to be due to transitions from the ground level ($^4I_{9/2}$) stark components ($\mu = 5/2$, 1/2 and 3/2) to the two stark components ($\mu = 3/2$, 1/2) of $^2D_{3/2}$ level at about 33200 cm.$^{-1}$

REFERENCES

1. Spedding, F. H. and Hamlin, H. F. *J. Chem. Phys.*, 1937, **5**, 191 and 429.
2. Ewald, H. .. *Ann. Phys.*, 1939, **34**, 209.
3. Satten, R. A. .. *J. Chem. Phys.*, 1953, **21**, 637.
4. Dieke, G. H. and Heroux, L. *Phys. Rev.*, 1956, **103**, 1227.
5. Carlson, E. H. and Dieke, G. H. *J. Chem. Phys.*, 1961, **34**, 1602.
6. Agrawal, R. M., *et al.* .. *Proc. Ind. Acad. Sci.*, 1962. **55**, 106.
7. Wybourne, B. G. .. *J. Chem. Phys.*, 1960, **32**, 639.
8. Wong, E. Y. .. *Ibid.*, 1961, **35**, 544.

THE INFLUENCE OF DISTURBED CONDITIONS AND INCREASED SOLAR ACTIVITY ON GEOMAGNETIC DISTORTION OF THE EQUATORIAL IONOSPHERIC F2 REGION

By B. N. Bhargava and R. V. Subrahmanyan

(*Astrophysical Observatory, Kodaikanal*)

Received November 30, 1961

(Communicated by Dr. M. K. Vainu Bappu, F.A.SC.)

Abstract

The principal diurnal anomalies in the maximum electron density of ionospheric F2 layer over Kodaikanal are discussed. From an analysis of data obtained over half a solar cycle, it has been found that the phenomena of rapid increase in the electron densities following sunrise, the diurnal asymmetry and the maintenance of abnormally high ionic densities after sunset undergo systematic changes during stormy conditions. In order to examine whether these changes are accounted for by additional movements during disturbed conditions, magnitudes of movement terms of the continuity equation at three heights, for the quiet as well as the disturbed days, have been computed and discussed. The changes in the pattern of diurnal variation of N_mF2 with solar activity and the mechanism responsible for these changes are also discussed. From an analysis of published F2 layer data obtained at a number of stations with magnetic dip between ± 40°, it has been shown that the ratio of morning to afternoon peak densities yields a fair measure of equatorial F2 layer distortion anomaly. From solar cycle variation in diurnal asymmetry, an attempt has been made to estimate the extent by which the anomalous belt widens during sunspot maximum.

1. Introduction

It is well known that the morphology of the ionospheric F2 layer maximum ionic density is complex in space and time. The variation of maximum ionic density in the layer does not follow the solar zenith angle variation and is considerably subject to geomagnetic influence. On a world-wide basis, F2 layer ionization is found to be much more symmetric about the magnetic equator than the geographic equator. When the diurnal variation of the F2 layer maximum electron density at an equatorial station is considered, several anomalies are found to exist. The ionic density drops sharply during the pre-sunrise period and increases more rapidly following sunrise. Instead of an expected maximum at midday a dip is found to exist with a maximum in the late afternoon hours. There is also a tendency for high ionization to persist after sunset. These normal quiet day anomalies are found to be considerably altered during geomagnetically disturbed periods. In the present paper the magnitudes of these effects together with their diurnal, seasonal and solar activity cycle characteristics have been discussed for Kodaikanal (Geomagnetic Latitude: 0°·6 N; Dip. 3°·5 N). Vertical incidence day-time data since July 1952 and round-the-clock data since September 1955 have been utilized for this study.

2. DISTORTION ANOMALY AND IONIC DRIFTS

The geomagnetic distortion anomaly at low and moderate latitudes has been explained by Martyn (1954) in terms of his electrodynamic drift theory. According to this theory, the electrostatic (polarization) field E developed in the 'dynamo' region produces currents in the F region. These currents interact with the main magnetic field of the earth as a consequence of which vertical and horizontal drifts of ionization are caused. The vertical drift velocity v at a place with dip ϕ is given by:

$$v = \frac{E_y}{F} \cos \phi$$

where F is the main magnetic field and E_y is the eastward component of the electric field. Under the influence of the vertical drift loss of ionization takes place and the maximum divergence of the ionization occurs along the line of "zero" dip where the vertical transport velocity is directed upward during the day with maximum enhancement of its magnitude.

3. THE EFFECT OF INCREASED MAGNETIC ACTIVITY ON DIURNAL VARIATION IN N_mF2

The influence of magnetic storminess on F2 layer maximum ionic density has been examined by Berkner and Seaton (1940), Appleton and Piggott (1952) and Wright and Skinner (1955). At Kodaikanal N_mF2 values on disturbed days are, generally, in excess of those observed on quiet days. It has also been noticed that the magnitude of the noon-'bite-out' effect progressively decreases with increasing geomagnetic activity. In order to examine these effects systematically, all internationally quiet and disturbed days from September 1955 to June 1958 were classified into four categories. These were designated Very Quiet (V.Q.), Quiet (Q), Disturbed (D) and Very Disturbed (V.D.). Very quiet days were selected out of all international quiet days and very disturbed days out of international disturbed days. The magnetic activity and percentage of days in each category are given in Table I.

TABLE I

Sl. No.	Magnetic activity		Symbol	Magnetic activity	Percentage number of days in each group
1.	Very quiet	..	V. Q.	$\Sigma K_p \leqslant 7$	≈ 15
2.	Quiet	..	Q.	All international quiet days	≈ 53
3.	Disturbed	..	D.	All international disturbed days	≈ 47
4.	Very disturbed	..	V. D.	$\Sigma K_p \geqslant 38$	≈ 11

The averages of mean hourly values of $(\text{foF2})^2$ for all the days in each one of the four categories were obtained and these are plotted in Fig. 1. Both the characteristics of this station, *i.e.*, progressive increase in N_mF2, at all hours, with increased magnetic activity and reduced midday minimum are at once seen. The mean of 24-hourly values for very quiet and very disturbed days were also subjected to harmonic analysis and the results (Table II) indicate that the daily mean value of N_m is about 15% higher and the amplitude of the diurnal term lower on disturbed days. The amplitude of the semi-diurnal term is, however, considerably higher on disturbed days indicating that the perturbation of the quiet day (S_q) variations superposed on disturbed days (S_D) has not only a diurnal component but also a marked semi-diurnal component due to the effect of net disturbance current system. For equatorial latitudes, this current system is directed westwards at about noon and afternoon hours causing an increase in the magnitude of downward drift velocity associated with solar semi-diurnal tides in the ionosphere and pushing the region to lower levels at these times. Because of this contraction of the region on disturbed days, the ionization above the density peak descends to lower levels and adds to the ionization therein. Further, as seen in Fig. 1, night-time electron density is considerably enhanced on disturbed days.

$N_m \propto (f_oF_2)^2$

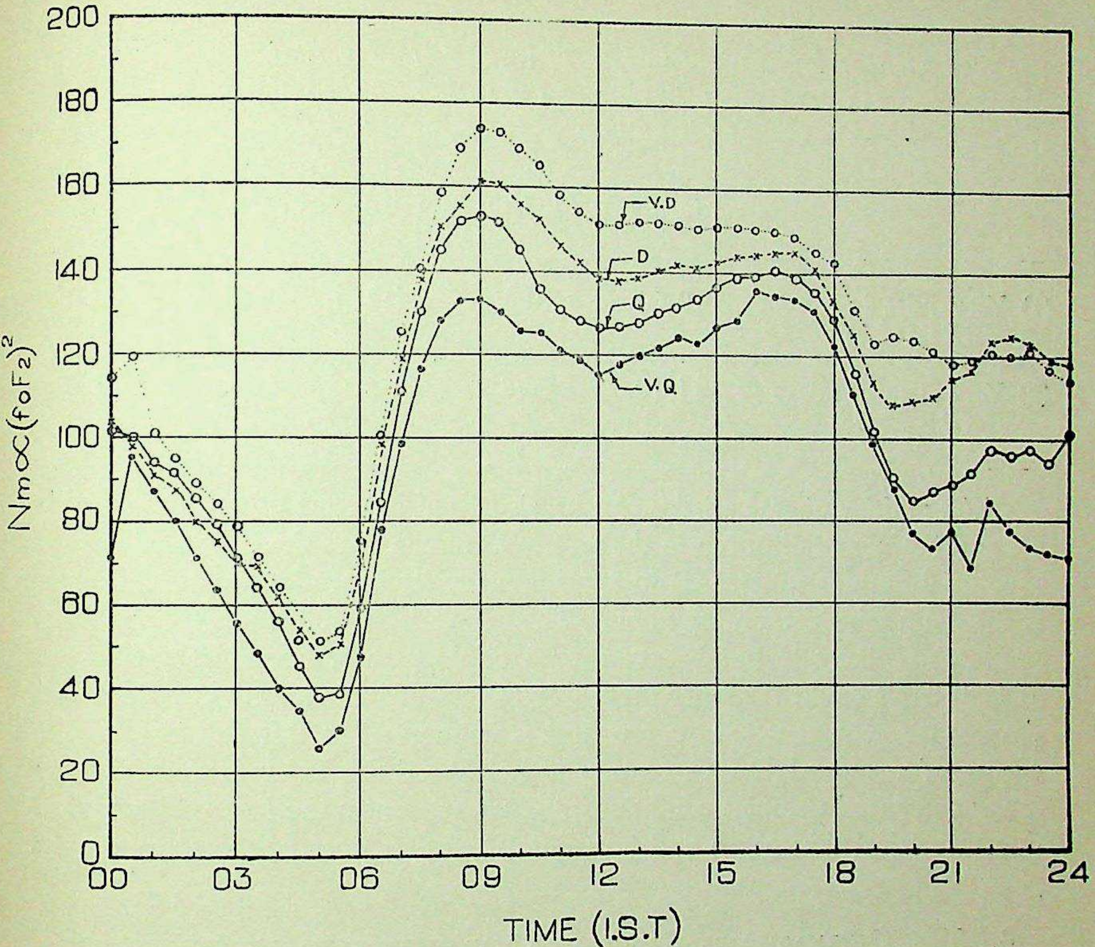

FIG. 1. **Diurnal Variation of NmF2 for Different Stages of Magnetic Activity.**

The basic continuity equation of electron density **N** is:

$$\frac{\partial N}{\partial t} = I(t) \cdot f(x, h) - \beta(h) \cdot N - \nabla \cdot (\bar{v}N) \qquad (a)$$

where I (t) represents the intensity of solar ionizing radiation, $f(x, h)$ represents the way in which the rate of ion production depends on solar zenithal angle x and height h, $\beta(h)$ is the attachment-like loss coefficient and $\nabla \cdot (\bar{v}N)$ is the movement term M, $\bar{v}$ being the transport velocity of electrons.

Immediately after sunset when $I(t) = 0$ and $\bar{v}$ is downwards, it can be shown that $\partial N/\partial t$ is positive if $(\partial/\partial z)(\bar{v}N)$ is $> \beta N$. At a given level z, therefore, the electron loss is more than compensated, on disturbed days, by an increase from enhanced downward drift. No significant differences are found to exist in the phases on quiet and disturbed days.

TABLE II

Summary of harmonic analyses of mean diurnal variation of foF2: (1) very quiet days and (2) very disturbed days

	R_0 Mc./sec.	R_1 Mc./sec.	t_1 (Hr.)	R_2 Mc./sec.	t_2 (Hr.)
(1) Very quiet days ($\Sigma K_p \leqslant 7$)	9·60	2·08	14·3	0·63	10·4
(2) Very disturbed days ($\Sigma K_p \geqslant 38$)	11·10	1·78	14·3	1·04	10·2

The midday characteristics can be visualized in terms of vertical spreading and horizontal diffusion in the layer. On quiet days the effects of intense equatorial current (electrojet) in spreading the layer are large and the layer is lifted up considerably at noon. Though vertical diffusion (proportional to $\sin^2\phi$) is likely to be absent at equatorial stations, horizontal diffusion at high levels could take place resulting in loss of ionization. On disturbed days, when geomagnetic H component is subnormal in this belt due to the effects of westward Dst currents, the height of the layer is considerably lower compared to quiet conditions and consequently the loss of ionization due to vertical divergence and horizontal diffusion does not appear to take place.

4. THE DIURNAL AND SEASONAL CHARACTERISTICS OF IONOSPHERIC STORMINESS

From data for the period September 1955 to June 1958 the ratios of foF2 for international disturbed days and quiet days are plotted in Fig. 2 for winter, equinoxes and summer conditions. It will be seen that the ratio D (foF2)/Q (foF2) exceeds unity during all seasons throughout the 24 hours except for a short night time period in summer. There is a marked increase in the ratio for the pre-sunrise and post-sunset periods. A moderate noon maximum also exists during all seasons. The values plotted in Fig. 2 were harmonically analyzed and the amplitudes and phases for the three seasons, given in Table III, indicate that the amplitude of the first harmonic is largest in winter. The second harmonic is higher than the first in summer and at the equinoxes but lower in winter. Significant phase differences exist in the semi-diurnal term between the equinoxes and summer on one hand and between the equinoxes and winter on the other, These may be attributed to slight shift in the vertical tide in the F2 region due to seasonal changes in electrical conductivities and in quiet day magnetic variation (Sq.).

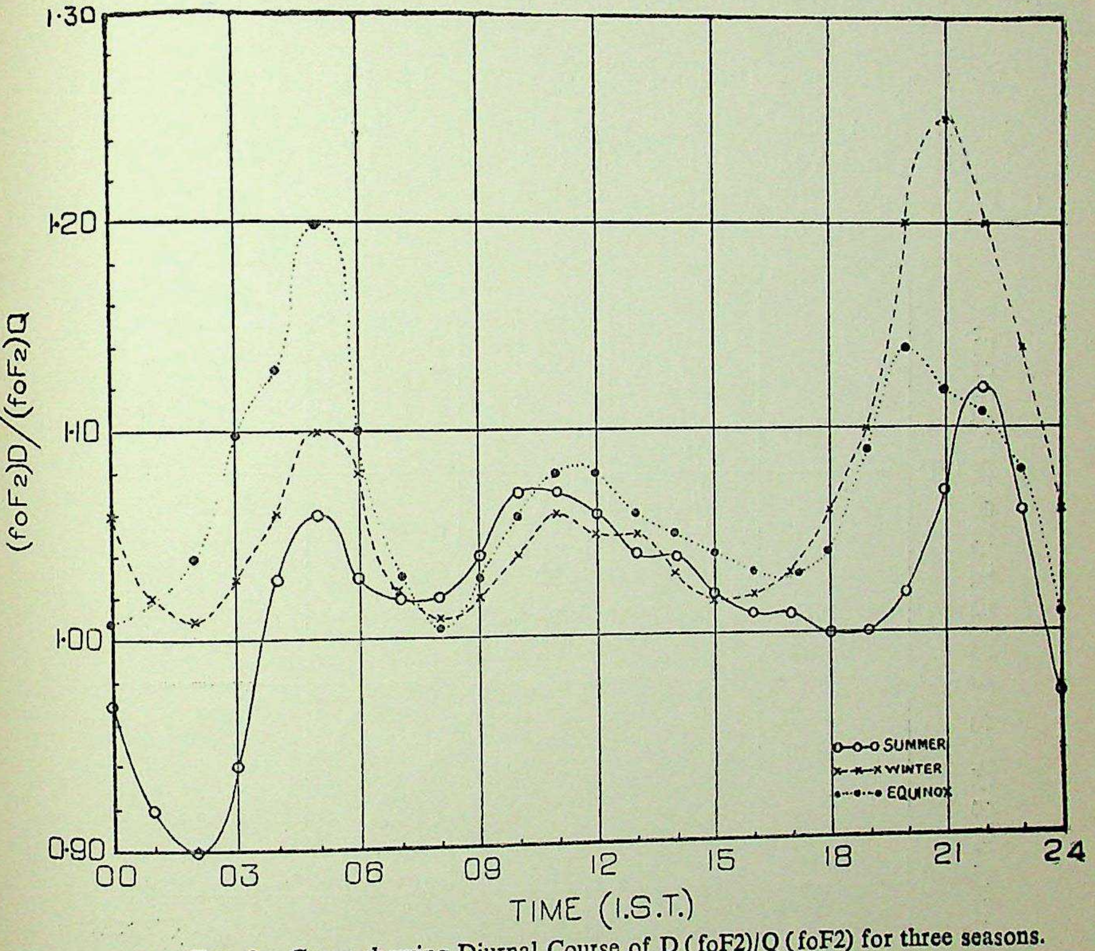

FIG. 2. Curve showing Diurnal Course of D (foF2)/Q (foF2) for three seasons.

TABLE III

	Summer Unit × 10^{-2}Mc./sec.					Equinoxes Unit × 10^{-2}Mc./sec.					Winter Unit × 10^{-2}Mc./sec.				
	R_0	R_1	ϕ_1	R_2	ϕ_2	R_0	R_1	ϕ_1	R_2	ϕ_2	R_0	R_1	ϕ_1	R_2	ϕ_2
$\frac{D}{Q}$(fo F2) ..	102·4	2·61	209°	3·47	272°	106·5	2·49	31°	3·90	207°	106·1	4·42	311°	3·18	259°

5. IONOSPHERIC BEHAVIOUR DURING A SINGLE STORM

In order to find the magnitude and nature of movements during a typical storm, ionospheric data of September 4, 1958, when a severe magnetic storm of range 532 γ in H was recorded at Kodaikanal, were analysed together with similar data for a 'control' day, two days earlier to the storm, when the magnetic character figure Ci was $0 \cdot 1$. The selected 'control' day was preceded and followed by quiet conditions and, therefore, free of residual storminess.

For three selected heights of 250, 300 and 350 km., $N-h$ profiles were obtained from $h'-f$ records using the appropriate coefficients given by Schmerling and Ventrice (1959) for both the storm and control days. The $(N-t)_h$ curves obtained from $N-h$ profiles are plotted in Fig. 3.

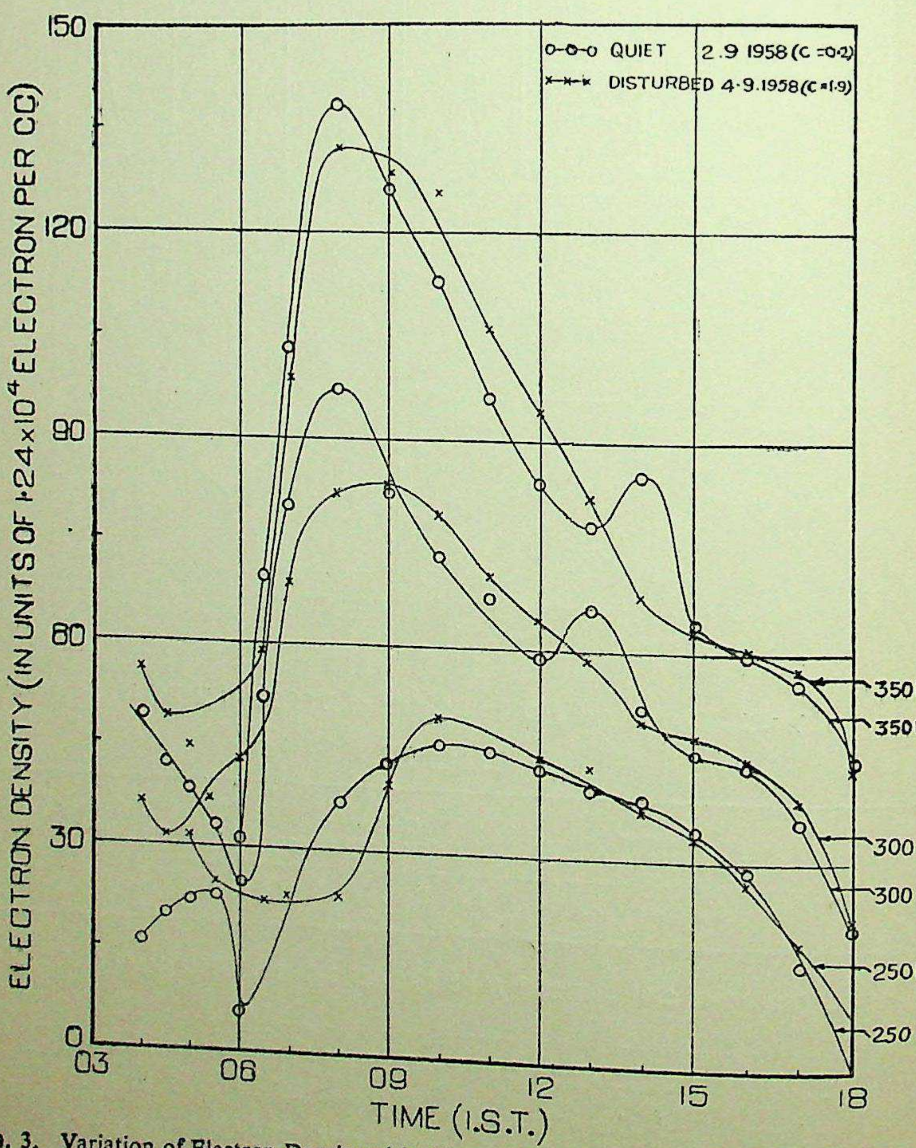

FIG. 3. Variation of Electron Density with Time at Fixed Heights during Sunspot Maximum for Disturbed and Quiet Days.

Using values of N and dN/dt from these curves and computing β (h) after Ratcliffe *et al.* (1956) and $f(x, h)$ and $I(t)$ from the usual expressions, the magnitudes of the movement terms were obtained, at intervals of one hour, from the continuity equation.

The control day movement term Mq for a selected true height of 300 km. together with the difference $\triangle$ M (= $M_Q - M_D$) for the same level is plotted in Fig. 4. These curves together with $(N - t)\,h$ curves of Fig. 3 indicate

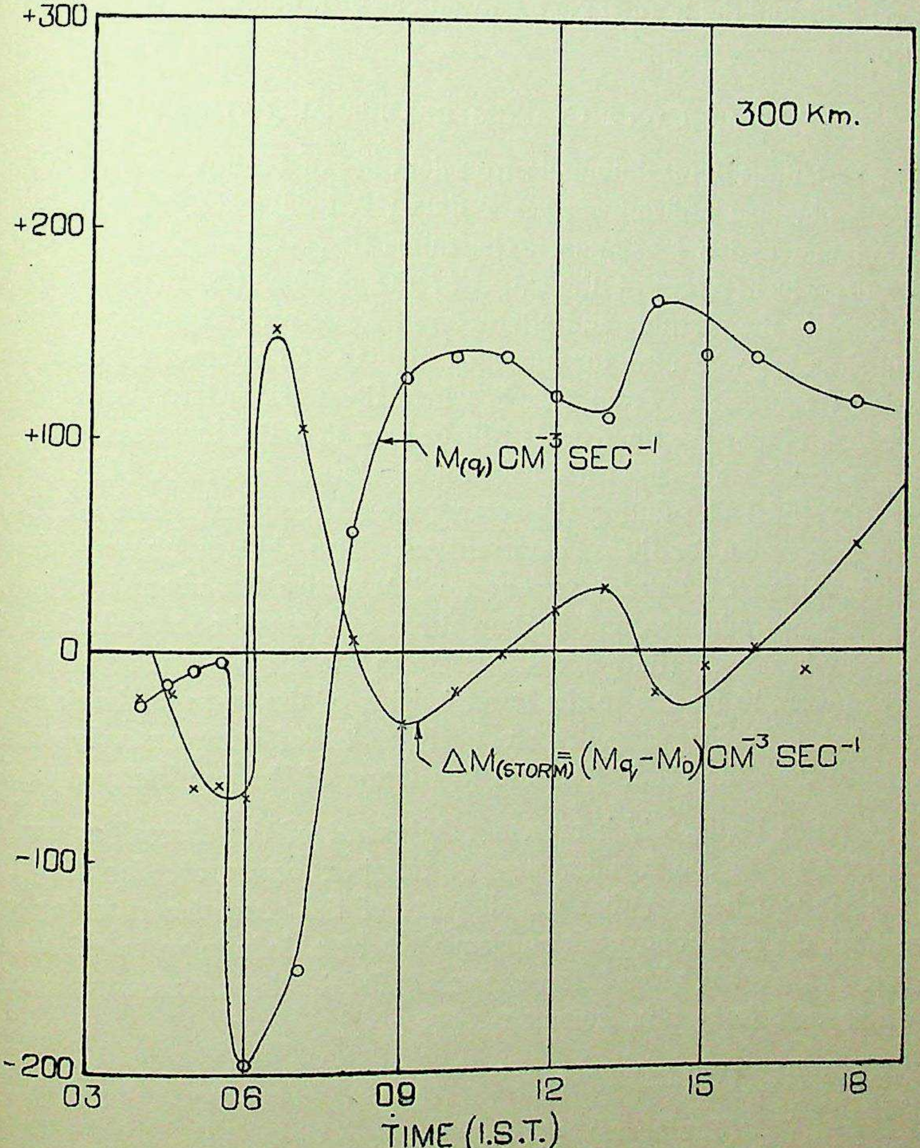

FIG. 4. Variation of Movement Term M (Quiet) = (N.dw/dh) cm.$^{-3}$. sec.$^{-1}$ with time together with $\triangle$ M (due to storm). For 300 km. level.

that normal quiet day N_mF2 characteristics were substantially modified due to the existence of additional movements on disturbed days; such movements also eliminated the midday decrease. According to Martyn (1953), the additional movement term during a storm is due to the electrostatic (polarisation) field created by currents set up in the auroral zone by incoming solar particles. This polarisation field spreads all over the earth during a storm and sets up currents in the F2 region; these currents, in turn, distort the region to a considerable extent through interaction with the earth's main magnetic field and the normal N_mF2 variations of a quiet day are, therefore, modified.

6. SOLAR CYCLE CHANGES IN DIURNAL ASYMMETRY

The variations in maximum electron densities of F2 layer at Kodaikanal have been obtained utilizing six years' data (1952–58) covering both a sunspot minimum and a maximum. The ratios $P_m = (f_1 - f_2)/f_2$ and $P_a = (f_3 - f_2)/f_2$ which represent the extent of the midday distortion in N_mF2 with respect to the morning and afternoon peaks respectively were computed from f_1, f_2 and f_3 which are the morning, midday and afternoon peak values of critical frequencies. From Fig. 5, where these ratios have been plotted as functions of sunspot number, it will be seen that P_m increases gradually and P_a decreases rapidly with increasing solar activity. A shift in the phases of vertical tide during the solar cycle (Hirono and Maeda, 1954) is perhaps responsible for these characteristics. This shift in phase is due to change in phase of diurnal variation of 'effective' conductivity, in the pattern of ion production and in the pattern of atmospheric oscillation due to irregular heating. The gradual increase in the morning peak with solar activity appears to be due to the lower heights of the layer in the forenoon hours when drift characteristics are likely to be of comparatively smaller importance than the production and loss terms of the continuity equation.

The ratios P_m/P_a which represent the extent of the diurnal asymmetry are plotted in Fig. 6 against sunspot number, separately for the three seasons. It will be seen that for all parts of the year, the morning peak approaches the afternoon peak and equals it at a definite value of sunspot number. This value, given below separately for the three seasons, is smallest in winter and largest in summer.

R_z (Winter) ≈ 89

R_z (Equinoxes) ≈ 142

R_z (Summer) ≈ 173

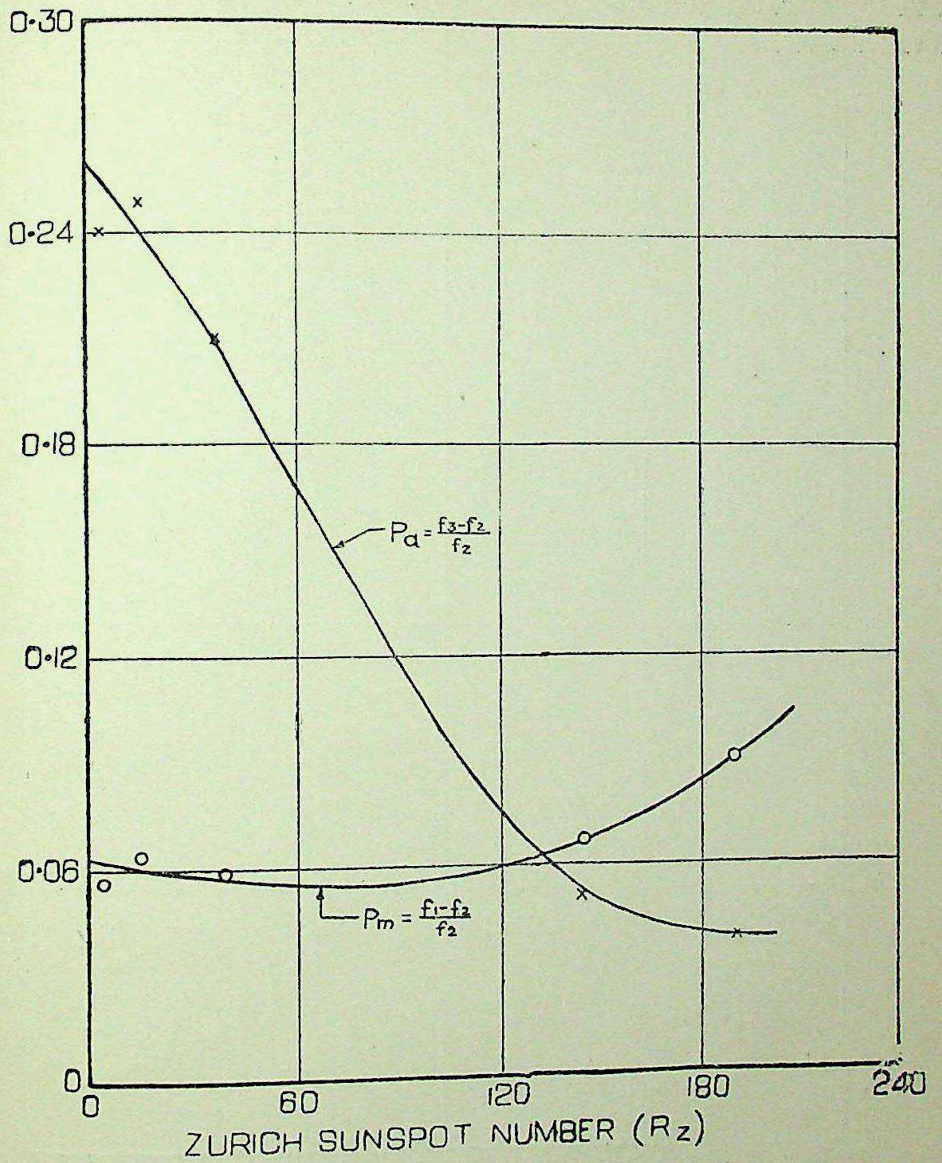

FIG. 5. Comparative Behaviour of Morning and Afternoon Peaks with Sunspot Activity.

At an equatorial station like Kodaikanal where the F2 region is lowest in winter months and highest in summer, the magnitude of drift effects in winter will be comparatively smaller than in summer because of the larger contribution from the electron production and loss terms of the continuity equation during the winter. As the diurnal asymmetry arises from vertical transport of ionization, the magnitudes of the drifts are of different orders during winter and summer. The large differences in the values of R_z for which the morning and afternoon peak ionization are equal are, therefore, understandable.

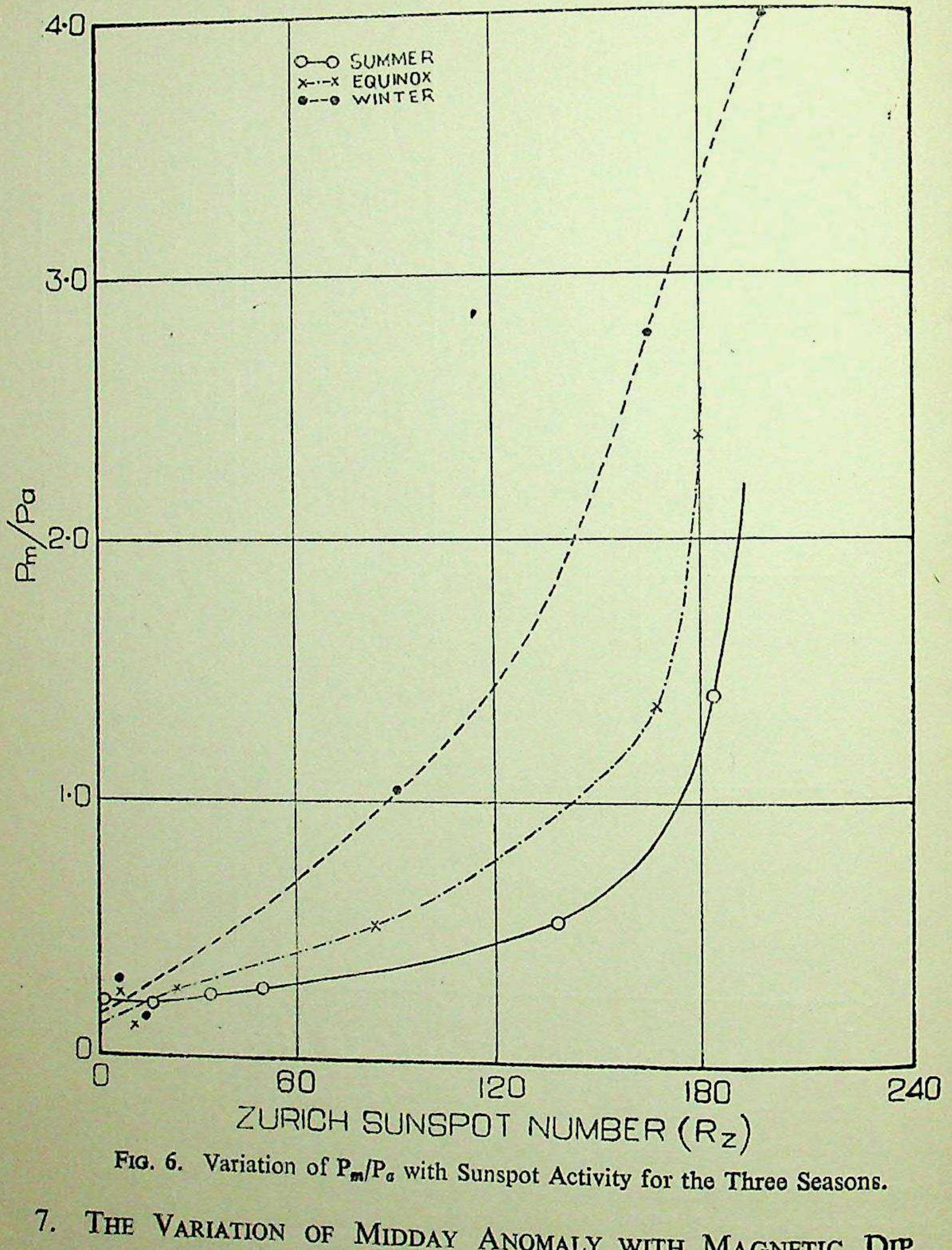

FIG. 6. Variation of P_m/P_a with Sunspot Activity for the Three Seasons.

7. THE VARIATION OF MIDDAY ANOMALY WITH MAGNETIC DIP

In order to obtain the variation in the noon anomaly with magnetic dip and in the extent of the anomalous belt from a sunspot minimum to a maximum, ionospheric data from several low latitude stations with their magnetic dip between 19°·0 N and 28°·5 S listed in Table IV, for the years

1954 and 1957 were examined. The plots of foF2 averaged over a year indicated that for the year 1954 it was possible to identify both the morning and the afternoon peaks only for stations which were located within a dip zone from 14°·0 N to 16°·0 S. For the year 1957, however, it was noticed that these peaks could be identified for stations substantially farther from the dip equator. The three frequencies f_1, f_2 and f_3 were read from the foF2 plots for each one of the stations and the values were utilised to obtain the magnitudes of the midday distortion, represented by the ratio P_m/P_a. The ratios are plotted against the respective dip of the station in Figs. 7 (*b*) and 7 (*c*) for the years 1954 and 1957 respectively.

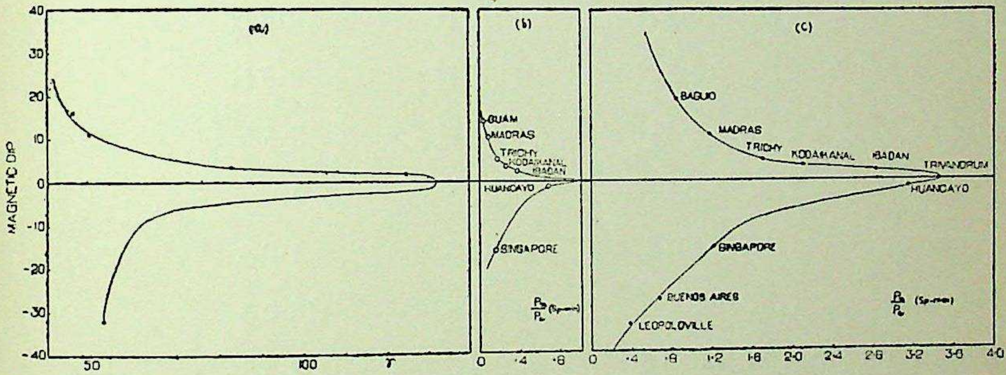

FIG. 7. (*a*) Distribution of Ranges of Daily Variation of the Horizontal Force against Magnetic Dip (After J. Egedal). (*b*) Variation of P_m/P_a with Magnetic Dip (Sp-min.). (*c*) Variation of P_m/P_a with Magnetic Dip (Sp-max.).

TABLE IV

Sunspot minimum (1954)

Station		Latitude		Dip ϕ	P_m/P_a
		Geogr.	Geomag.		
		(°)	(°)	(°)	
Guam	..	13·5 N	3·9 N	14·0 N	0·06
Madras	..	13·0 N	3·1 N	10·5 N	0·10
Trichy	..	10·5 N	1·3 N	4·8 N	0·18
Kodaikanal	..	10·2 N	0·6 N	3·5 N	0·26
Ibadan	..	7·2 N	10·4 N	2·5 N	0·37
Huancayo	..	12·0 S	0·6 S	1·0 S	0·69
Singapore	..	1·2 N	10·1 S	16·0 S	0·18

TABLE IV—(*Contd.*)

Sunspot maximum (1957)

Station	Latitude		Dip ϕ	P_m/P_a
	Geogr.	Geomag.		
	(°)	(°)	(°)	
Baguio ..	16·2 N	7·0 N	19·0 N	0·83
Madras ..	13·0 N	3·1 N	10·5 N	1·18
Trichy ..	10·5 N	1·3 N	4·8 N	1·67
Kodaikanal ..	10·2 N	0·6 N	3·5 N	2·08
Ibadan ..	7·2 N	10·4 N	2·5 N	2·81
Trivandrum ..	8·4 N	0·5 S	0	3·43
Huancayo ..	12·0 S	0·6 S	1·0 S	3·18
Singapore ..	1·2 N	10·1 S	16·0 S	1·21
Buenos Aires ..	34·5 S	23·1 S	28·5 S	0·71
Leopoldville ..	4·3 S	3·1 S	33·5 S	0·39

It will be seen that the magnitude of the ratio P_m/P_a is largest along 'zero' dip and that it further increases rapidly with solar activity from about unity at sunspot minimum to about 3·4 at sunspot maximum. The variations also indicate that the distortion anomaly belt is much wider during periods of high solar activity than those of low activity. With increased solar activity, geomagnetic distortion appears at stations with comparatively large dip like Baguio (Dip: 19° N), Beunos Aires (Dip: 28°·5 S) and Leopoldville (Dip: 33°·5 S). This indicates that in spite of the downward movement of ionization due to vertical diffusion (Ferraro, 1945) the 'effective' conductivity becomes, during high solar activity, adequate for the occurrence of drifts and consequent divergence of ionization around noon at these stations. Recently, Appleton (1960), in his plots of equatorial foF2 data for 1958 (a year of sunspot maximum) with magnetic latitude for different hours of the day, found that the equatorial 'trough', centred on the magnetic equator, is more extensively exhibited at Sp-max. than at Sp-min. From curves (*b*) and (*c*) of Fig. 7 we have obtained values of dip at Sp-min. (1954) and close to Sp-max. (1957) corresponding to P_m/P_a ratios between 0·2 and 0·8 (Table V). It will be seen that from the point of view of F2 layer anomaly, the extent of the belt during Sp-max. covered stations whose magnitudes of dip were greater by about 25°.

TABLE V

P_m/P_a	1954	1957	Extension of geomagnetic anomalous belt
	Dip ϕ	Dip ϕ	Dip ϕ
	(°)	(°)	(°)
0·2	14·5	40·0	25·5
0·4	6·0	33·0	27·0
0·6	3·0	29·0	26·0
0·8	0·8	24·0	23·2
		Mean	25·4

8. DISTORTION ANOMALY AND EQUATORIAL ELECTROJET

In Fig. 7 *a*, Egedal's (1947) curve of the variation in daily range in horizontal force with dip is reproduced along with the variation of P_m/P_a. A remarkable similarity of the three curves is obvious. Similar variations with dip of intense sporadic E in the vicinity of magnetic equator was reported by Matsushita (1952). It appears that the ratio P_m/P_a which gives a measure of vertical divergence of N_mF2 around noon may be due to the effect of drifts associated with Hall polarisation field related to the intense eastward current—the so-called electrojet. The seasonal variation of this ratio appears to arise from possible movement of electrojet itself like that of the Sq. current system while the solar cycle variation of the ratio appears to be due to enhanced ionospheric conductivity resulting from increased solar activity to which the electrojet is sensitive.

9. ACKNOWLEDGEMENT

The authors wish to express their thanks to Dr. M. K. Vainu Bappu for his interest in this investigation.

10. REFERENCES

1. Appleton, E. V. and Piggott, W. R. *J. Atmosph. Terr. Phys.*, 1952, **2**, 236.
2. Applaton, E. V. .. "Some ionospheric results obtained during the I.G.Y.", *Proceedings of the Symposipm Organised by the URSI/ AGI Committee*, Brussels, (1959), Edited by W. J. G. Beynon, 1960, p. 4.
3. Berkner, L. V. and Seaton, S. L. *Terr. Mag. and Atmos. Elec.*, 1940, **45**, 419.
4. Egedal, J. .. *Ibid.*, 1947, **52**, 449.
5. Ferraro, V. C. A. .. *Ibid.*, 1945, **50**, 215.
6. Hirono, M. and Maeda, H. *J. Geomagn. Geoelectt* 1954, **6**, 127.
7. Martyn, D. F. .. *Proc. Roy. Soc.*, 1953, **218 A**, 1.
8. ——————— .. *Report of Conference on Physics of the Ionosphere*, Physical Society, London, 1954, 257.
9. Matsushita, S. .. *Proceedings of Mixed Commission on the Ionosphere*, Third Meeting (Canberra), 1952, p. 124.
10. Ratcliffe, J. A., Schmerling, E. R., Setty, C. S. G. K. and Thomas, J. O. *Phil. Trans.*, 1956, **248 A**, 621.
11. Skinner, N. J. and Wright, R. W. *J. Atmosph. Terr. Phys.*, 1955, **6**, 177.
12. Schmerling, E. R. and Ventrice, C. A. *Ibid.*, 1959, **14**, 249.

SYNTHESIS OF 3:4 DIHYDRO-5-METHYL-2H-PYRANO-(2, 3-*b*)-QUINOLINE

By V. T. Ramakrishnan and P. Shanmugam

(*Department of Organic Chemistry, University of Madras, Madras-25*)

Received February 28, 1962

(Communicated by Dr. K. N. Menon, F.A.SC.)

Raman, P. S. had found[1] that Allylacetoacetanilide (I) on cyclization with polyphosphoric acid did not give 3-allyl-4-methyl-2-quinolone (II) as expected, but underwent further cyclization to give a base, formulated to be III. It was

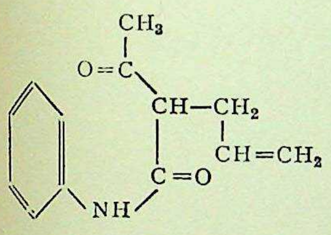
I

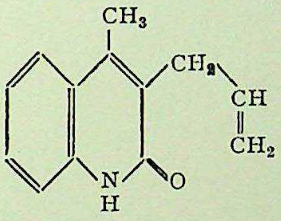
II

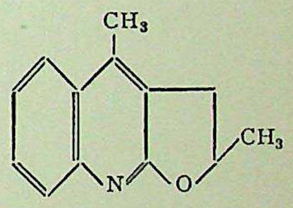
III

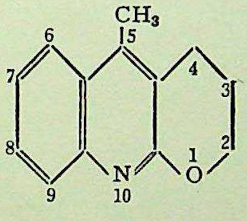
IV

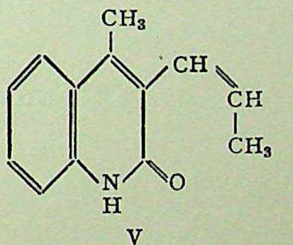
V

analogous to the formation of Dihydro-benzofurans,[2] from allyl-phenols, on treatment with acids. The alternate possible structure IV was ruled out on the basis of the absorption spectra. The correctness of the above formulation (III) for the product was shown, in the previous paper,[3] by obtaining it from V by ring closure.

Now it would be of interest to prepare IV by an unambiguous method and prove its non-identity with the product from allylacetoacetanilide, and compare its absorption spectrum with that of III, IV is synthesised according to the scheme,

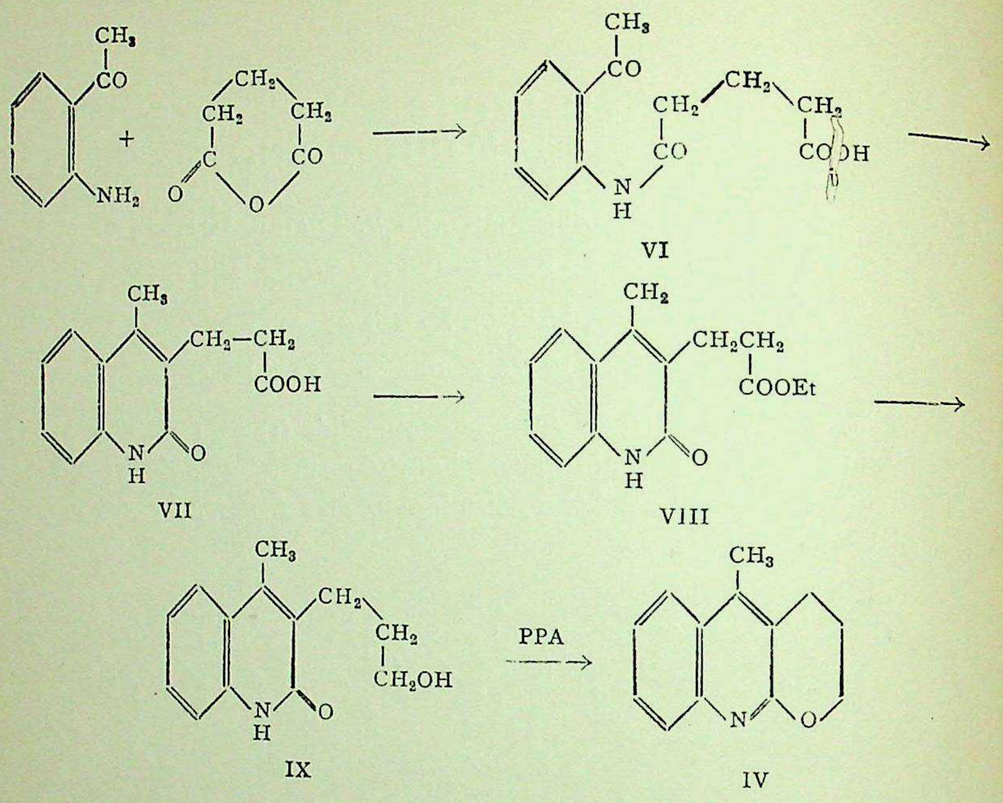

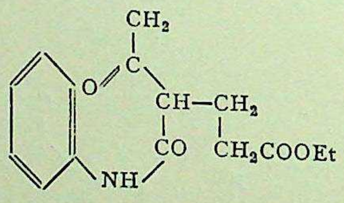

X

The key intermediate in the reaction scheme is 4 methyl-2 quinolone-3 propionic acid (VII). It was obtained in two ways: one by reacting *o*-amino acetophenone with glutaric anhydride and cyclizing the resulting product (VI) with aqueous alkali (as in the case of 2-quinolone-3-acetic acids[4]) and the other by reacting the sodio-derivative of acetoacetanilide with ethyl-β-iodo-propionate and cyclizing the product (X) with sulphuric acid (as in the case of 4-methyl-2-quinolone-3-acetic acid from acetoacetanilide and ethyl-bromo-acetate[5]). The ester (VIII) of the acid (VII) was then reduced with lithium-aluminium hydride to the alcohol (IX). The alcohol (IX) on ring closure with polyphosphoric acid furnished the pyranoquinoline IV. The pyranoquinoline melts at 137–38°, whereas the base (III) from allylacetoacetanilide melts at 119–20°. The U. V. absorption are also not identical.

The absorption of IV shows a batho-chromic shift.

The relevant absorption maxima are

	λ	ε	λ	ε	λ	ε
Substance III ..	272	5075	313	5723	326	6389
IV ..	280	5192	317	5841	331	7139

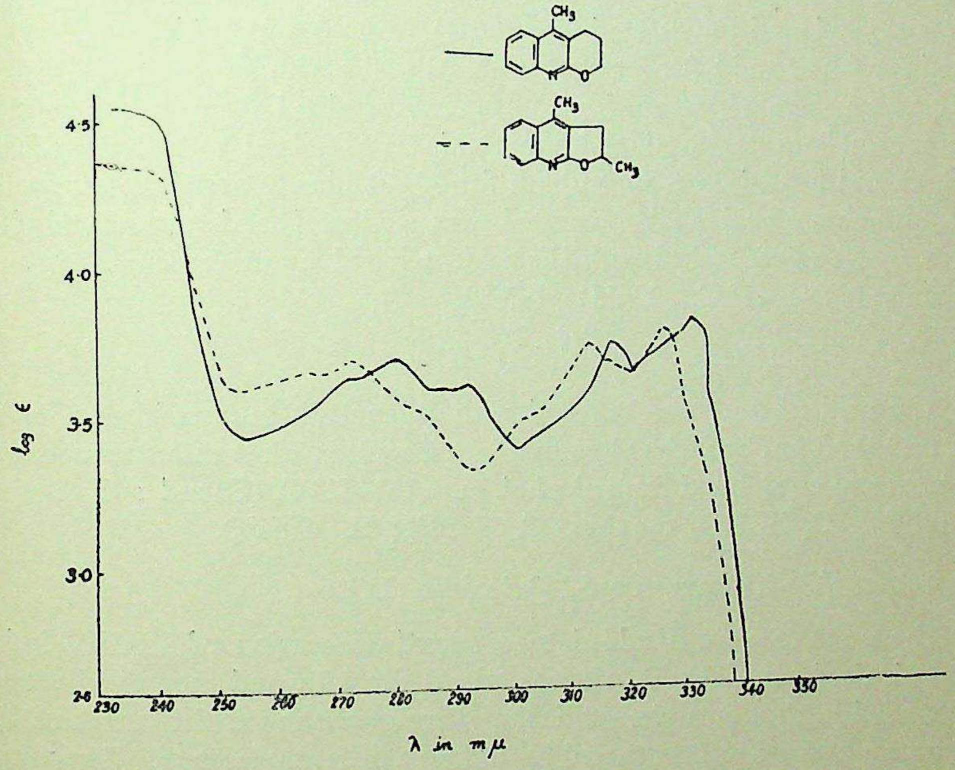

FIG. 1. U.-V. spectra of III and IV in ethanol.

The I.R. spectra of III shows a fairly intense band at 6·13 μ whereas the I.R. spectra of IV shows a band at 6·2 μ.

EXPERIMENTAL

(*i*) 4-*Methyl*-2-*Quinolone*-3-*Propionic Acid* (*VII*)

Method (*a*).—Ortho-amino acetophenone (7·0 gm.), glutaric anhydride (7·0 g.), in 20 c.c. of dry benzene was refluxed for 20 minutes, cooled and the product (VI) was collected and crystallised from benzene, m.p. 113–14° C. (Found: C, 62·85%; H, 5·89%. $C_{13}H_{15}NO_4$ requires C, 62·65%; H, 6·03%).

The above product was dissolved in slight excess of 2% aq. KOH and refluxed for 1 hr., cooled and acidified with HCl, when the quinolone acid (VII) separated. Crystallised from alcohol, m.p. 245–47° C. Yield: 7 gm. (Found : C, 67·71%; H, 5·78%. $C_{13}H_{13}NO_3$ requires C, 67·53%; H, 5·63%.

Method (*b*).—To a suspension of sodium (0·7 g.) in abs. benzene (75 ml.) acetoacetanilide (5·0 g.) was added. The mixture was refluxed with stirring for 4 hrs. when the sodio-derivative was completely formed; it was cooled and ethyl-β-iodopropionate (6·5 g.) was added. It was refluxed for 4 hrs. and left overnight. After dilution with ice-water, the benzene layer was separated, washed with water, and dried over anhyd. $MgSO_4$. The solvent was removed and the residue was mixed with conc. H_2SO_4, (20 ml.) and heated on a steam-bath for 30–40 mins. Poured into ice-water. The quinolone acid that separated was collected and crystallised from alcohol. It was identical with the acid prepared by method (*a*). M.p. and mixed m.p. 245–47° C. Yield: 4·7(g.).

(*ii*) *Ethyl Ester* (*VIII*) *of the Acid* (*VII*)

The acid (5·0 g.) was refluxed with ethanol (70 ml.) and conc. H_2SO_4 (3·0 ml.) for 4 hr., cooled and poured into ice-water, when the ester separated, collected and crystallised from alcohol, m.p. 161–62° C. (Found : C, 69·63%; H, 6·49%. $C_{15}H_{17}NO_3$ requires C, 69·50%; H, 6·56%).

(*iii*) 4-*Methyl*-3′-*Hydroxypropyl*-2-*Quinolone* (*IX*)

The ester (5 g.) was added to a stirred suspension of $LiAlH_4$ (2·5 g.) in tetrahydrofuran (30 ml.). It was stirred for 4 hr. and then the flask was sorrounded with hot water and the stirring continued for another ½ hr. The excess hydride was destroyed by adding a little ethylacetate. The solvent was removed under vacuum and the residue was treated with cold dil. H_2SO_4, the alcohol was collected and crystallised from dil. alcohol, m.p. 154–55° C. Yield: 2·9 gm. (Found: C, 69·19%; H, 7·09%. $C_{13}H_{15}NO_2\cdot\frac{1}{2}H_2O$ requires: C, 69·02%; H, 7·08%).

(*iv*) 3:4-*Dihydro*-5-*Methyl*-2-*H*-*Pyrano*-(2, 3-*b*)-*Quinoline* (*IV*)

The alcohol (IX) (1·0 g.) was heated with polyphosphoric acid (prepared from 5·0 g. of P_2O_5 and 3 ml. of orthophosphoric acid) on a steam-bath for 3 hr. Poured into ice-water and filtered and the clear filtrate was then basified with ammonia. The base was collected, washed with water and then dried. Crystallised from petroleum ether (60–80°) in feathery needles, m.p. 137–38° C. (Found: C, 78·4%; H, 6·4%. $C_{13}H_{13}NO$ requires C, 78·4%; H, 6·5%).

SUMMARY

The synthesis of 3 : 4-dihydro-5-methyl-2H-pyrano-(2, 3-*b*)-quinoline is described and its U.-V. spectra is compared with that of 2 : 3-dihydro-2 : 4-dimethyl-furo-(2, 3-*b*)-quinoline.

ACKNOWLEDGMENT

Thanks are due to Dr. S. Swaminathan and Dr. K. N. Menon for their encouragement, and to Dr. Albert Bernhardt (of Microanalytical Laboratory, Max Planck Institute, West Germany) for the analysis.

REFERENCES

1. Raman, P. S.	.. *Proc. Ind. Acad. Sci.*, 1958, **47**, 244.
2. Hurd, C. D. and Hoffman, W. A.	.. *J. Org. Chem.*, 1940, **5**, 212.
3. John, J. P. and Shanmugam, P.	*Proc. Ind. Acad. Sci.*, 1962, **55**, 227–231.
4. Shanmugam, P.	.. *Ibid.*, 1960, **51**, 75–83.
5. Raman, P. S.	.. *Ibid.*, 1957, **45**, 260.

INVESTIGATION OF SECONDARY FLOW ON AN INFINITE YAWED CYLINDER WITH 15 PER CENT. THICK JOUKOWSKI PROFILE AS SECTION

By Rajeshwar Prasad Singh

(*Department of Mathematics, Patna University*)

and

Dr. K. D. P. Sinha, Ph.D.

(*Department of Mathematics, Science College, Patna*)

Received October 12, 1961

(Communicated by Dr. N. S. Nagendra Nath, F.A.Sc.)

Abstract

This paper contains a theoretical investigation of the secondary flow in the laminar incompressible boundary layer on an infinite yawed cylinder with chordwise section as Joukowski profile of 15 per cent. thickness at zero incidence and with homogeneous suction, the suction mass flow coefficient being equal to 0·2085. The secondary flow profiles are obtained at different points of the wing section and for various angles of sweepback. It is found that in favourable pressure gradients and at pressure minimum, the secondary flow profiles have negative values. In regions of adverse pressure gradients after the pressure minimum the secondary flow changes sign from negative to positive values and have points of inflexion. The change of sign starts from the surface and extends to the edge of the boundary layer downstream. At some points in adverse pressure gradients the secondary flow profiles have double points of inflexion and values of both signs simultaneously. It is also found that an adverse pressure gradient produces more powerful secondary flow than a favourable pressure gradient of the same strength.

Introduction

On an infinite yawed cylinder the boundary layer flow is three dimensional.[1] In the presence of a pressure gradient the chordwise potential velocity varies, whereas the spanwise potential velocity is constant. Therefore, the path of the streamline becomes curved. This path becomes a straight line in the case of a flat plate. In order to maintain this curved potential streamline, there exists a pressure gradient normal to it, which is balanced by the centrifugal force acting on the fluid particle. Due to the boundary layer approximation, the pressure field of the potential flow is transmitted unchanged through the boundary layer. Under this curved potential streamline as the boundary is approached, velocities of the fluid particles in planes parallel to the span continuously decrease to become zero on the boundary. Consequently the streamlines increase their curvature in planes parallel to the span in order to restore the centrifugal force to its required value. In this process, fluid flows towards the concave side of the potential streamline. At any point in the boundary layer, the velocity component in plane parallel to the span is composed of two components, one parallel to the potential streamline direction, and the other normal to it. The velocity component parallel to the potential streamline direction is called the 'Primary flow', and the velocity component normal to it is called the 'Secondary flow'.

Sowerby[2] has shown analytically that in a three-dimensional boundary layer there must be secondary flow unless the streamlines are straight. He and Loos[3] obtained the solution for the secondary flow in the boundary layer on a plate, where the potential streamlines are parabolic.

The secondary flow on a sweptback wing is of considerable importance, because it has been associated with the inflexional type of instability causing early transition near the leading edge.

In the present paper the approximate numerical solutions of the boundary layer are used to investigate the secondary flow on an infinite yawed symmetrical Joukowski profile of 15 per cent. thickness, at zero incidence and with homogeneous suction, the suction mass flow coefficient being equal to $0 \cdot 2085$.

SYMBOLS

x, y, z = Co-ordinates measured in the tangential direction, spanwise direction and normal to the surface respectively (Fig. 1).

u, v, w = Velocity components in the boundary layer in x, y and z directions respectively.

U = Chordwise velocity at the edge of the boundary layer.

U_0 = Chordwise component in the free stream.

V_0 = Spanwise component in the free stream.

U_1 = $(U^2 + V_0^2)^{\frac{1}{2}}$ = Resultant velocity parallel to the boundary at the edge of the boundary layer.

$\bar{U}$ = U/U_0 = Non-dimensional chordwise velocity distribution in the potential flow.

ν = Kinematic viscosity.

Λ = Angle of sweepback.

θ_e = $\mathrm{Tan}^{-1}(V_0/U)$ = Inclination of the edge streamline to the chordwise direction.

v_1 = Velocity component of the secondary flow in the boundary layer.

v_1/U_1 = Non-dimensional velocity of the secondary flow.

k_x = Form parameter for the chordwise profile.

k_y = Form parameter for the spanwise profile.

θ_x = Momentum thickness of the chordwise boundary layer.

θ_y = Momentum thickness of the spanwise boundary layer.

δ_x = A measure of the chordwise boundary layer thickness.

δ_y = A measure of the spanwise boundary layer thickness.

$g_x(k_x)$ = θ_x/δ_x = Ratio of the chordwise momentum thickness to the measure of the chordwise boundary layer thickness.

$g_y(k_y)$ = θ_y/δ_y = Ratio of the spanwise momentum thickness to the measure of the spanwise boundary layer thickness.

H_x = δ_x/θ_x = Shape factor for the chordwise profile in the boundary layer.

H_y = δ_y/θ_y = Shape factor for the spanwise profile in the boundary layer.

H_t = A variable to denote H_x or H_y, equation (1.6).

K_t = A variable to denote K_x or K_y, equation (1.6).

g_t = A variable to denote g_x or g_y, equation (1.7).

c = Length of wing chord.

$\overline{\theta}_x$ = $\theta_x(U_0/c\nu)^{\frac{1}{2}}$ = Non-dimensional chordwise momentum thickness.

ζ = $z(U_0/c\nu)^{\frac{1}{2}}$ = A non-dimensional variable in the case of an aerofoil.

q = θ_y/θ_x = Ratio of the momentum thickness of the boundary layer in the spanwise and chordwise directions.

η_x = z/δ_x = A non-dimensional variable.

η_y = z/δ_y = A non-dimensional variable,

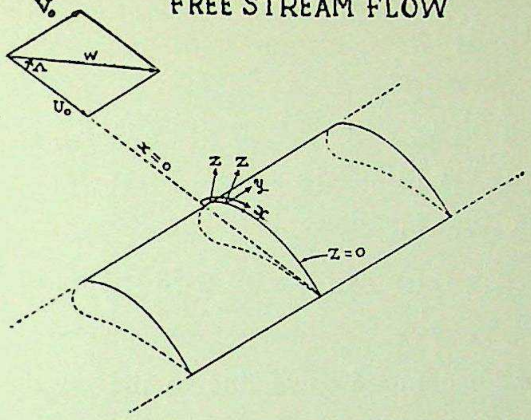

FIG. 1. Sketch showing the orthogonal curvilinear co-ordinates for the flow past an infinite, yawed, uniform cylinder.

METHOD FOR THE CALCULATION OF THE SECONDARY FLOW

A method for the calculation of the secondary flow has been developed by Sinha.[4] He has shown that the secondary flow profiles are given by

$$\frac{v_1}{U_1} = \frac{1}{2}\sin 2\theta_e \left(\frac{v}{V_0} - \frac{u}{U}\right) \tag{1.1}$$

where,

$$\frac{u}{U} = \text{Chordwise profile}$$

and

$$\frac{v}{V_0} = \textbf{Spanwise profile.}$$

Using Schlichting's approximate profiles, the chordwise profile is given by

$$\begin{aligned}\frac{u}{U} &= (1 + K_x)(1 - e^{-\eta_x}) - K_x \sin(\pi/6\ \eta_x), \quad 0 \leqslant \eta_x \leqslant 3,\\ &= 1 - (1 + K_x)\, e^{-\eta_x}, \qquad \eta_x \geqslant 3\end{aligned} \tag{1.2}$$

where,

$$\eta_x = \left\{\frac{g_x(K_x)}{\theta_x}\right\} \cdot \zeta. \tag{1.3}$$

Similarly, the spanwise profile is given by

$$\begin{aligned}\frac{v}{V_0} &= (1 + K_y)(1 - e^{-\eta_y}) - K_y \sin[(\pi/6)\,\eta_y], \quad 0 \leqslant \eta_y \leqslant 3,\\ &= 1 - (1 + K_y)\, e^{-\eta_y}, \qquad \eta_y \geqslant 3\end{aligned} \tag{1.4}$$

where,

$$\eta_y = \left\{\frac{g_y\,(K_y)}{q\bar{\theta}_x}\right\} \cdot \zeta. \tag{1.5}$$

The calculation, then, proceeds as follows:

The chordwise layer[4] being given, $\bar{\theta}_x$ and H_x are known. Hence K_x is determined from the equation:

$$0{\cdot}02358\, H_tK_t^2 - (0{\cdot}09014 + 0{\cdot}06656\, H_t)\, K_t + 1 - \tfrac{1}{2}\, H_t = 0. \tag{1.6}$$

Consequently g_x becomes known due to the relation

$$g_t = \tfrac{1}{2} + 0{\cdot}06656\, K_t - 0{\cdot}02358\, K_t^2. \tag{1.7}$$

Thus η_x is calculated for given values of ζ from the relation (1.3) and u/U is obtained for those values of ζ. Similarly the profile v/V_0 is calculated, because the spanwise layer parameters[4] H_y and q are also known, using the same relations (1.6), (1.7) and (1.5).

It is well known[4] that the smallest value of H_y is $2{\cdot}0$ for the asymptotic suction case. This value is also taken as the lower limit for H_x, although Thwaites[5] has obtained some values of H_x less than 2. If H_t equals the minimum value $2{\cdot}0$, the product of the two roots of K_t becomes zero. One root $K_t = 0$ gives the asymptotic suction profile and the other root is positive which is excluded by Schlichting.[6] For all $H_t \geqslant 2$ the product of the two roots of K_t is always negative, and only the negative roots are permissible. Thus one value of H_t yields only one relevant value of K_t.

Thus the chordwise profile u/U and the spanwise profile v/V_0 both being known, the secondary flow profile can be calculated at any point of the yawed cylinder for given Λ and $\bar{U}$ using the formula (1.1).

RESULTS OF CALCULATIONS

The secondary flow is calculated at points $x/c = 0{\cdot}0148$, $0{\cdot}1445$ and $0{\cdot}734$ for the sweep angles 15°, 30°, 45°, 60° and 75° as shown in Figs. 2, 3 and 4. These secondary flow profiles have also been calculated for sweep angles 15°, 45° and 75° at various points of the wing section as shown in Figs. 5, 6 and 7. Figs. 2, 3 and 4 show the variation of the secondary flow at a particular point for various sweep angles whereas Figs. 5, 6 and 7 show the variation of the secondary flow for a given sweep angle at different points of the wing section. The points on the wing section chosen for the calculation have been taken to lie in regions of different types of pressure gradients.

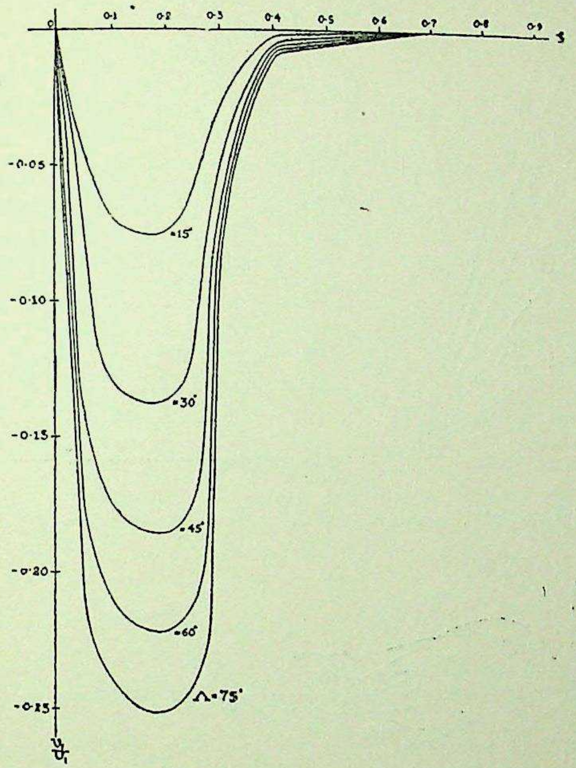

FIG. 2. Nature of the secondary flow profiles at $x/c = 0{\cdot}0148$.

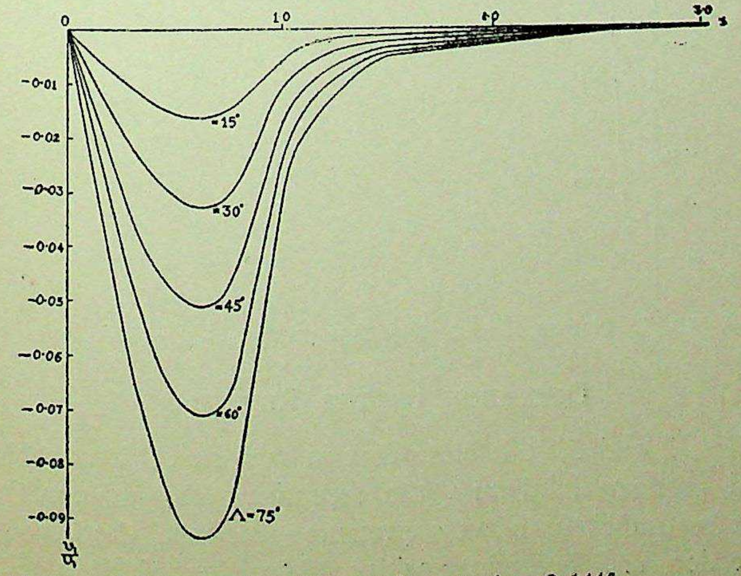

FIG. 3. Nature of the secondary flow profiles at $x/c = 0{\cdot}1445$.

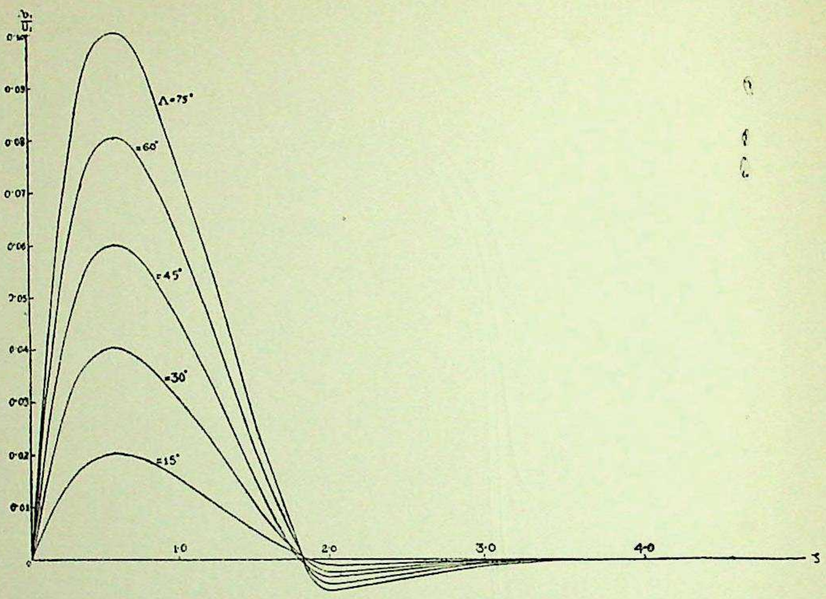

FIG. 4. Nature of the secondary flow profiles at $x/c = 0 \cdot 734$.

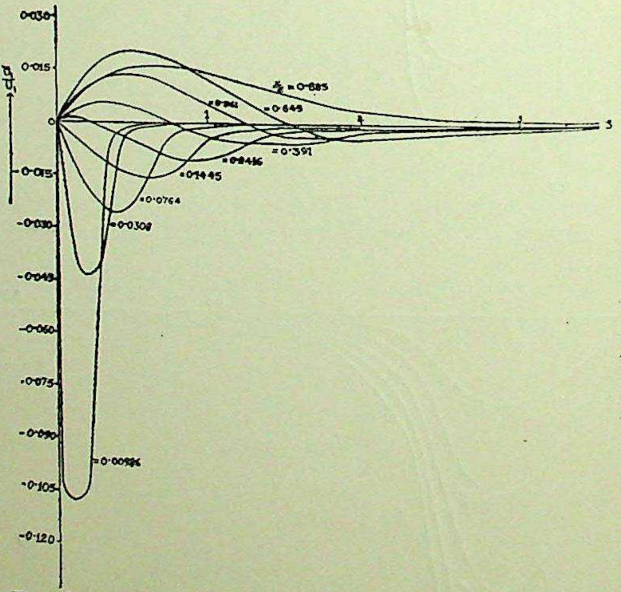

FIG. 5. Nature of secondary flow profiles at $\Lambda = 15°$.

DISCUSSION OF THE RESULTS

From Figs. 2 and 3, it is clear that in regions of favourable pressure gradient and pressure minimum, the secondary flow is negative. From Fig. 4, it is seen that in adverse pressure gradients, the secondary flow changes direction and becomes positive. Moreover, it is also seen that

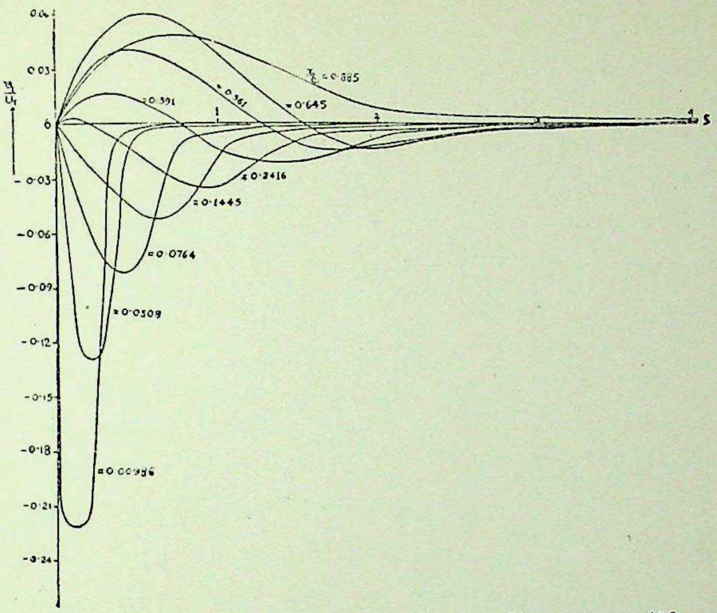

FIG. 6. Nature of the secondary flow profiles at $\Lambda = 45°$.

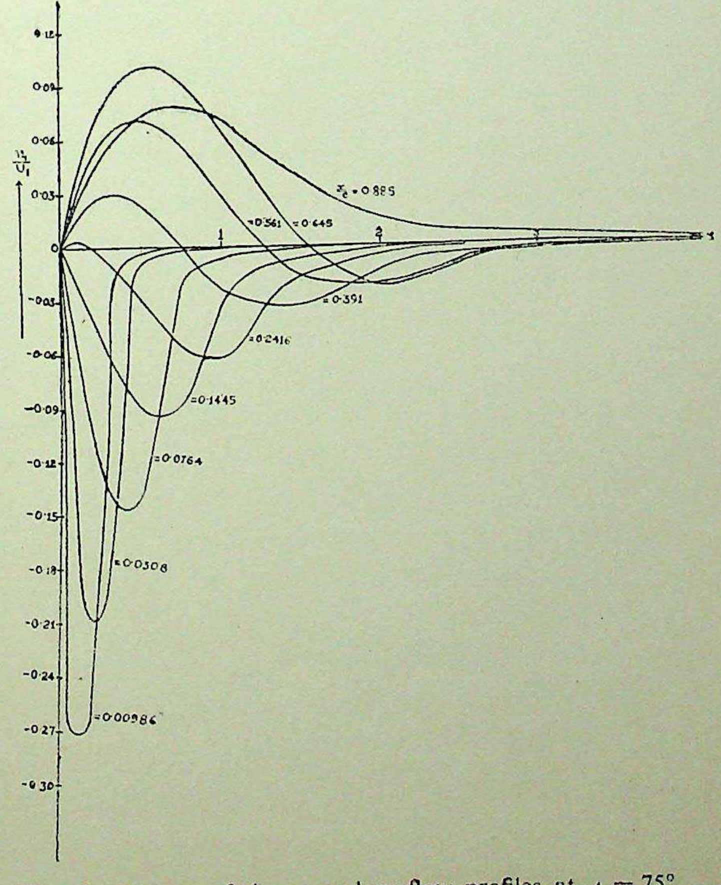

FIG. 7. Nature of the secondary flow profiles at $\Lambda = 75°$.

the change in the direction starts after the pressure minimum and from the surface. It is also seen from Fig. 4 that at some points after the pressure minimum, the secondary flow profiles are both positive and negative and have points of inflexion for different sweep angles. From Figs. 5, 6 and 7, it is seen that the magnitude of the secondary flow increases at all points of the wing section with the increase in the sweep angles. These figures also show that at some points of the wing section in regions of adverse pressure gradients, the secondary flow profiles have double points of inflexion.

CONCLUSIONS

The following is a brief statement of the conclusions to which the present paper leads:—

(1) The secondary flow is zero when the angle of sweepback is zero [Equation (1.1)].

(2) The magnitude of the secondary flow increases with increasing sweep angle at any point of the wing section.

(3) For zero pressure gradient, there is no secondary flow in the boundary layer on an infinite yawed cylinder.

A pressure gradient, whether favourable or adverse, produces a secondary flow which increases with the magnitude of the pressure gradient.

(4) The secondary flow velocities are all negative in the pressure fall domain.

(5) At pressure minimum also the secondary flow profiles have negative values and the values are not the least here.

(6) The secondary flow profiles begin to change their signs (from negative to positive) a little distance downstream of the pressure minimum. The change begins from the surface and the region of change increases to the edge of the boundary layer.

(7) In regions of adverse pressure gradients, some secondary flow profiles are both positive and negative, have points of inflexion and are unstable.

(8) At some points of the wing section in regions of adverse pressure gradients, the secondary flow profiles have velocities of both signs and double points of inflexion. These are likely to be more unstable.

(9) Ultimately in large adverse pressure gradients, the secondary flow profiles become completely positive and become free from any point of inflexion.

(10) Adverse pressure gradients produce more powerful secondary flows than favourable pressure gradients of the same numerical strength.

ACKNOWLEDGEMENTS

We are sincerely thankful to Dr. N. S. Nagendra Nath, Principal, Science College, Patna, for his valuable discussions and comments during our work.

REFERENCES

1. Schlichting, H. .. *Boundary Layer Theory*, Translated by Dr. J. Kestin, 1955.
2. Sowerby, L. .. "Secondary flow in a boundary Layer," *R.A.E. Report No. Aero.* 2512, 1954, A.R.C. 16832.
3. Loos, H. G. .. "A simple laminar boundary layer with secondary flow," *Jour. of Aero. Sciences*, 1955, **22**, 35.
4. Sinha, K. D. P. .. "Dissertation submitted for the degree of Ph.D. in the University of Cambridge," 1956.
5. Thwaites, B. .. "The development of laminar boundary layers under conditions of continuous suction. Part II. Approximate methods of solutions," *A.R.C.* 12699, *F.M.* 1296 *a*, 1949.
6. Schlichting, H. .. "An approximate method for the calculation of the laminar boundary layer with suction for bodies of arbitrary shape," *N.A.C.A. T.M.* 1216, 1949.

STUDIES IN HETEROCYCLIC N-OXIDES

Part III.* 8-Hydroxyquinoline N-Oxide

BY K. RAMAIAH AND V. R. SRINIVASAN

(*Department of Chemistry, Osmania University, Hyderabad-7*)

Received March 22, 1962

(Communicated by Prof. N. V. Subba Rao, F.A.Sc.)

8-Hydroxyquinoline (I) is a well-known analytical reagent which also exhibits antimicrobial properties.[1–2] The basis for such uses of this compound lies in its ability to form a five-membered chelate with metals. However, on account of the lack of selectivity in its chelation properties it forms complexes with a wide range of metals. A certain amount of specificity has been sought in the use of (I) as an analytical reagent either by variation of the conditions of precipitation or by preferential extraction of these complexes with appropriate solvents.[3] Greater selectivity has also been aimed at by structural modification of the reagent through nuclear substitution.[4–6]

An entirely different type of structural modification results on the conversion of 8-hydroxyquinoline to its N-oxide (II) which may be expected to confer greater selectivity in the metal precipitating ability of this compound. In view of this interest in 8-hydroxyquinoline N-oxide, several attempts have been made to evolve a satisfactory procedure for its preparation.[7–10] All the earlier methods involve a preliminary preparation of an oxidising agent such as, monoperphthalic acid or perbenzoic acid or result in low yields when hydrogen peroxide and acetic acid alone were used.

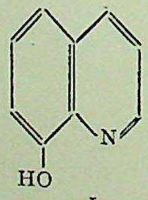

I

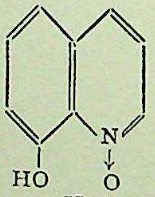

II

The present communication describes a convenient procedure for the preparation of 8-hydroxyquinoline N-oxide in a pure state and in fair yields.

---

* This paper forms a part of the work submitted in 1960, to the Osmania University, for the Ph.D. Degree by K. Ramaiah. Part II, *Proc. Ind. Acad. Sci.*, 1962, **55**, 221–26.

This method involves the oxidation of 8-hydroxyquinoline by peracetic acid generated *in situ* by 30% aqueous hydrogen peroxide and glacial acetic acid. The unconverted 8-hydroxyquinoline has been effectively separated from the N-oxide by steam distillation of the reaction mixture.

Intramolecular hydrogen bonding in 8-hydroxyquinoline N-oxide.—8-Hydroxyquinoline is a typical example of a five-membered chelate. Intramolecular hydrogen bonding is also possible in 8-hydroxyquinoline N-oxide which would form a six-membered chelate. In general, it has been observed that a six-membered system of intramolecular association is sterically as favourable as a five-membered one. The study of intramolecular association in (II) and a comparison of the relative strengths of association in (I) and (II) have been carried out in the present investigation by determining the infra-red absorption characteristics of these two compounds together with that of 8-ethoxyquinoline N-oxide. The relevant results are presented in Table I.

TABLE I

Infra-red absorption data in the hydroxyl stretching region

	Compound		Frequencies cm.$^{-1}$	Concentration M
1.	8-Hydroxyquinoline in $CHCl_3$	..	3660 3400	0·3147
2.	do.	..	3660 3400	0·1573
3.	8-Hydroxyquinoline N-oxide in $CHCl_3$	..	2857–2440	0·3125
4.	do.	..	2857–2440	0·1562

8-Hydroxyquinoline shows a strong band at 3400 cm.$^{-1}$ and a weak one at 3660 cm.$^{-1}$ in a region where hydroxyl stretching vibrations generally absorb. These absorption bands are in accord with those recorded earlier by Badger and Moritz.[11] The band at 3400 cm.$^{-1}$ which is unaffected by dilution with the solvent used and which is about 200 cm.$^{-1}$ lower than the one expected for an unbonded hydroxyl group has been assigned to the weak intramolecular hydrogen bonding in (I). The weak absorption band at 3660 cm.$^{-1}$ in this spectrum has been assigned to an unbonded hydroxyl vibration caused by the presence of a small amount of the trans isomer.[11]

In 8-hydroxyquinoline N-oxide there is no absorption either at 3660 cm.$^{-1}$ or at 3400 cm.$^{-1}$ Instead, this spectrum shows a broad band of moderate intensity in the 2857—2440 cm.$^{-1}$ region, which is independent of the concentration of the solution. These features point to the presence of intramolecular hydrogen bonding involving the O–H and the N–O groups in this compound. 8-Ethoxyquinoline N-oxide, where there is no possibility of intramolecular association, does not absorb in this region; thus confirming the presence of chelation in 8-hydroxyquinoline N-oxide.

The stretching vibration of an unbonded hydroxyl appears as a strong band in the region of 3600 cm.$^{-1}$ A shift of this band to lower frequencies is usually accepted as a criterion for the presence of hydrogen bonding. It is well established that the stronger the internal association, the greater is the shift towards lower frequencies. The relatively large shift of the hydroxyl band by about 1000 cm.$^{-1}$ towards lower frequencies in the spectrum of 8-hydroxyquinoline N-oxide, as compared to a shift of only about 200 cm.$^{-1}$ in 8-hydroxyquinoline, indicates an appreciably greater strength of internal association in this N-oxide. This appears explainable not merely in terms of a six-membered chelate, sterically as favourable as a five-membered one, but also by a stronger intramolecular association of an [O–H $\cdots$ O] type. This increased strength may be on account of the flanking of the hydrogen atom on either side by the two oxygen atoms. On the other hand the environment of the bonded hydrogen in 8-hydroxyquinoline is between an oxygen atom and a less electronegative nitrogen.

Very strong manifestations of such [O–H $\cdots$ O] type of hydrogen bonding are encountered both in six- as well as in five-membered chelates. The broad absorption centred around 2700 cm.$^{-1}$ in β-diketones, such as, acetyl acetone[12] and the 3200–2200 cm.$^{-1}$ absorption in nujol mull or in chloroform solution of 2-hydroxypyridine N-oxide[13] appear to be pertinent examples of this type of intramolecular association, consisting of a six- and a five-membered chelate, respectively.

Metal precipitating ability of 8-hydroxyquinoline N-oxide.—Isolated instances of the use of 8-hydroxyquinoline N-oxide either in metal complex formation[8] or in the estimation of uranium and Ferric ions[14] have been reported. Since 8-hydroxyquinoline N-oxide possesses a strong intramolecular hydrogen bond it may be expected to form stable six-membered chelates with only some cations of favourable atomic dimensions, a feature that may confer greater selectivity to 8-hydroxyquinoline N-oxide in metal precipitation reactions. In order to investigate this possibility, a preliminary study of the metal-complexing ability of this compound on twenty-three cations has been undertaken now. The procedure of Irving and co-workers[15] has been adopted for this screening. The action of 8-hydroxyquinoline on the same set of cations has also been investigated, in order to provide comparable data on metal-complex formation by 8-hydroxyquinoline N-oxide in relation to the un-N-oxidised 8-hydroxyquinoline. These results are presented in Tables II and III.

Out of the twenty-three metals tested, only seventeen reacted with 8-hydroxyquinoline N-oxide forming metal complexes as indicated either by formation of precipitates or by colour changes. Three of these cations, *viz.*, Cu^{++}, Fe^{++} and Ni do not form precipitates with 8-hydroxyquinoline N-oxide, but merely exhibit colour changes.

Be, Hg^{++}, Pb, Sb, Bi and Cr ions do not form insoluble complexes or exhibit complex formation by colour change with the N-oxide under these conditions. 8-Hydroxyquinoline, as expected, precipitated or gave indications of complex formation through change of colour with all the twenty-three metal ions in one or more of the buffers used.

The inability of 8-hydroxyquinoline N-oxide to form complexes with the aforesaid cations may possibly be due to several factors such as the size of the entering ion and the solubility, stability or otherwise of the metal complex. Further investigations on these features of 8-hydroxyquinoline N-oxide and its development into an analytical reagent are in progress.

EXPERIMENTAL

Preparation of 8-hydroxyquinoline N-oxide.—8-Hydroxyquinoline (14·5 g.), glacial acetic acid (30 ml.) and hydrogen peroxide (30%, 10 ml.) were heated on a water-bath at 65–75° C., for four hours. Additional amounts of hydrogen peroxide (10 ml.) were added in three equal portions, while heating, at intervals of one hour each. The reaction product was concentrated under reduced pressure and rendered alkaline with saturated aqueous sodium carbonate solution. Chloroform (60 ml.) was added to it and kept overnight. The solution was filtered, the chloroform layer was separated from the filtrate and dried over anhydrous sodium sulphate. The chloroform was distilled off and the residue was subjected to steam distillation in order to remove the unconverted 8-hydroxyquinoline. The residual aqueous solution was filtered hot to remove the red sticky-material, the filtrate was cooled to yield 8-hydroxyquinoline N-oxide (5·96 g.), shining yellow needles, m.p. 139° C.

TABLE II*

Complex formation tests with 8-hydroxyquinoline N-oxide

Metal ion	Buffer A pH = 5·2	Buffer B pH = 8·4	Buffer C pH = 12·4
Cu^{++}	NP[1]	NP[1]	NP[1]
Be	NP	NP	NP
Mg	Yellow[3]	NP	Yellow[3]
Ca	NP	NP	Yellow[3]
Sr	NP	NP	Bright yellow[2]
Ba	NP	White[2]	Bright yellow[2]
Zn	NP	NP	White[3]
Cd	NP	NP	Yellow[2]
Hg^{++}	NP	NP	NP
Pb	NP	NP	NP
Sb	NP	NP	NP
Bi	NP	NP	NP
Cr	NP	NP	NP
Mo	NP	Pale yellow[2]	NP
Mn	NP	NP	White[2]
Fe^{++}	NP[1]	NP[1]	NP[1]
Co	White[3]	White[3]	White[3]
Ni	NP[1]	NP[1]	NP
Ce^{++++}	Brown[3]	NP[1]	NP
Zr	Yellow[3]	NP	NP
Th	Pink[3]	NP[1]	NP
Uo_2	NP	Yellowish red[3]	NP[1]
Tl^{+}	White[3]	NP	Bright yellow[3]

* Key to table of results.

Colours indicated in the table refer to the colour of the precipitate obtained.

NP: No precipitate even after warming the solution.

[1] Change in the colour of the solution indicating the formation of a metal complex, which, however, is not precipitated out.

[2] Precipitate obtained at room temperature itself.

[3] Precipitate obtained only after warming the test mixture.

TABLE III*

Complex formation tests with 8-hydroxyquinoline

Metal ion	Buffer A pH = 5·2	Buffer B pH = 8·4	Buffer C PH = 12·4
Cu^{++}	Green^{2}	Green^{2}	Green^{2}
Be	NP	NP^{1}	NP
Mg	NP^{1}	Yellow^{2}	Yellow^{2}
Ca	NP	NP^{1}	White^{2}
Sr	NP	NP^{1}	White^{2}
Ba	NP	White^{2}	White^{2}
Zn	Yellow^{2}	Yellow^{2}	Yellow^{2}
Cd	NP^{1}	Yellow^{2}	Yellow^{2}
Hg^{++}	Orange^{2}	Yellow^{2}	NP
Pb	NP	Yellow^{2}	NP
Sb	NP^{1}	Yellow^{2}	NP
Bi	Yellow^{2}	Yellow^{2}	NP
Cr	NP	NP	Greenish-yellow^{2}
Mo	Yellow^{2}	Yellow^{2}	Yellow^{2}
Mn	Yellow^{2}	White^{2}	White^{2}
Fe^{++}	Black^{2}	Brown^{2}	Dark brown^{2}
Co	Yellow^{2}	Yellow^{2}	Yellow^{2}
Ni	Green^{2}	Green^{2}	Pale yellow^{3}
Ce^{++++}	Brown^{2}	Brown^{2}	White^{2}
Zr	White^{3}	Yellow^{3}	NP^{1}
Th	Yellow^{2}	Yellow^{2}	NP
Uo$_{2}$	Orange^{2}	Orange^{2}	White^{3}
Tl^{+}	NP^{1}	NP^{1}	NP^{1}

---

* The significance of the notations used are the same as those given in Table II.

The infra-red absorption spectra were obtained by using a Perkin-Elmer Model 21 Recording Spectrophotometer. A pair of matched cells (0·94 mm.) were used for recording spectra in chloroform solution.

The authors express their gratitude to Professor N. V. Subba Rao, F.A.SC., Head of the Department of Chemistry, Osmania University, for his kind interest and helpful discussions.

SUMMARY

A convenient method for the preparation of 8-hydroxyquinoline N-oxide in fair yields has been reported. The presence of strong intramolecular association in 8-hydroxyquinoline N-oxide has been demonstrated. A preliminary appraisal of the utility of this compound as an analytical reagent has been carried out and it has been found that 8-hydroxyquinoline N-oxide is more selective in metal-complex formation than 8-hydroxyquinoline.

REFERENCES

1. Albert, A., Rubbo, S. D., Goldacre, R. J. and Balfour, B. G. *Brit. J. Exptl. Pathol.*, 1947, **28**, 69.
2. —, Gibson, M. I. and Rubbo, S. D. *Ibid.*, 1953, **34**, 119.
3. Lacroix, S. .. *Anal. Chim. Acta*, 1947, **1**, 260.
4. Berg, R. and Kustenmacher, H. *Z. anorg. Chem.*, 1932, **204**, 215.
5. Merritt, L. L. and Walker, J. K. *Ind. Eng. Chem. Anal. Ed.*, 1944, **16**, 387.
6. Irving, H., Hollingshead, R. G. W. and Harris, G. *Analyst*, 1955, **80**, 260.
7. Schchukina, M. N. and Savitskaya, N. V. *J. Gen. Chem.* (U.S.S.R., English translation), 1952, **22**, 1269.
8. Murase, I. .. *J. Chem. Soc.* (Japan), 1954, **75**, 1180.
9. Khaletskii, A. M., Pesin, V. G. and ChouTs'in *J. Gen. Chem.* (U.S.S.R., English translation), 1958, **28**, 2386.
10. Petrow, V. and Sturgeon, B. *J. Chem. Soc.*, 1954, 570.
11. Badger, G. M. and Moritz, A. G. *Ibid.*, 1958, 3437 and references therein.
12. Rasmussen, R. S., Tunnicliff, D. D. and Brattain, R. R. *J. Amer. Chem. Soc.*, 1949, **71**, 1068.
13. Gardner, J. N. and Katritzky, A. R. *J. Chem. Soc.*, 1957, 4375.
14. Bhat, A. N. and Jain, B. D. *J. Sci. Industr. Res.* (*India*), 1960, **19 B**, 16 and 295.
15. Irving, H., Butler, E. J. and Ring, M. F. *J. Chem. Soc.*, 1949, 1489.

ANGULAR DISTRIBUTION OF JETS PRODUCED BY HEAVY PRIMARY COSMIC-RAY NUCLEI

By E. Balea, E. M. Friedländer, C. Potoceanu and M. Sahini

(*Cosmic Ray Laboratory, Institute of Atomic Physics, Bucharest, Rumania*)

Received October 16, 1961

(Communicated by Dr. B. V. Thosar, F.A.SC.)

Abstract

A statistical method is developed for analyzing the angular distribution of meson jets produced by heavy primary cosmic-ray nuclei, enabling detection and elimination of the proton jet due to evaporation of the residual incident nucleus. The procedure is applied to 50 high-energy collisions of heavy primary nuclei. It is shown that a significant fraction of the heavy primaries produce bi-modal meson jets consistent with the two-centre model.

I. Introduction

Recent observations by the Polish–Zech group[1] have brought evidence for double-maximum angular distributions of secondaries from meson jets. Thus, for the first time, experimental proof was brought forward for the consistency of theoretical models describing the process of meson production at the collision of two very high-energy nucleons by the formation of two "hot centers" emitting independently mesons, in relative motion with respect to the center of mass system.[2–4] Although the statistics gathered up to date as to nucleon-nucleon interactions is relatively poor, the bi-modality of such jets has been recently proved beyond any statistical doubt.[5–6] These features of high energy jets offer prospects for a direct use of the results obtained by means of the two center-model in the study of nucleon structure. Whereas the first attempts in this direction treated the meson field of the nucleon as some sort of a continuous medium, [7–8] recent results at lower energies[9–14] hinted at the existence of structural elements, *viz.*, appearance at the moment of the collision of cuasi-free pions in the meson cloud surrounding the colliding nucleons.

Similar results have been obtained in cloud-chamber experiments for proton and pion induced jets, at energies around loo Bev.[15]

As far back as 1957 one of the authors[16] suggested that high energy heavy nuclei of the primary cosmic radiation have to be preferred as compared to individual nucleons as jet-producing particles in such a study for the following reasons :

(*a*) A heavy primary can be considered (at energies sufficiently high to neglect the binding energies in complex nuclei) as a monokinetic beam of nucleons. If such a "beam" interacts with a complex nucleus, the occurrence of quite different types of collisions (*e.g.*, central or peripheric) may show up in some way or other in the angular distribution.

(*b*) Due to its characteristic appearance, a heavy nucleus can be easily identified as a primary particle, in distinction to $Z = 1$ particles, whose identification is usually ambiguous.

(*c*) Detection of heavy primary induced jets can be made easily in an unbiased way by following along the track.

These advantages of the heavy primary induced jets are partly counterbalanced by a spurious effect, *viz.*, partial or total evaporation of that part of the incident nucleus, which has not been directly concerned with meson production. In those cases in which this evaporation leads to a relatively large number of protons which cannot be readily distinguished from the mesons of the jet, the protons can easily distort the apparent angular distribution of the meson jets. Thus, *e.g.*, the superposition of the narrow proton beam, due to the evaporation of the residual heavy primary nucleus, over a meson jet distributed isotropically in its own center of mass system, may give the whole jet the appearance of a double maximum angular distribution, characteristic for the two center model.

The present investigation is concerned with a study of the angular distributions characteristic for jets induced by heavy primary nuclei; after eliminating from such events the influence of the evaporation jets, a picture of the interaction is obtained, which contains a greater wealth of information than is the case of jets induced by individual nucleons or pions.

Anticipating our final conclusions we wish to state here that we succeeded in developing a new method for the detection of the evaporation jet; in this way we were able to show that in some cases the angular distributions of secondaries from interactions of high energy heavy primary nuclei, with the nuclei of photographic emulsion, have a polimodal shape, consistent with that observed in interactions produced by particles of unit charge.

Some preliminary results of this investigation have been published previously.[17–19]

II. ANGULAR DISTRIBUTION OF THE EVAPORATION JET

Let γ_0 and Z be the energy per nucleon and the charge of a primary nucleus measured in the laboratory system (L system, *see* Appendix I), interacting with an emulsion nucleus. Part of the incident nucleus interacts with the target nucleus, while the rest of the primary nucleus is evaporated isotropically in the frame of reference in which the incident nucleus is at rest (the anti-laboratory system denoted hereafter by $\bar{\mathrm{L}}$, *see* Appendix I). The energy distribution of the protons evaporated in this system is well known from measurements on stars observed in photographic emulsion (the mirror picture of the evaporation of the incident nucleus) (for numerical values *see e.g.*, [20]).

As is well known the Lorentz transform of angles from $\bar{\mathrm{L}}$ to the L system is:

$$\gamma_0 t_g \psi_{\mathrm{L}} = \frac{\sin \psi_{\bar{\mathrm{L}}}}{\dfrac{\beta_0}{\beta_{\bar{\mathrm{L}}}} + \cos \psi_{\bar{\mathrm{L}}}} \tag{1}$$

where ψ_{L} is the emission angle of the evaporated particles with respect to the direction of motion of the incident nucleus in the L system,

$\psi_{\bar{\mathrm{L}}}$ is the corresponding angle in $\bar{\mathrm{L}}$,

$\gamma_0 \equiv (1 - \beta_0{}^2)^{-\frac{1}{2}}$ and

$\beta_{\bar{\mathrm{L}}}$ is the velocity of motion of the evaporated particle in the $\bar{\mathrm{L}}$ system.*

By means of the above transform, an estimate can be obtained for γ_0 in the case of pure evaporation (without meson production) using the approximate formula of Peters[21]:

$$\gamma_0 \approx \frac{\text{const.}}{\sqrt{\overline{\psi_{\mathrm{L}}{}^2}}} \tag{2}$$

where $\cos \psi_{\bar{\mathrm{L}}}$ is neglected as compared to the ratio $\beta_0/\beta_{\bar{\mathrm{L}}}$ and only an average value for $\beta_{\bar{\mathrm{L}}}$ is used.

The use of this formula is nevertheless limited by the existence of a relatively long high energy tail in the energy spectrum of the evaporation protons,[20] which may lead to relatively large transverse momenta and hence destroy the clear delimitation of the evaporation and the meson jets.

---

* Hereafter $c = 1$.

In order to obtain a more complete picture of the evaporation jet, it appears useful to characterize its angular distribution in the L system by the variance:

$$S_{ev} \equiv \left[\frac{1}{n_{ev}-1}\sum\left(\log ctg\,\psi_{\mathrm{L}} - \overline{\log ctg\,\psi_{\mathrm{L}}}\right)^2\right]^{\frac{1}{2}} \tag{3}$$

where n_{ev} is the number of protons of the evaporation jet. It is well known that in the case of the meson jets the angles θ_{L} of the mesons with respect to the primary direction have such a distribution that the quantity $\log tg\theta_{\mathrm{L}}$ is distributed approximately normally; in the case of isotropy in the meson center of mass system (C sytsem, *see* Appendix I) the corresponding variance s_{mes} has an expectation value $\sigma_{mes} \approx 0{,}39$.†

The normal distribution of $\log tg\theta_{\mathrm{L}}$ in the L system is a direct consequence of the approximation $\beta\pi'/\beta_c \approx 1$ in the expression analogous to equation (1) written for mesons of velocity β_π' in the C system. This equality is violated in a flagrant manner by the proton and α-particle velocities in the $\overline{\mathrm{L}}$ system. This led us to the idea that may be the expectation value σ_{ev} of s_{ev} is also sensibly different from σ_{mes} ; if so, this fact should in principle allow a clear detection of the evaporation jet.

In order to get an answer to the statistical problems raised by the existence of the evaporation jet, we used a Monte-Carlo procedure, whose block diagram is shown in Fig. 1 (*see* Appendix II, for a detailed description). The energy spectrum of the protons has been taken from reference (²⁰). The value of γ_0 is irrelevant for the estimation of s_{ev} as long as λ_0 is large enough ($\beta_0 \approx 1$).

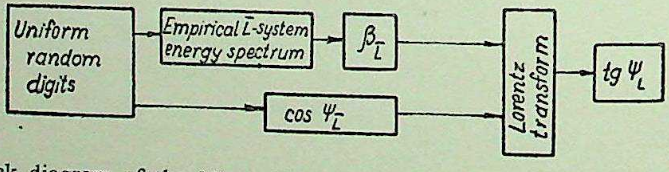

FIG. 1. Block diagram of the Monte-Carlo procedure for simulating evaporation jets.

In view of the large frequency of incident carbon nuclei, we simulated evaporation jets consisting of 6 protons; in order to get an idea about the influence of fluctuations in very small samples, we simulated also evaporation jets consisting of 3 protons each. The results of the estimation of S_{ev} for these two classes of artificial evaporation jets are given in Fig. 2;

---

† In decimal logarithms.

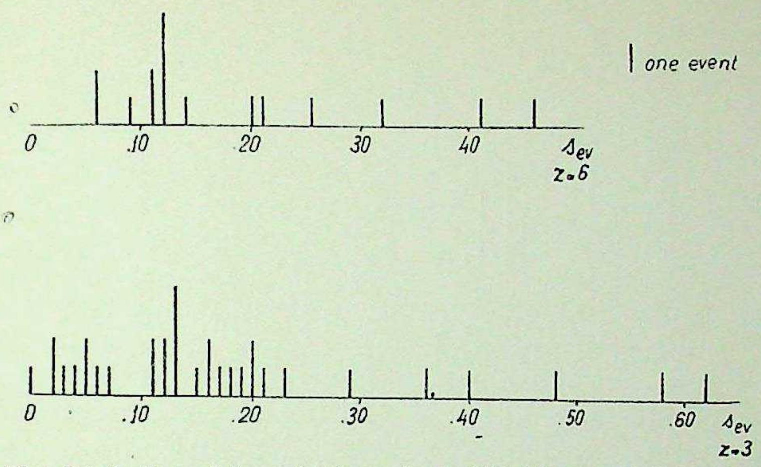

FIG. 2. The distribution of the estimate s_{ev} for artificial jets consisting of 6 and 3 evaporation protons, respectively.

the corresponding average values are:

$$\bar{s}_{ev} = 0{,}18 \pm 0{,}03 \qquad \text{for } Z = 6.$$

$$\bar{s}_{ev} \mathrel{\hat{=}} 0{,}17 \pm 0{,}03 \qquad \text{for } Z \mathrel{\hat{=}} 3. \tag{4}$$

In the above computation we used the same approximation as in Peters' formula, *viz.*, $\cos\theta_{\bar{L}} \ll \beta_0/\beta_{\bar{L}}$. We also applied the correct transformation formula to a restricted sample of events and obtained only negligible differences as compared to the approximate calculation.

Thus our results show that the evaporation jet has, in the L system, an angular distribution of much narrower shape than the angular distribution of a meson jet with the same Lorentz factor; on a Duller-Walker diagram[22] this is equivalent to a straight line much stronger inclined, with respect to the abscissa axis (slope ≈ 4). This feature of the evaporation jet has been used in the following for separating it from the meson jet.

III. EXPERIMENTAL

The jets studied in the present work have been collected in three stacks of nuclear emulsions, exposed in the 1953 Sardinian expedition, and in the 1957 and 1958 Po-Valley expeditions respectively.

The α-particle induced jets have been obtained by area scanning, while those induced by primaries of $Z \geqslant 3$ (H P jets) by following along the track heavy nuclei detected by area scanning in the marginal plates.

The charge distribution of the primaries is shown in Fig. 3. All charges have been estimated from δ-ray densities in the course of another investigation at present under way in our laboratory. The jets accepted for measurement had to show a visible collimation and had a median track length per plate of $\sim 3000\,\mu$.

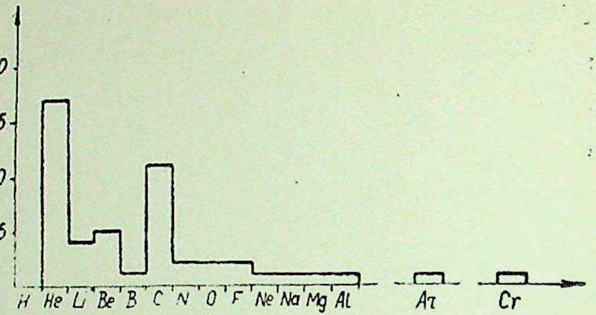

FIG. 3. Charge distribution of the primary nuclei.

The spatial angles ϕ_L of the secondaries of unit charge‡ with respect to the primary direction have been obtained by co-ordinate measurements on Koristka MS-2 and Leitz-Ortholux microscopes.

The following analysis concerns 50 interactions (17-α and 33 H P jets). The total number of incident nucleons was 546 and the total number of relativistic secondaries 1158. For each jet we computed the Lorentz factor γ_c of the center of mass system (assuming that all particles have been produced from a single center of mass) by means of the Castagnoli formula [23]; this formula was corrected for the non-monoenergic spectrum of mesons in the C system according to references ([24–25]).

The degree of anisotropy of each jet has been characterised as usual by the parameter:

$$S \equiv \left[\frac{1}{n_s - 1} \sum \left(\log ctg\, \phi_L - \overline{\log ctg\, \phi_L}\right)^2\right]^{\frac{1}{2}} \qquad (5)$$

where n_s is the number of secondary particles of unit charge.

The values of γ_c spanned the range 2–15, corresponding to energies between 10–500 Bev per incident nucleon. The median energy was approximately 35 Bev per nucleon.

IV. RESULTS

For each jet we constructed the integral Duller-Walker diagram[22] and the corresponding differential distribution of the quantity log *ctg* ϕ_L. According to the shape of these diagrams the jets have been divided into three classes, *viz.*,

(A) Unimodal jets.

(B) Bimodal ones.

(C) Jets with a complex structure showing up several maxima in the differential distribution.

---

‡ No matter whether they were mesons or evaporation protons.

Typical examples of such jets, all produced by carbon nuclei, are shown in Figs. 4 *a*, *b*, *c* which illustrate the great diversity of types realised by one and the same primary nucleus.

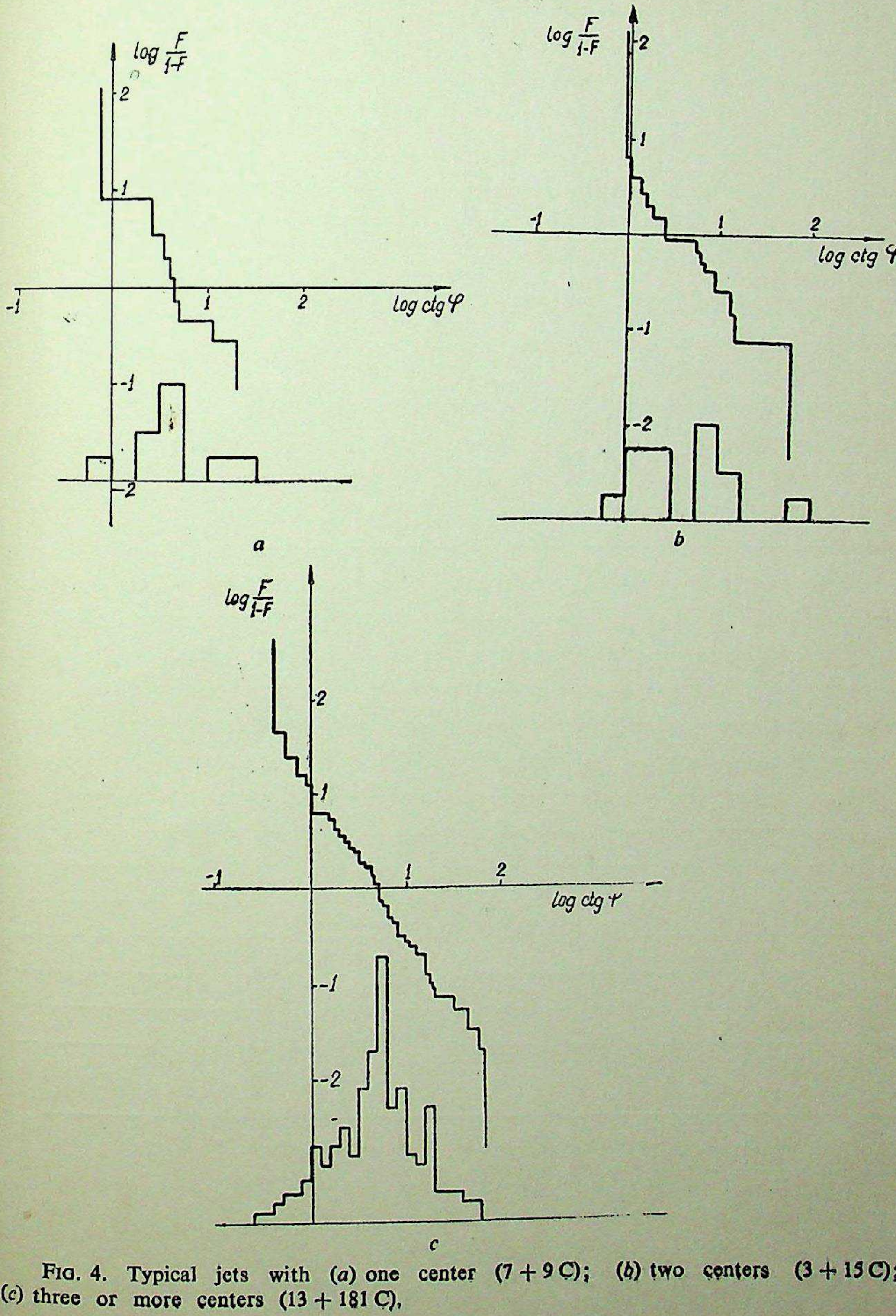

a

b

c

FIG. 4. Typical jets with (*a*) one center (7 + 9 C); (*b*) two centers (3 + 15 C); (*c*) three or more centers (13 + 181 C).

The detailed angular distributions of all our jets are given in Figs. 5 *a*, *b* and *c*.

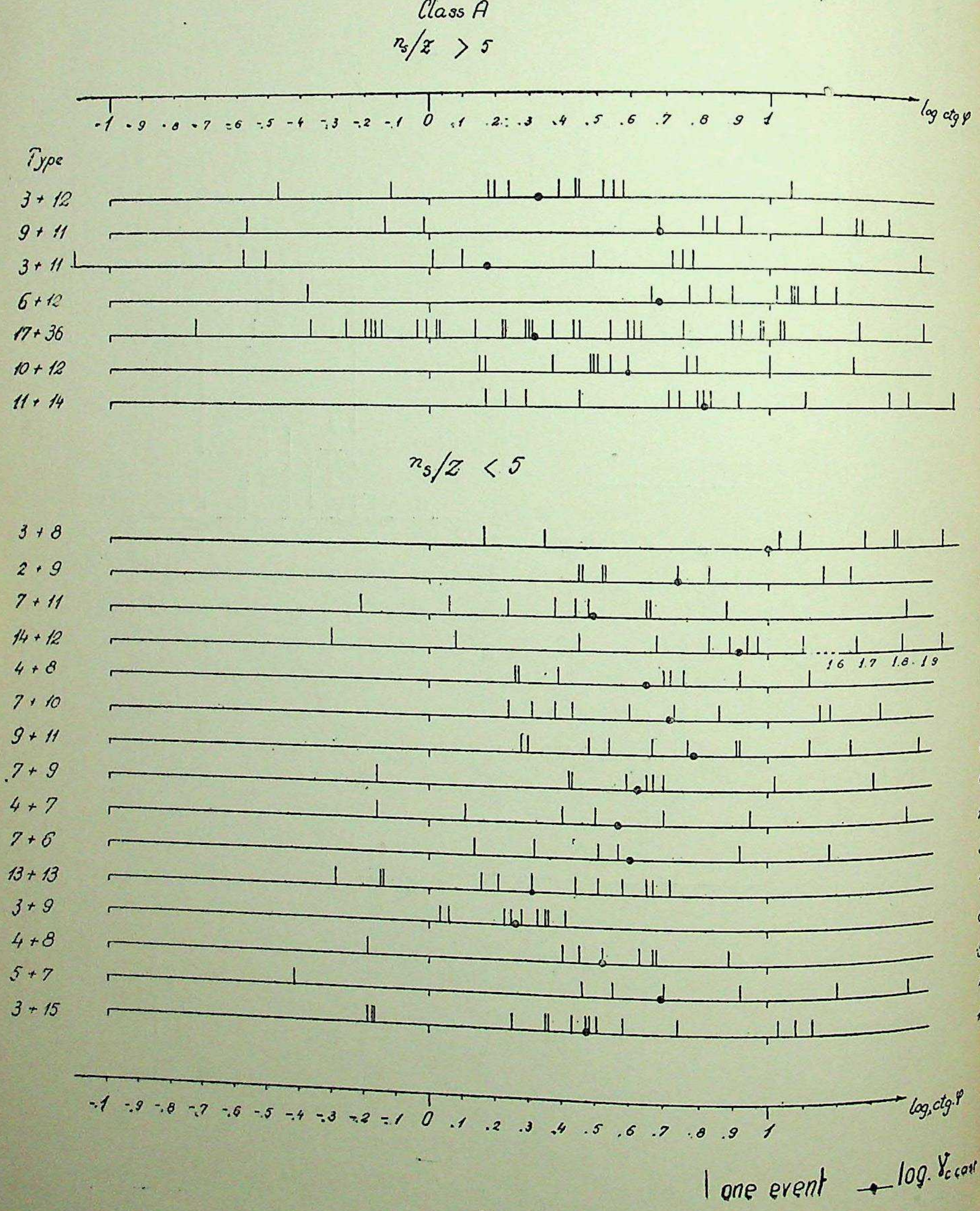

FIG. 5 *a*

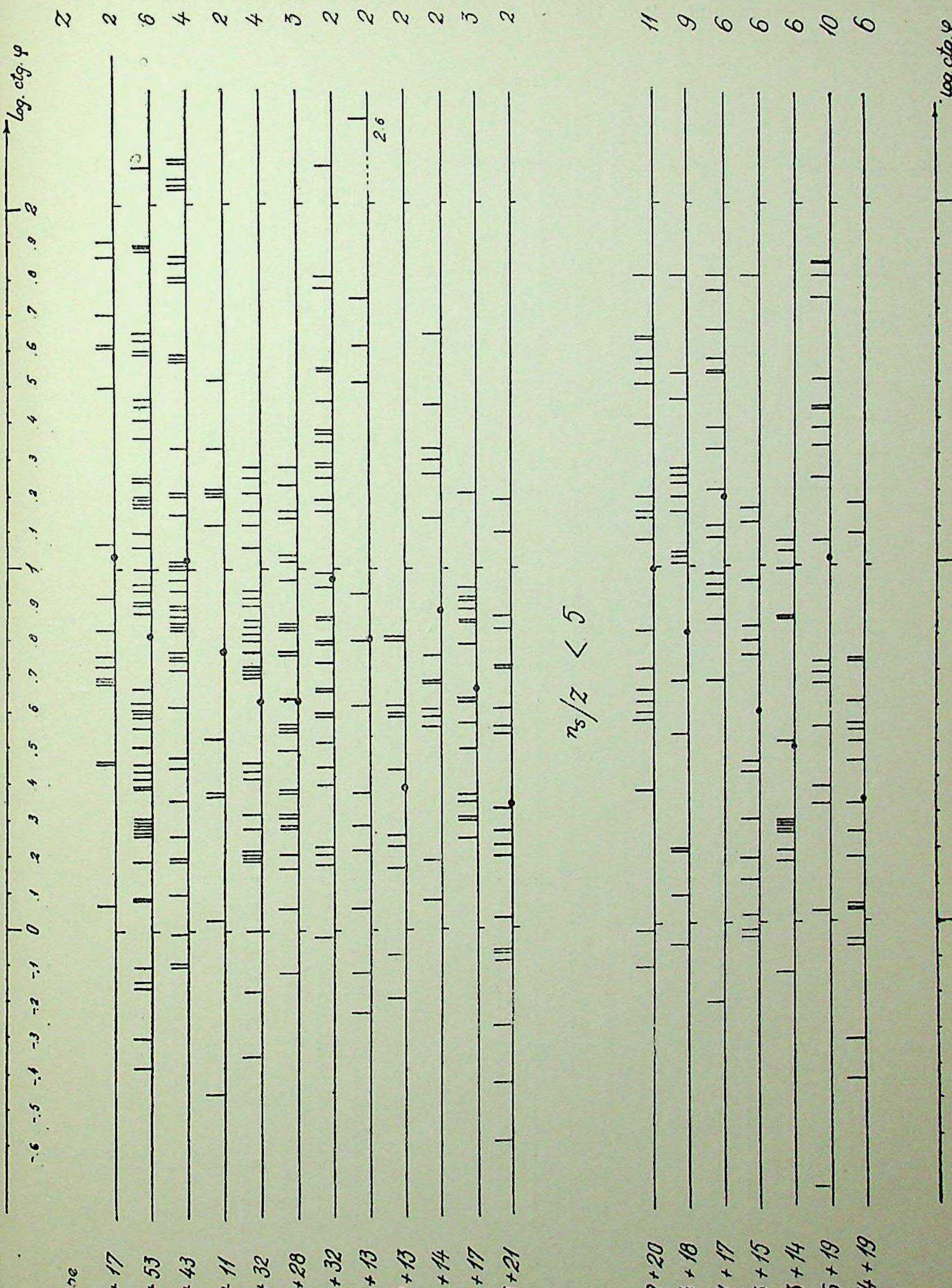
Z
log. ctg. φ
-.6 -.5 -.4 -.3 -.2 -.1 0 .1 .2 .3 .4 .5 .6 .7 .8 .9 1 .1 .2 .3 .4 .5 .6 .7 .8 .9 2
$n_s/Z > 5$
$n_s/Z < 5$
2.6
2 6 4 2 4 3 2 2 2 2 3 2
11 9 6 6 6 10 6
+17
0+53
3+43
7+11
2+32
16+28
6+32
4+13
12+13
3+14
9+17
13+21
2+20
4+18
11+17
3+15
3+14
6+19
14+19

FIG. 5 b

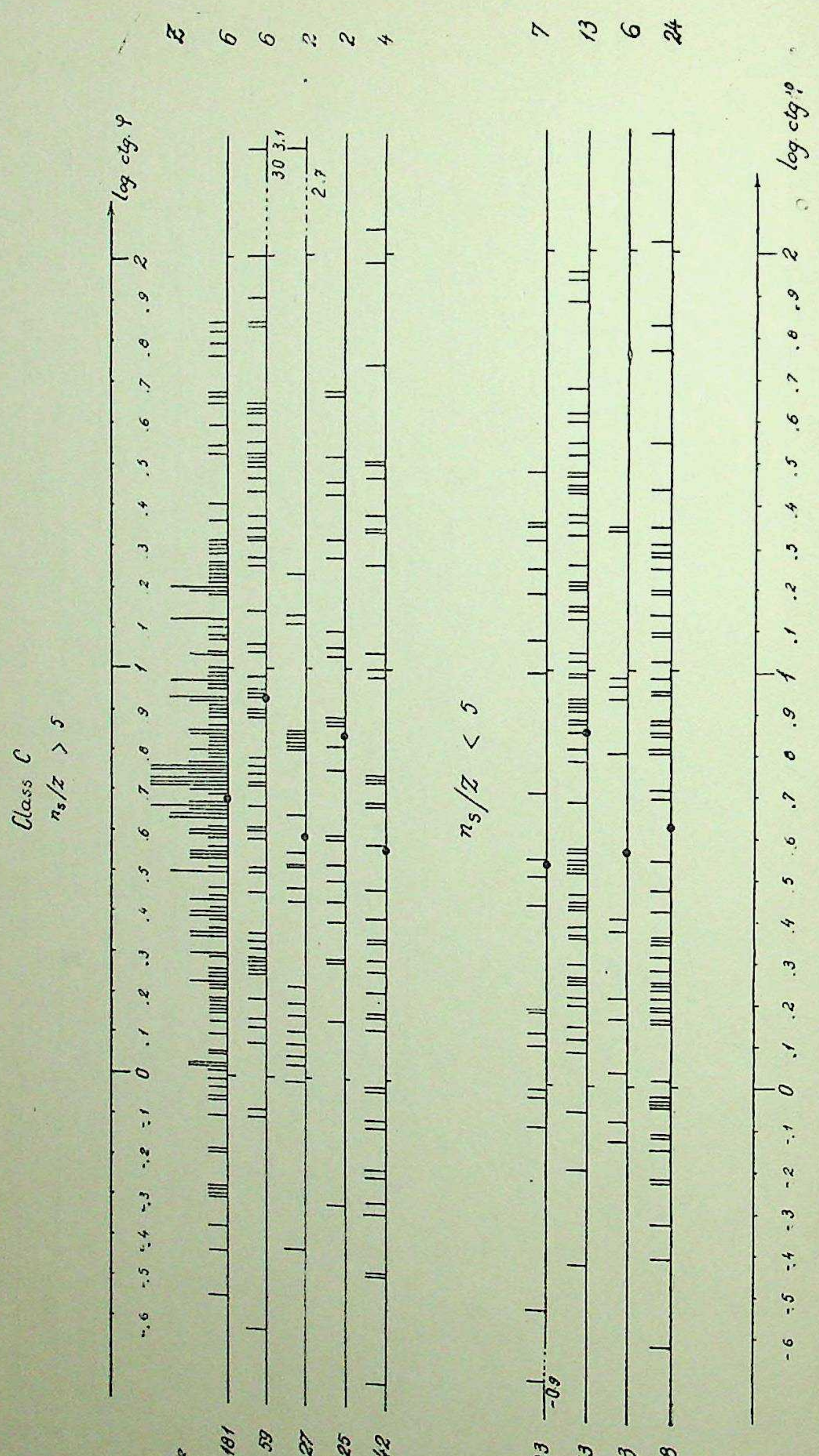

FIG. 5 c

FIG. 5. Detailed angular distributions in log *ctg* φ co-ordinates of all the 50 jets analysed in the present work.

(1) First we analysed the jets with a double maximum shape. As already stated we were here faced with the problem of the superposition of the evaporation jet on a single-maximum meson jet, as an explanation for the observed bimodal shape. We chose as a criterium for distinguishing between the two possible types of interactions (with, and without evaporation jet) the ratio n_S/Z. The distribution of the observed values of this ratio is shown in Fig. 6, in which there appear two distinct groups of jets characterized by either very large or very low values of the ratio n_S/Z.

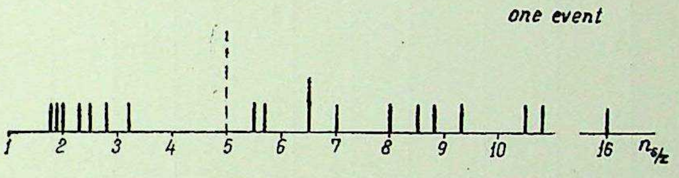

FIG. 6. The distribution of the ratio n_s/Z for experimental bimodal jets.

The average multiplicity per incident nucleon of the jets with $n_S/Z > 5$ (Table I) is in good agreement with the results obtained for protons of comparable energy.[26] The jets with $n_S/Z < 5$ have a low average multiplicity per incident nucleon, of the same order as that observed in accelerator experiments at energies below 10 Bev, although the average values of the Lorentz factor γ_c for the two groups of jets are very near to one another (*see* Table I).

This contradiction can be explained in the easiest way by the assumption that in the jets with $n_S/Z < 5$ the estimate $\overline{\log ctg\, \phi_L}$, for the Lorentz factor, is distorted (enhanced) most probably by the influence of the evaporation jet. In order to check this assumption we studied the angular distribution cumulated from all the corresponding jets in reduced co-ordinates[5]:

$$t \equiv \frac{\log ctg\, \phi_L - \overline{\log ctg\, \phi_L}}{S} \tag{6}$$

separately for jets of each of the two classes (Fig. 7 *a*, *b*).

For each of these distributions we computed by means of a Monte-Carlo procedure a group of artificial jets under the following assumptions:

(*a*) the meson jet is unimodal and has an isotropic distribution in its own center of mass system (C system, *see* Appendix I). In the L system this jet appears as the wide cone with a Lorentz factor γ_-.

(*b*) the narrow cone is due to the evaporation of the incident nucleus so that its Lorentz factor γ_+ is actually a measure of γ_0 (*i.e.*, of the velocity of the L system). The number of tracks chosen for simulating the evapora-

TABLE I

Experimental data and estimated parameters

	$n_s/Z > 5$			$n_s/Z < 5$		
	A	B	C	A	B	C
N ..	7	12	5	15	7	4
$Z = 2$ ..	6	7	2	2	0	0
$Z \geqslant 3$ ..	1	5	3	13	7	4
$\overline{Z}$ ..	$2\cdot6 \pm 0\cdot5$	$2\cdot8 \pm 0\cdot4$	$4\cdot0 \pm 0\cdot8$	$6\cdot5 \pm 1\cdot1$	$7\cdot7 \pm 0\cdot8$	$12\cdot5 \pm 3\cdot6$
$\bar{n}_s$ ..	$15\cdot4 \pm 3\cdot2$	$24\cdot5 \pm 2\cdot7$	$66\cdot8 \pm 7\cdot2$	$9\cdot5 \pm 0\cdot6$	$17\cdot4 \pm 0\cdot8$	$39\cdot3 \pm 11\cdot0$
$\overline{N}_h$ ..	$8\cdot4 \pm 1\cdot8$	$6\cdot6 \pm 1\cdot6$	$10\cdot6 \pm 2\cdot7$	$6\cdot1 \pm 0\cdot9$	$6\cdot1 \pm 1\cdot6$	$13\cdot0 \pm 3\cdot6$
$\overline{n_s/Z}$ ..	$6\cdot0 \pm 0\cdot2$	$8\cdot6 \pm 0\cdot8$	$15\cdot5 \pm 3\cdot3$	$2\cdot0 \pm 0\cdot6$	$2\cdot4 \pm 0\cdot2$	$3\cdot2 \pm 0\cdot7$
Z ..	18	34	20	97	54	50
Z_{ev} ..	2	16	2	25	21	32
$2(Z - Z_{ev})$	32	36	36	114	66	36

$n\pi$	..	108	294	334	128	122	157
$\overline{n\pi/\mathrm{nucleon}}$	..	3·4 ±0·1	7·2 ±0·2	9·2 ±0·5	0·88±0·13	1·73 ±0·07	3·64±0·80
$\overline{\gamma_{0\ cast}}$	..	4·0 ±0·8	5·6 ±0·8	5·3 ±0·7	4·0 ±0·8	6·7 ±1·6	3·4 ±0·8
$\bar{\gamma}_+$	..	..	14·4 ±3·7	25·3 ±7·0	..	14·0 ±3·7	..
$\bar{\gamma}_-$	..	..	2·1 ±0·2	1·6 ±0·3	..	2·6 ±0·5	..
$\overline{\gamma_+/\gamma_-}$	..	..	5·9 ±0·8	17·8 ±5·5	..	..	..
$\bar{\bar{\gamma}}$	..	..	1·39±0·08	2·10±0·29	..	..	..
$\bar{\sigma}$	..	0·52±0·10	0·49±0·08	0·54±0·05	0·40±0·04	0·48±0·04	0·49±0·02
$\overline{\mathrm{D}}$	..	..	0·15±0·03	0·02±0·07	..	0·11±0·06	0·27±0·09
$\bar{\gamma}_0$	..	40±13	77±22	61±18	52±13	127±55	32±21

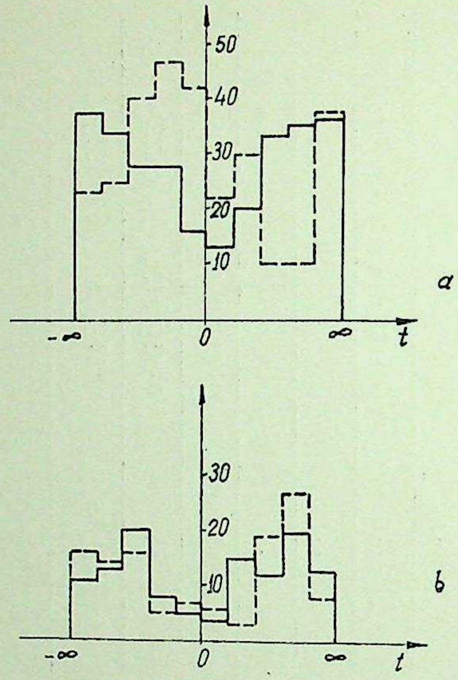

FIG. 7. The angular distribution (in reduced co-ordinates) of bimodal experimental jets (full line) and artificial jets from a mixed population (dotted line). (*a*) Jets with $n_s/Z > 5$; (*b*) jets with $n_s/Z < 5$.

tion jet has been taken equal to $Z - Z_{ev}$, where Z_{ev} is the charge carried by the heavy evaporated nuclear fragments (secondary nuclei with $Z \geqslant 2$).

(*c*) γ_- and γ_0 are assumed to be connected by:

$$\gamma_0 = 2\gamma_-^2 - 1. \tag{7}$$

The block diagram of the Monte-Carlo calculation is given in Fig. 8, and the procedure is described in Appendix II. The unimodal meson jets were simulated by means of a procedure described in a previous paper.[27] Then we superposed an evaporation jet constructed under the exaggerated assumption that it contains exactly Z protons. Actually both initial assumptions (*a* and *b*) are exaggerated in so far as they enhance the influence of the evaporation jet in the angular distribution of the resulting jet.

The angular distribution of these artificial jets is shown by a dotted line in Fig. 7. As can be seen for $n_s/Z < 5$ the experimental and the artificial distribution are in good agreement, while for $n_s/Z > 5$ there appears a strong discrepancy. The consistency of each pair of distributions was checked by means of Pearson tests, the results of which are given in Table II. These results prove that interactions with $n_s/Z < 5$ are mostly

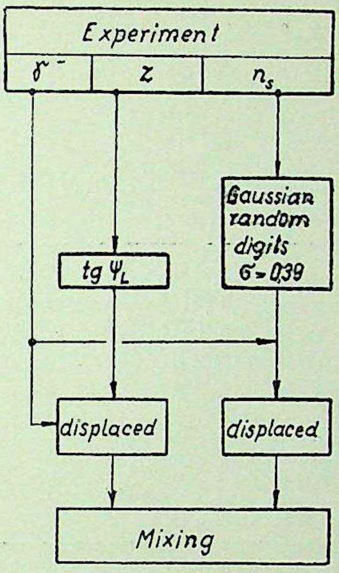

FIG. 8. Block diagram of the Monte-Carlo calculation for simulating artificial jets from a mixed population (mesons + evaporation).

evaporation jets superposed on unimodal meson jets, while events with $n_s/Z > 5$ are mostly true bimodal jets.

It is interesting to note that as ought to be expected, the average charge of the incident nuclei is sensibly larger for the group $n_s/Z < 5$ (Table I).

For each experimental jet with $n_s/Z < 5$ we computed the quantity s_{ev} separately for the narrow cone. As was to be expected the average value of s coincides with that obtained by the Monte-Carlo method for artificial evaporation jets, *viz.*,

$$\bar{s} = 0{,}17 \pm 0{,}03.$$

Now, the true bimodal jets ($n_s/Z > 5$) have been analysed from the point of view of the two center model. Before processing the experimental data we eliminated those (few) tracks which most probably were evaporation protons. For this purpose we computed for each jet observed in experiment three artificial evaporation jets with the same γ_0 and Z as the experimental jet. The whole jet was processed as a meson jet only if not one single track of the experimental jet fell inside the angular interval covered by the whole of the artificial evaporation jets. Otherwise all tracks falling inside the doubtful interval were eliminated. It is easily seen that in this way the bias introduced has only a tendency to underestimate the true bimodality.

TABLE II

Consistency tests: χ^2 *and* P_{χ^2} *values*; $n' = 9$ *except for values denoted by an asterisk where* $n' = 4$

		Experimental jets		Artificial jets from mixed population
		Test against normality	Mutual consistency with artificial jets from mixed population	Test against normality
$n_s/Z > 5$	.. A	11 .. 28%	..	..
	.. B	16 6* 7% 20%	37 $<10^{-4}$	52 $\ll 10^{-4}$
	.. C	9* 6%	37 $<10^{-4}$	53 $\ll 10^{-4}$
$n_s/Z < 5$	.. A	9 44%	..	..
	.. B	18 4%	11 28%	43 $\ll 10^{-4}$
	.. C	34 $<10^{-4}$	13 16%	43 $\ll 10^{-4}$
Artificial jets from a truly bimodal population		Test against normality	Mutual consistency with experimental jets of class B ($n_s/Z > 5$)	
		4* 41%	6* 20%	

In a previous paper[28] it has been shown that the interpretation of the two centers as the result of a pair of cuasi-independent peripheric collisions between nucleon cores and pions of the meson cloud of the collision partners, leads to a well-defined relationship between the Lorentz factors γ_+ and γ_- of the two cones; this interpretation allowed also computation of the Lorentz factor $\bar{\gamma}$ of relative motion of the two centers with respect to the

C system and implicitly the computation of σ.[1] Table III gives the result of the corresponding computation and shows the values of $\bar{\gamma}$, σ, γ_+/γ_- and D (the bimodality coefficient defined in reference ⁽⁵⁾). As can be seen within the experimental errors, good agreement between our results and the theoretical expectation is obtained. It should nevertheless be stressed that just because of the relatively low energy of our primaries the expected effects in the case of each of the estimated parameters are relatively low and hence considerably larger statistics than the ones available here are necessary in order to prove this effect beyond any statistical doubt.

TABLE III

Comparison of the true bimodal jet parameters with the values expected from the pion-exchange two center model (in brackets results of the Monte-Carlo computation)

	Experiment	Theoretical expectations
$\bar{\gamma}$ ..	$1{\cdot}39 \pm 0{\cdot}08$	$1{\cdot}41$
γ_+/γ_-	$5{\cdot}9 \pm 0{\cdot}8$	$5{\cdot}9$
σ	$0{\cdot}49 \pm 0{\cdot}08$	$0{\cdot}54$
D	$0{\cdot}15 \pm 0{\cdot}03$	$0{\cdot}09$ $(0{\cdot}11 \pm 0{\cdot}06)$

As a supplementary check of the reality of the bimodal jets ($n_s/Z > 5$) we computed by means of a Monte-Carlo procedure a sample of artificial bimodal jets of the same multiplicity as the experimental ones. (The block diagram is given in Fig. 9 and the detailed description is again in Appendix II).

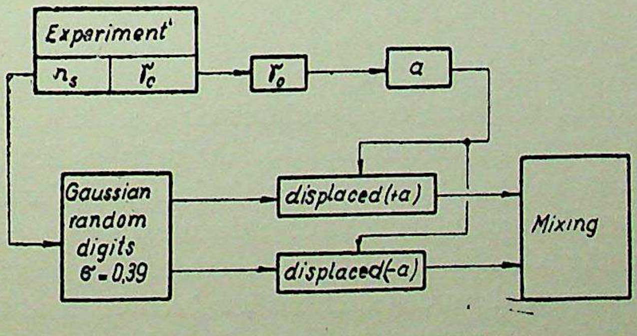

FIG. 9. Block diagram of the Monte-Carlo procedure for simulating true bimodal meson jets.

The angular distribution of these artificial jets is compared in Fig. 10 with the experimental data; the mutual consistency of these distributions has been checked by means of a Pearson test, the result of which is also given in Table II.

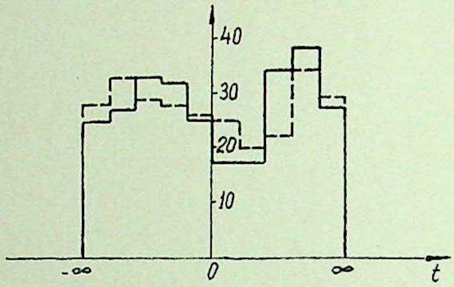

FIG. 10. Comparison (in reduced co-ordinates) of angular distributions from experimental true bimodal jets with artificial jets from a bimodal population, according to the cloud collision two center model (full line experimental jets, dotted line artificial ones).

Table III gives also the value of the bimodality coefficient D of the artificial jets ($n_s/Z > 5$) which is in as good agreement with the theoretical expectations, as were the experimental data.

(2) As already stated in § 1, collisions of heavy primary nuclei with emulsion nuclei offer favourable conditions for the simultaneous observation of peripheral and central collisions in one and the same jet, in view of the larger number of participating nucleons. As was the case in accelerator experiments[9] one might expect here again an angular distribution structured into several maxima. The extreme maxima are expected to be due to peripheral collisions ($\pi - N$ and $N - \pi$), while $N - N$, $N - 2N$ and $\pi - \pi$ collisions should be located at intermediate positions. This kind of angular distribution (with several maxima) has been actually observed in the jets of class C, characterized by high values of the incident charge as well as by a larger number of evaporation tracks from the target nucleus (*see* Table I).

Here again one had to solve first the problem of the influence of the evaporation jet; actually the events of this class could also be divided into two subclasses according to the value of the ratio n_s/Z. Then the events were processed in an analogous way to the one used for the bimodal jets. The angular distribution in reduced co-ordinates[5] is shown in Fig. 11 *a, b* together with the distribution of the corresponding artificial jets. The mutual consistency of these distributions has been checked by Pearson tests, the results of which are given in Table II. These results show that the class C jets, with $n_s/Z > 5$, cannot be interpreted as a superposition of an evaporation jet on a bimodal meson jet as well.

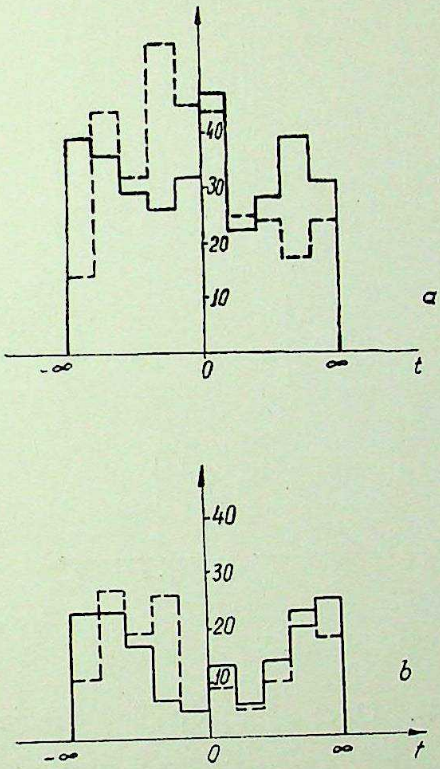

FIG. 11. Angular distribution (in reduced co-ordinates) for experimental and artificial jets of class C (full line experimental jets, dotted line artificial ones). (*a*) Jets with $n_s/Z > 5$; (*b*) jets with $n_s/Z < 5$.

This characteristic feature of the class C jets (the appearance of several maxima in the differential angular distribution) appears especially clearly in a very high multiplicity jet (13 + 181 C, Fig. 12). Similar results have been obtained recently on jets of comparably high multiplicity.[29–30]

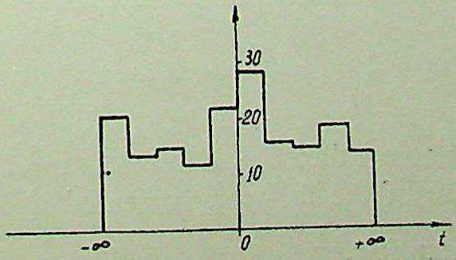

FIG. 12. Angular distribution (in reduced co-ordinates) of the 13 + 181 C jet.

(3) The angular distribution of the apparently unimodal jets (class A) is given in Fig. 13 *a*, *b*. Here the Pearson tests (Table II) show that the angular distribution in the C system cannot be distinguished from an isotropic one (*see* Fig. 14). Once again dividing the jets according to the criterion n_s/Z it appeared that some jets were built up almost entirely from evaporation protons. The very low multiplicity of these jets and the relatively low value of the Lorentz factor γ_c show that most probably the events of class A are a mixture of the following types of events:

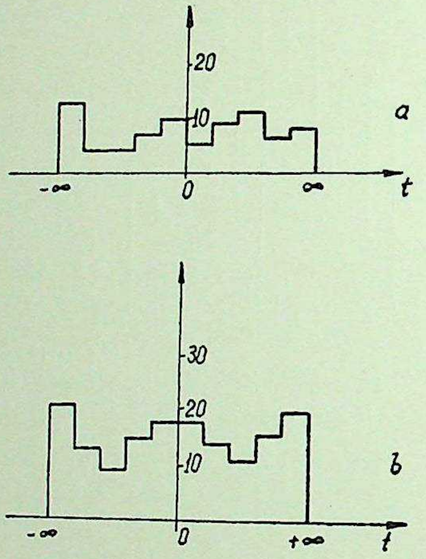

FIG. 13. Angular distribution (in reduced co-ordinates) of unimodal experimental jets. (*a*) Jets with $n_s/Z > 5$; (*b*) jets with $n_s/Z < 5$.

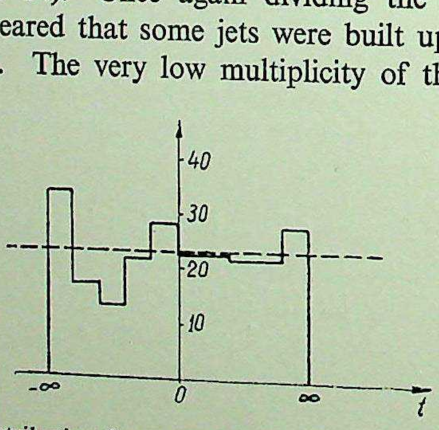

FIG. 14. Angular distribution (in reduced co-ordinates) of all unimodal jets (dotted line —normal distribution).

(*a*) Pure evaporation jets.

(*b*) Unimodal meson jets due to medium energy central collisions.

(*c*) Bimodal meson jets of such low energy that the two cones cannot be distinguished.[28]

(*d*) Mixed events.

For the class A events any clear distinction between these types of interactions is practically impossible and hence a more detailed analysis of these jets does not appear to be justified.

V. CONCLUSIONS

Our results show that the main obstacle in the way of any use of the heavy primary induced jets for the study of the elementary process, *viz.*, the presence of the evaporation jet of the incident nucleus, can be eliminated in a significant manner by means of the pair of criteria n_s/Z and s_{ev}. Thus there appears the possibility of studying with better statistics in an unbiased manner peripheral nucleon-nucleon interactions at high energies by means of heavy primary nuclei. The results obtained in the present work as to the true bimodal jets—which should be considered as preliminary in view of their relatively poor statistics—are in qualitative agreement with the results obtained up to now in nucleon-nucleon collisions.

VI. ACKNOWLEDGMENTS

We are indebted to Dr. E. Fenyves, Dr. J. Pernegr and Dr. P. K. Malhotra for communicating previous to publication their data on jets of high multiplicity measured in the Budapest, Prague and Bombay laboratories; our thanks go to Prof. J. Ausländer for useful discussions, to Miss M. Spîrchez who performed the charge determination on the primary and secondary nuclei, and to our scanner group for locating the events.

VII. REFERENCES

1. Ciok, P., Coghen, J., Gierula, J. Holyński, R., Jurak, A., Mięsowicz, M., Saniewska, J. and Pernegr, J. *Nuovo Cim.*, 1958, **10**, 741.
2. Takagi, S. .. *Progr. Theor. Phys.*, 1952, **7**, 123.
3. Kraushaar, W. L. and Marks, L. J. *Phys. Rev.*, 1954, **93**, 326.
4. Feinberg, E. L. and Černavsky, D. S. *D.A.N.*, 1951, **81**, 795.

5. Gierula, J., Mięsowicz, M. and Zielinski, P. *Nuovo Cim.*, 1960, **18**, 102.
6. ——————Haskin, D. and Lohrmann, E. *Phys. Rev.*, 1961, **122**, 626.
7. Bhabha, H. J. . . *Proc. Roy. Soc.*, 1953, **219**, 293.
8. Friedländer, E. M. . . *Acta Phys. Hung.*, 1956, **6**, 237.
9. —————— . . *Nuovo Cim.*, 1959, **14**, 796.
10. Winzeler, H., Klaiber, B., Koch, W., Nicolić, M. and Schneeberger, M. *Ibid.*, 1960, **17**, 8.
11. Derado, I. . . *Ibid.*, 1960, **15**, 853.
12. Wang-Show-Feng *et al.* . . *J.E.T.F.*, 1960, **39**, 957.
13. Friedländer, E. M., Marcu, M. and Spîrchez, M. *Nuovo Cim.*, 1960, **18**, 623.
14. Grote, L. C., Krecker, U., Kundt, U., Lanius, K., Manske, G. and Meier, H. W. *Nuclear Phys.*, 1961, **24**, 300.
15. Awunor-Renner, E. R. T., Blaskovitch, L., French, B. R., Chesquière, C., de Minvielle-Devaux, J. B., Neale, W. W., Pelletier, C., Rivet, P., Sahiar, A. B. and Skillicorn, J. O. *Nuovo Cim.*, 1960, **17**, 134.
16. Friedländer, E. M. . . *Cosmic Ray Meeting*, Warsaw, 1957.
17. Balea, E., Friedländer, E. M., Oncescu, M., Potoceanu, C. and Sahini, M. *Intern. Meet. Cosmic Rays*, Bucharest, 1959, p. 32.
18. —————— . . *Rev. de Phys.*, 1960, **5**, 91.
19. —, —, Potoceanu, C. and Sahini, M. *C.R. (Paris)*, 1960, **251**, 1487.
20. Camerini, U., Lock, W. O. and Perkins, D. H. *Progr. Cosmic Ray. Phys.*, 1952, **1**, 43.
21. Peters, B. . . *Ibid.*, 1952, **1**, 213.
22. Duller, N. and Walker, W. *Phys. Rev.*, 1954, **93**, 215.
23. Castagnoli, C., Cortini, C., Franzinetti, C., Manfredini, A. and Moreno, D. *Nuovo Cim.*, 1953, **10**, 1539.
24. Friedländer, E. M. . . *Ibid.*, 1959, **12**, 483.
25. Jain, P., Lohrmann, E. and Teucher, M. W. *Phys. Rev.*, 1959, **115**, 643.

26. Hansen, L. F. and Fretter, W. B. *Phys. Rev.*, 1960, **118**, 812.

27. Friedländer, E. M. .. *Nuovo Cim.*, 1962, **23**, 261.

28. ——————— .. *Phys. Rev. Letters*, 1960, **5**, 212.

29. Bozoki, G., Fenyves, E., Pernegr, J. and Vrana, J. *Proc. Weimar High. Energy Conf.*, 1960.

30. Malhotra, P. K. and Tsuzuki, Y. *Nuovo Cim.*, 1960, **18**, 982.

APPENDIX I

REFERENCE FRAMES

A. Before collision

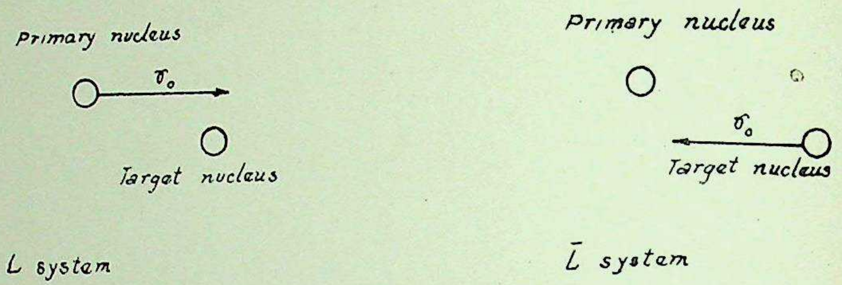
Primary nucleus
v_0
Target nucleus
L system
Primary nucleus
v_0
Target nucleus
$\bar{L}$ system

APP. I, 1

B. After collision

1. Pure evaporation of the two nuclei seen from the L and $\bar{L}$ systems.

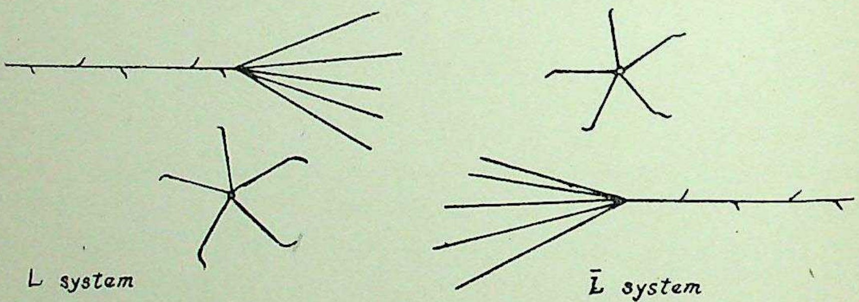
L system
$\bar{L}$ system

APP. I, 2

2. Unimodal meson jet (c.m.s. isotropical, full line) + evaporation jet (dotted line).

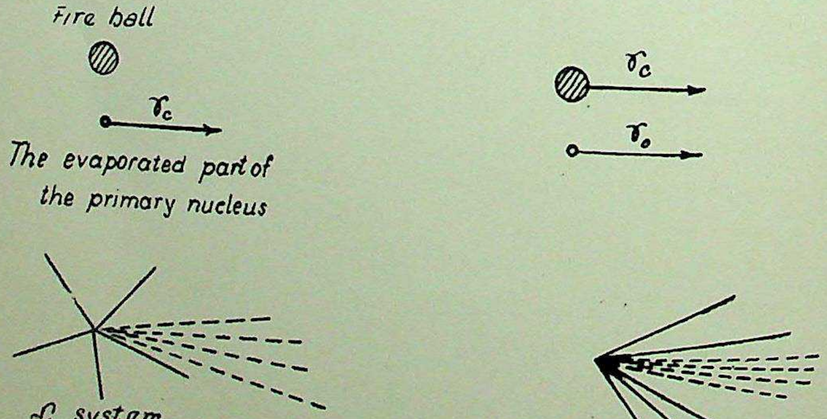
Fire ball
v_c
The evaporated part of the primary nucleus
C system
v_c
v_0
L system

APP. I, 3

112120

3. Pure bimodal meson jet (no accompanying evaporation).

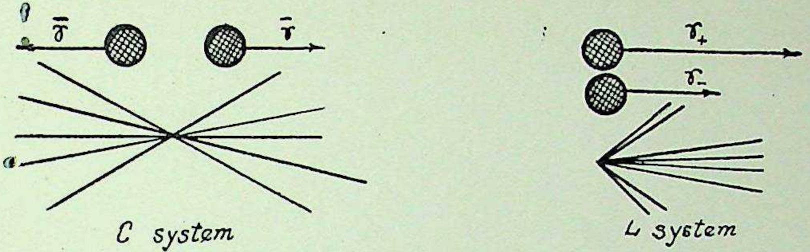

App. I, 4

APPENDIX II

MONTE-CARLO PROCEDURE

I. Simulation of the evaporation jet

In order to obtain the values of s_{ev} in artificial jets we proceeded as follows:

The emission angle $\psi_{\bar{L}}$ has been chosen from an isotropical population (uniform in cos $\psi_{\bar{L}}$). A second random number gave *via* the integral energy distributions of the protons (computed from the data of reference (20)) the value of $\beta_{\bar{L}}$. These two values were then used in the standard Lorentz transform for angles and the values of ψ_L obtained in this way were treated exactly as any experimentally obtained ones. (Eq. 3) for the computation of s_{ev}.

II. Simulation of mixed jets (superposition of an evaporation jet on an unimodal meson jet)

For each double maximum experimental jet, an artificial jet of the same multiplicity was computed. The evaporation jet was constructed according to Fig. 8 (*see* also preceding point). As initial data we took from experiment the values of Z (the maximum number of the evaporation protons) and the Lorentz factor γ_- (of the wide cone) assumed to pertain to the meson jet. γ_- was used as well as a measure for γ_0 (Eq. 7). The transform $\psi_{\bar{L}} \rightarrow \psi_L$ was thus performed by means of γ_0; the $(n_s - Z)$ mesons have been chosen from an isotropic distribution in C. (Log *ctg* $\theta_{\bar{L}}$ has been chosen from a normal population of zero mean and variance 0,39) and displaced by γ_- for the transform to the L system.

112120

III. Simulation of pure bimodal meson jets

The procedure has been exactly the same as the one used in reference (27). The experimental values yielded the multiplicity n_s and the Lorentz factor γ_c of the center of mass system. We assumed validity of the cloud collision two center model[28] which leads at the relatively low energies studied here to a Lorentz factor $\bar{\gamma} \approx 1{,}4$. By means of this value we computed the separation $2\,a$ of the two centers in a $\log tg\,\phi_L$ scale, which was used to displace the isotropic forward jet by $\log \gamma_c + a$ and the isotropic backward jet by $\log \gamma_c - a$.

पुस्तकालय
गुरुकुल कांगड़ी विश्वविद्यालय
हरिद्वार

376-62. Printed at the Bangalore Press, Bangalore City, by T. K. Balakrishnan, Superintendent, and Published by B. S. Venkatachar, Editor, "Proceedings of the Indian Academy of Sciences", Bangalore

NOTICE TO AUTHORS

Scientific papers intended for publication in the *Proceedings of the Indian Academy of Sciences* can be accepted only when they are communicated by a Fellow of the Academy whose duty shall be to satisfy himself that such communications are fit to be read at the Meeting of the Academy and published in its *Proceedings*.

Papers should not ordinarily exceed fifty pages of foolscap. MSS. should be either typewritten or written in legible hand on one side of the paper. All papers should be carefully revised by the authors and should be absolutely in final form for printing. Position for text-figures should be indicated. Each paper shall conclude with a critical summary not exceeding 350 words.

Drawings, diagrams or other illustrations should be made on larger scale (preferably) twice the size than the ones in which they are intended to appear. They should be done in Indian ink on bristol board with lettering in pencil. Scale of magnification of camera lucida tracings should be indicated by the side of drawings. In certain special cases arrangements will also be made for monochrome lithographic and other colour plates. Reduction of illustrations desired should be indicated in pencil. Appropriate legends should accompany all drawings. Names of authors are to be marked in pencil on the left-hand corner of drawing sheets. Photomicrographs should be securely mounted with colourless paste.

All tables, quotations and footnotes which will be set hereafter (beginning from Vol. I, No. 2) in types smaller than the text, should be typewritten on separate sheets and placed with the text in proper sequence. Footnotes should be numbered in Arabic numerals.

References to literature in the text should be given, whenever possible, in chronological order, only the names of authors and years of publication, in brackets, being given. They should be cited in full after the summary, the authors' names following in alphabetical order. Thus,

Name or Names of author; Name of Journal (abbreviation) with a single underline; Year of publication; Number of Volume with a double underline, and lastly page. The following would be a useful illustration:—

Bergmann and Stather . . . . Z. Physiol. Chem., 1926, 152, 189.

Two copies of slip-proof and wherever possible, a page proof for final revision will be sent to authors. All corrections are best made on the slip-proof which should be transmitted to the Office of the Academy. All proof corrections involve heavy expenses which would be negligible if the papers are carefully revised by the authors before submission.

Fifty free reprints including plates and with cover will be supplied for each paper. Additional copies can be supplied at cost on previous intimation.

Blocks appearing in the *Proceedings* will be available for purchase by their respective authors. Orders for the same should be sent along with the corrected proofs and in any case not later than one month after the date of publication of the paper. The price charged would be 25% of the actual cost of the blocks *plus* freight and despatching charges. If the blocks are reproduced in other journals or publications, due acknowledgment should be made in them to the *Proceedings*.

The original drawings and plates of blocks appearing in the *Proceedings* will be returned to such of the authors as may require them provided the cost of despatching such originals is borne by them.

CONTENTS

PAGE

Ultra-violet Absorption Spectra and Higher Excited States of Nd^{3+} in $LaCl_3$ at 77° K. . . . . R. M. Agrawal, R. K. Asundi, R. C. Naik, D. Ramakrishnan and Shobha Singh 325

The Influence of Disturbed Conditions and Increased Solar Activity on Geomagnetic Distortion of the Equatorial Ionospheric F2 Region . . . . B. N. Bhargava and R. V. Subrahmanyan 330

Synthesis of 3 : 4 Dihydro-5-Methyl-2H-Pyrano-(2, 3-*b*)-Quinoline . . . . V. T. Ramakrishnan and P. Shanmugam 345

Investigation of Secondary Flow on an Infinite Yawed Cylinder with 15 per cent. Thick Joukowski Profile as Section . . . . Rajeshwar Prasad Singh and K. D. P. Sinha 350

Studies in Heterocyclic N-oxides. Part III. 8-Hydroxyquinoline N-Oxide . . . . K. Ramaiah and V. R. Srinivasan 360

Angular Distribution of Jets Produced by Heavy Primary Cosmic-Ray Nuclei . . . . . . E. Balea, E. M. Friedländer, C. Potoceanu and M. Sahini 367

Compiled

यह पुस्तक वितरित न [illegible]
NOT TO BE ISSUED

सन्दर्भ
REFERENCE BOOK